Jurassic–Paleogene Intra–Oceanic Magmatic Evolution of the Ankara Mélange, North–Central Anatolia, Turkey

Ender Sarifakioglu[1], Yildirim Dilek[2] and Mustafa Sevin[1]

[1]General Directorate of Mineral Reseach & Exploration, Department of Geology, TR–06520 Ankara, Turkey, esarifakioglu@mta.gov.tr

[2]Department of Geology & Env. Earth Science, Miami University, Oxford, OH 45056, USA, dileky@miamioh.edu

Abstract

Oceanic rocks in the Ankara Mélange along the Izmir–Ankara–Erzincan suture zone (IAESZ) in North–Central Anatolia include locally coherent ophiolite complexes (~179 Ma and ~80 Ma), seamount or oceanic plateau volcanic units with pelagic and reefal limestones (96.6±1.8 Ma), metamorphic rocks with ages of 256.9±8.0 Ma, 187.4±3.7 Ma, 158.4±4.2 Ma, and 83.5±1.2 Ma indicating Northern Tethys during the late Paleozoic through Cretaceous, and subalkaline to alkaline volcanic and plutonic rocks of an island arc origin (~67–63 Ma). All but the arc rocks occur in a shaly–graywacke and/or serpentinite matrix, and are deformed by south–vergent thrust faults and folds that developed in the Middle to Late Eocene due to continental collisions in the region. Ophiolitic volcanic rocks have mid–ocean ridge (MORB) and island arc tholeiite (IAT) affinities showing moderate to significant large ion lithophile elements (LILE) enrichment and depletion in Nb, Hf, Ti, Y and Yb, which indicate the influence of subduction–derived fluids in their melt evolution. Seamount/oceanic plateau basalts show ocean island basalt (OIB) affinities. The arc–related volcanic rocks, lamprophyric dikes and syeno–dioritic plutons exhibit high–K shoshonitic to medium–to high–K calc–alkaline compositions with strong enrichment in LILE, rare earth elements (REE) and Pb, and initial ε_{Nd} values between +1.3 and +1.7. Subalkaline arc volcanic units occur in the northern part of the mélange, whereas the younger alkaline volcanic rocks and intrusions (lamprophyre dikes and syeno–dioritic plutons) in the southern part. The Late Permian, Early to Late Jurassic, and Late Cretaceous amphibole-epidote schist, epidote–actinolite, epidote–chlorite and epidote–glaucophane schists represent the metamorphic units formed in a subduction channel in the Northern Neotethys. The Middle to Upper Triassic neritic limestones spatially associated with the seamount volcanic rocks indicate that the Northern Neotethys was an open ocean with its MORB–type oceanic lithosphere by the early Triassic (or earlier). The Latest Cretaceous–Early Paleocene island arc volcanic, dike and plutonic rocks with subalkaline to alkaline geochemical affinities represent intraoceanic magmatism that developed on and across the subduction–accretion complex above a N–dipping, southward–rolling subducted lithospheric slab within the Northern Neotethys. The Ankara Mélange thus exhibits the record of ~120–130 million years of oceanic magmatism in geological history of the Northern Neotethys.

Keywords: Ankara Mélange (Turkey), Northern Neotethys, seamount volcanics, suprasubduction zone ophiolites, subduction–accretion complex, island arc magmatism

1. Introduction

In the circum-Mediterranean mountain chains belonging to the Alpine-Himalayan system, subduction-related tectonic mélanges during pre-collisional stages are described, but they generally overprinted by arc-continent and continent-continent collisions (Festa et al., 2010 and references therein). In northern Turkey, the 2600-km-long IAESZ extends from west to east, connecting Vardar Suture in west and Sevan-Akera Suture Zone in east. The ophiolitic mélanges and ophiolite slabs are observed along this zone. At the central part of IAESZ, in the vicinity of Ankara, Kırıkkale, Çankırı and Çorum, the Ankara Mélange, first described by Bailey and McCallien (1950), is a well-known subduction-accretion type mélange of the world. They defined metamorphic, limestone and ophiolitic rock blocks in age from Paleozoic to Mesozoic in the mélange. In previous works, three major tectonic units are identified in the Ankara Mélange from the northwest to the southeast. These are metamorphic block mélange, limestone block mélange and ophiolitic mélange (Norman, 1984; Akyürek et al., 1984; Koçyiğit, 1991; Tüysüz et al., 1995; Tankut et al., 1998). The metamorphic block mélange contains a chaotic mixture of variably metamorphosed sedimentary, basic-ultrabasic, and pyroclastic rocks in age from Permian to Triassic while the limestone block mélange consists of neritic to pelagic limestone blocks in age ranging from Permian through Albian in a shale-graywake matrix. The ophiolitic mélange includes several kilometer-size thrust sheets of mantle peridotite, oceanic basic crustal rock, and blocks of serpentinite, massive to pillow basaltic lava flows, radiolarite, chert and neritic-pelagic limestone in pelitic and/or serpentinite matrix (Norman, 1984; Akyürek et al., 1984; Koçyiğit, 1991; Tüysüz et al., 1995). Tankut et al. (1998) emphasized that the ophiolitic mélange unit of the Ankara Mélange is represented by two major mappable coherent units as ophiolitic fragments and volcanic seamounts. They determined that N-MORB character of the Neo-Tethyan oceanic crust along with its seamounts was overprinted by a chemical signature related to subduction zone processes and associated magmatism prior to their incorporation into the subduction-accretion mélange. Göncüoğlu et al. (2001) proved that the ocean-floor generation in the Izmir-Ankara oceanic branch started in early late Carnian from the radiolarian fauna in the blocks of basalt-radiolarite association. Tekin and Göncüoğlu (2007) have presented the radiolarian fauna giving late Ladinian to early middle Carnian from the ribbon-cherts within the Bornova Flysch Zone, western part of IAESZ. Çelik et al. (2011) reported the amphibolites in the ophiolitic mélange near Çankırı giving dates between 177.08±0.96 Ma and 166.9±1.1 Ma from $^{40}Ar/^{39}Ar$ amphibole ages.

In this study, we mapped the ophiolitic rocks, the megablocks and/or thrust sheets of seamount and metamorphic rocks in the Ankara Mélange, and the products of island-arc

magmatism. Also, we document the internal structure of the Ankara Mélange along the IAESZ in North–Central Anatolia, and present new geochemical and geochronological data from various magmatic rock assemblages that make up distinct tectonic units in this mélange. Our geochemical data and interpretations indicate that all units within the Ankara Mélange are intraoceanic in origin and appear to have formed during the seafloor spreading, seamount volcanism and island arc magmatism stages of the Northern Neotethys. We also present new Pb–Sr–Nd isotopic compositional data, and radiometric data belonging to both magmatic arc rocks and basic rocks from the Ankara Mélange. Thus, the Ankara Mélange displays a complete record of ~120–130 m.y. of intraoceanic magmatism that took place prior to the continental collisional events in Anatolia in the Eocene.

2. Regional Geology

The IAESZ forms the tectonic boundary between the Pontide tectonic belt including the Sakarya Continent which represents the southern margin of Eurasia in the north and the Anatolide–Tauride block including the Central Anatolian Crystalline Complex (CACC) in the south. The suture zone is marked by ophiolite units, ophiolitic mélanges, and seamount fragments. The Sakarya Continent in the Pontides represents the southern margin of Eurasia (Figs. 1 and 2). Carboniferous (330–310 Ma), high–grade metamorphic rocks (gneiss, migmatite, amphibolite and marble), currently exposed in the Kazdağ, Söğüt, Devrekani, and Pulur massifs (from west to east), make up the continental basement of the Sakarya Continent (Topuz et al., 2004, 2006; Okay et al., 2006; Nzegge et al., 2006). These metamorphic basement rocks are intruded by the Carboniferous (295 Ma) granitoids (Çoğulu et al., 1965; Delaloye and Bingöl, 2000). The Triassic Karakaya Complex, representing a subduction–accretion complex, tectonically overlies the crystalline basement units (Tekeli, 1981). It includes the Lower Karakaya, which comprises metabasite, marble and phyllite rocks, and the Upper Karakaya consisting mainly of unmetamorphosed clastic and basic volcanic rocks with blocks of Carboniferous and Permian neritic limestones (Bingöl et al., 1975; Okay et al., 2002; Okay and Göncüoğlu, 2004).

The CACC consists mainly of Paleozoic–Mesozoic metamorphic massifs (Kırşehir, Akdağ, and Niğde massifs) and Cretaceous–Paleocene granitoids (Fig. 2). The metamorphic massifs comprise metacarbonate, metapelite and amphibolite–gneiss rocks that are the products of varied P/T conditions of metamorphism (Whitney and Dilek 1998). The Late Cretaceous granitoids and the Eocene–Upper Miocene volcanic rocks crosscut and overlie (respectively) the crystalline basement units of the CACC (Güleç, 1994; Boztuğ, 2000; Kadıoğlu et al., 2003, 2006; İlbeyli et al., 2004). The Late Cretaceous plutons are composed

of *Granite*, *Monzonite* and *Syenite Supersuites* with ages of 77.7±0.3 Ma, 70±1.0 Ma and 69.8±0.3 Ma, respectively (Kadıoğlu et al., 2006). They display a chemical progression from high–K calc–alkaline and high–K shoshonitic to alkaline compositions, representing the development of within–plate magmatism across the CACC with time (Kadıoğlu et al., 2006).

3. Internal Structure and Tectonic Units of the Ankara Mélange

The most important component of the IAESZ in its central segment in northern Anatolia is the Ankara Mélange, extending from Ankara in the west to Çorum in the east (Fig. 2). The Ankara Mélange is a well known subduction–accretion complex (Bailey and McCallien, 1950, 1953), consisting of blocks of Paleozoic limestone and metamorphic rocks, Jurassic–Cretaceous ophiolitic units, and Jurassic–Cretaceous seamount volcanic assemblages in a shaly–graywacke and/or serpentinite matrix (Figs. 3a, 3b and 4; Norman, 1984; Akyürek et al., 1984; Koçyiğit, 1991; Tüysüz et al., 1995; Tankut et al., 1998; Dilek and Thy, 2006; Dangerfield et al., 2011).

Megablocks and imbricated thrust sheets of oceanic rocks occur as mappable units enveloped in a pelitic (clayey, sandy–silty), serpentinite or volcanic matrix within the Ankara Mélange (Fig. 5). In some of these blocks or thrust sheets the mafic–ultramafic rock units and the associated sedimentary rocks make up coherent ophiolite complexes (e.g. the Eldivan ophiolite) (Figs. 6 and 7), representing the Neotethyan oceanic lithosphere. Plagiogranite dikes intruding the serpentinized peridotites near Eldivan (Çankırı) revealed U–Pb zircon ages of 179 Ma (Dilek and Thy, 2006), indicating that part of the Neotethyan oceanic crust preserved in the mélange is as old as the Early Jurassic. The radiolarian fauna in the chert blocks have yielded Late Carnian–Middle Norian, and Middle Jurassic to Middle Cretaceous ages (Sarifakioglu et al., 2011). However, the whole–rock $^{40}Ar/^{39}Ar$ dating of basaltic pillow lava from an ophiolitic thrust sheet farther south in the Ankara Mélange has revealed an age of 80.3±7.6 Ma, indicating that Late Cretaceous oceanic crustal rocks also exist within the mélange (Table 1).

The Senomanian–Santonian flyschoidal sedimentary rocks with pebblestone, sandstone, mudstone and clayey limestone with interbedded chert layers unconformably rest on the ophiolitic rocks (Figs. 3a and 4). However, Kimmeridgian–Hauterivian flyschoidal sedimentary rocks cover the ophiolitic pillow lavas farther south in the Ankara Mélange (Sarifakioglu et al., unpublished data). The Upper Santonian–Maastrichtian, thin– to medium–layered clayey to sandy limestone and volcanic detrital rocks rest unconformably on these flyschoidal sedimentary and ophiolitic rocks around Yapraklı (Çankırı) and Laloğlu

(Çorum), and represent the forearc basin strata (Figs. 6 and 7). The ophiolitic, flyschoidal and forearc basin rocks are imbricated along south–directed thrust faults (Sarifakioglu et al., 2011).

Blocks (km–size) of alkaline volcanic and pyroclastic rocks, debris flow deposits, and coarse–grained reefal limestones representing seamount and/or oceanic plateau fragments also occur in the Ankara Mélange (Fig. 8). We have obtained Middle–Upper Triassic and Cretaceous biostratigraphic ages from the reefal limestones overlying the seamount volcanic units, and $^{40}Ar/^{39}Ar$ whole–rock ages of 96.6±1.8 Ma from the alkaline pillow lavas that are stratigraphically associated with the pink colored pelagic limestones (Sarifakioglu et al., 2011). Rojay et al. (2004) obtained the Late Barremian–Early Aptian biostratigraphic ages from the reefal limestones resting on the pillow lavas with ocean island basalt (OIB) geochemical affinities. Blocks of these neritic carbonates and the underlying alkaline pillow lavas are also embedded in a turbiditic sequence consisting of chert and volcanic rock clasts in a fine–grained sandstone matrix. Volcanic debris flow deposits also occur within the turbiditic sequence.

In addition to the blocks of ophiolitic, seamount and oceanic plateau rocks, the Ankara Mélange also contains blocks of metamorphic rocks, mainly epidote–glaucophane, epidote–chlorite, and epidote–actinolite schists (Fig. 6). The geochemical fingerprinting of these rocks suggests that their protoliths were made of seamount volcanics and ophiolitic basic rocks, and related sediments. Detailed descriptions and documentation of these metamorphic rocks will be presented elsewhere. We interpret these metamorphic rocks to have formed in an intra–oceanic subduction zone. The $^{40}Ar–^{39}Ar$ dating of the epidote–glaucophane, epidote–chlorite and epidote–actinolite schists revealed the cooling ages of 83.5±1.2 Ma, 158.4±4.2 Ma, and 187.4±3.7 Ma, respectively whereas phyllite, actinolite schist and amphibole–epidote schist yielded 119.8±3.3 Ma, 177.4±5.8 Ma, 256.9±8.0 Ma, respectively (Tables 2 and 3).

Overlying the Ankara Mélange tectonically or unconformably are volcanic and volcaniclastic rocks of an island arc origin (Figs. 9 and 10). Nearly 20 km north of Kalecik subalkaline to alkaline volcanic rocks (Dönmez et al., 2009), intercalated with clayey and sandy limestone, calcareous sandstone, pebblestone, sandstone and shale, overlie the Ankara Mélange units and the flyschoidal sedimentary rocks (Hakyemez et al., 1986; Rojay and Süzen, 1997). The volcanic rocks are locally overlain by the Upper Cretaceous reefal limestones and sandstones containing rudist fossils (Fig. 10a and b). Both pillowed and massive lava flows with cooling joints occur (Figs. 9c and 10d); the massive lava flows contain cm–size augite

and leucite phenocrysts. Mafic dikes locally crosscut the volcaniclastic rocks of the arc sequence (Fig. 9d). The $^{40}Ar–^{39}Ar$ whole–rock dating of an arc–related pillow lava has yielded an age of 67.8±4.9 Ma (Table 4a).

Lamprophyre dikes and a syeno–diorite pluton of an island arc origin are intruded into the ophiolitic and seamount rocks and the mélange matrix along the Kizilirmak River near and east of Kalecik (Fig. 11). The brownish grey colored lamprophyric dikes continue along–strike for 200 to 1000 m, and are displaced by local thrust faults. The $^{40}Ar–^{39}Ar$ whole–rock dating and the $^{40}Ar–^{39}Ar$ biotite age from the lamprophyric dikes revealed ages of 67.2±1.2 Ma and 63.6±1.2 Ma, respectively (Table 4b and c).

We have also obtained an $^{40}Ar–^{39}Ar$ biotite age of 75.9±1.3 Ma from a syeno–dioritic pluton, approximately 1 km in diameter, indicating that the arc magmatism started as early as the Campanian and that it progressed with alkaline volcanism and dike emplacement throughout the Maastrichtian and Early Paleocene (Table 4d). Andesitic lavas and volcaniclastic and pyroclastic rocks are intercalated with the Upper Cretaceous–lower Paleocene turbiditic rocks in the region. These turbiditic and flyschoidal rocks contain volcanic pebbles in the lower stratigraphic levels and grade upwards into sandstone and shale. The Paleocene rocks (Dizilitaslar Formation) are conformably overlain by the lower to Middle Eocene sandstone, shale, clayey limestone and marl units that collectively make up the Mahmutlar Formation (Akyürek et al., 1984). All these Paleogene sedimentary rocks were deformed by south–vergent thrust faults and folds, indicating that they underwent N–S–directed contractional deformation in the Middle to Late Eocene.

4. Petrography

In this section we describe the primary and secondary mineral assemblages and the textures of the main lithological types associated with the Neotethyan oceanic crust, seamount volcanic units, and island arc assemblages (e.g. volcanic rocks, lamprophyre dikes and syeno–diorite plutons) that we investigated in the study area.

4.1. Basalt

The seamount-related alkaline basaltic rocks consist mainly of plagioclase (55–60%) and clinopyroxene (approximately 40%), displaying an intergranular texture (Fig. 12a). Some of the basalt samples contain olivine phenocrysts (about 15%) ranging in size from 0.2 mm to 2 mm. Clinopyroxene grains (titanaugites) are partially altered into chlorite, olivine to serpentine and iddingsite, and plagioclase to sericite and chlorite. Apatite and opaque

minerals (Fe–Ti oxide) occur as accessory minerals. Amygdals are filled with secondary carbonate and chlorite minerals.

Tholeiitic basaltic rocks of the Neotethyan oceanic crust comprise microlitic plagioclase and clinopyroxene crystals in a fine–grained texture (Fig. 12b). They are partially or completely spilitized, with plagioclase replaced by albite, sericite, chlorite and epidote (saussuritization), whereas clinopyroxene replaced by actinolite (uralitization) and chlorite. The glassy material in the matrix is transformed into chlorite. Leucoxene and opaque minerals are present as accessories. Vesicles in the basaltic lavas are filled by secondary carbonate and chlorite.

The island-arc basaltic rocks consist mainly of plagioclase (about 55%) and clinopyroxene (45%) crystals in the porphyritic textures with chloritized glassy and microcrystalline groundmass. Clinopyroxene (diopside) grains range in size from 0.2 mm to 2 mm in length (Fig. 12c and d), and locally display twinning. The plagioclases are partly altered to chlorite and carbonate minerals. Accessory minerals are made of fine crystalline Fe–Ti oxides. Basaltic andesites contain plagioclase, clinopyroxene, minor olivine and biotite within porphyritic and glomeroporphyritic textures (Fig. 12e). Ferromagnesian minerals are locally 1.5 cm-long. Fe–Ti oxide minerals are accessories. The groundmass consists of plagioclase microlites, and chloritized and/or devitrified glass. Basaltic lavas include vesicles filled by secondary carbonate, chlorite, and zeolite.

4.2. Basanite

The ultrabasic volcanic rocks consist of clinopyroxene, plagioclase and minor olivine occurring as euhedral and subhedral grains in a hyalomicrolitic, porphyritic texture. Plagioclase forms microlites or micro–phenocrysts, and is commonly altered to clay minerals. Clinopyroxene is mainly augite, and displays zoning and twinning. Olivine is surrounded by a groundmass that is made entirely of serpentine minerals. Small analcime crystals occur as a replacement of leucite between plagioclase and clinopyroxene crystals within the groundmass.

4.3. Tephrite

This fine–grained basaltic rock comprises clinopyroxene (augite), leucite, rare olivine and black mica (phlogopite) crystals within a hyalomicrolitic or porphyritic texture. Plagioclase microlites, ultra fine–grained clinopyroxene, phlogopite, leucite and glassy material form the groundmass, whereas clinopyroxene and leucite occur as euhedral to subhedral

241 microphenocrysts. The leucite contents in the leucite-tephrite rock are up to ~25% (Fig. 12d).
242 Small, anhedral or subhedral opaque minerals are found as accessory minerals.

243 Some tephrites display characteristic features of phonolitic tephrite with feldspar crystals
244 (plagioclase > K–feldspar) and mafic minerals (phlogopite, hornblende) in a microcrystalline
245 porphyritic texture. Plagioclase is partially altered to sericite and chlorite, whereas sanidine is
246 partially altered to sericite and clay minerals. Leucite occurs as subhedral grains, is mostly
247 altered to sanidine microlites, zeolite and clay minerals, and is surrounded by small
248 phlogopite flakes. Euhedral apatite crystals and anhedral opaque minerals (Fe–Ti oxides) are
249 present as accessories.

250 **4.4. Lamprophyre**

251 These alkaline dike rocks consist mainly of small prismastic clinopyroxene (diopside), minor
252 phlogopite and leucite pseudomorphs embedded in a groundmass composed of feldspars
253 (orthoclase>plagioclase), analcime crystals and glassy material (Fig. 12f and g). Both
254 plagioclase and orthoclase are partly or completely altered to carbonate, clay and zeolite
255 minerals; phlogopite is replaced by chlorite along its rims. Small, interstitial apatite laths are
256 enclosed in the orthoclase crystals. In addition, euhedral prismatic apatite crystals up to 0.7
257 mm in length are also present in the groundmass. Opaque minerals occur as accessory
258 crystals.

259 **4.5. Syeno–diorite**

260 The main minerals in this intrusive rock include feldspar (plagioclase ≥ orthoclase),
261 clinopyroxene, hornblende and biotite (Fig. 12h). Subhedral to anhedral plagioclase crystals
262 form a granular texture; some large orthoclase crystals (~2.5 cm) locally give the rock a
263 porphyry texture. Plagioclase grains (An_{28}–An_{48}) are locally surrounded by orthoclase. K–
264 feldspar grains display a perthitic texture. Subhedral to anhedral clinopyroxene (diopside),
265 hornblende and biotite crystals show partial chloritization. Subhedral hornblende crystals
266 have opacite rims around them as a result of metasomatism during their reaction with melt
267 (Plechov et al., 2008). The subhedral prismatic apatite and anhedral granular opaque
268 minerals are present as accessories.

269 **5. Analytical Methods**

270 We analyzed fifthy–one (51) rock samples for major, trace, and rare–earth element chemistry
271 at ACME Analytic Laboratory (Canada). Inductively coupled plasma–emission spectroscopy

has been used for major–element analysis, and inductively coupled plasma–mass spectroscopy has been used for the analysis of both trace elements and rare–earth elements (REE). The results of these analyses are presented in Tables 5, 6, 7, 8 and 9.

$^{40}Ar/^{39}Ar$ age dating was done at the Geochronology and Isotopic Geochemistry Laboratory of Activation Laboratories Ltd. (Actlabs), Ancaster, Ontario, Canada. We obtained $^{40}Ar/^{39}Ar$ ages of biotite separates from two samples of the arc rocks. In addition, whole rock fractions of five rock samples were analyzed. The samples wrapped in Al foil was loaded in evacuated and sealed quartz vial with K and Ca salts and packets of LP–6 biotite interspersed with the samples to be used as a flux monitor. The sample was irradiated in the nuclear reactor for 48 hours. The flux monitors were placed between every two samples, thereby allowing precise determination of the flux gradients within the tube. After the flux monitors were run, J values (n x10-10 cc STP) were then calculated for each sample, using the measured flux gradient. LP–6 biotite has an assumed age of 128.1 Ma. The neutron gradient deed not exceeded 0.5% on sample size. The Ar isotope composition was measured in a Micromass 5400 static mass spectrometer. 1200°C blank of ^{40}Ar deed not exceed $n*10^{-10}$ cc STP.

Argon is extracted from the sample as degassing at ~100°C during two days in double vacuum furnace at 1700°C. Argon concentration is determined using isotope dilution with 38Ar spike, which is introduced to the sample system prior to each extraction. The obtained pure Ar is introduced into customer build magnetic sector mass spectrometer (Reinolds type) with Varian CH5 magnet. Measurement Ar isotope ratios is corrected for mass–discrimination and atmospheric argon assuming that 36Ar is only from the air. After each analysis the extraction temperature is elevated to 1800°C for few minutes. Then, Aliquot of the sample is weighted into graphite crucible with lithium metaborate/tetraborate flux and fussed using LECO induction furnace for K–analysis. The fusion bead is dissolved with acid. Standards, blanks and sample are analyzed on Thermo Jarrell Ash Enviro II ICP Spectrometer.

The Sr, Nd, and Pb isotopic compositions of six samples from the alkaline lamprophyric dikes have been determined at the ACT Analytical Laboratories Ltd., Canada (Table 9). The Sr isotope analysis was performed with a Triton multi–collector mass–spectrometer in static mode. The weighted average of 15 SRM–987 Sr–standard runs yielded 0.710258±9 (2s) for $^{87}Sr/^{86}Sr$. Sm and Nd were separated by extraction chromatography on hexyl di–ethyl hydrogen phosphate–covered Teflon powder. The analysis was performed on a Triton multi–collector mass spectrometer in static mode. $^{143}Nd/^{144}Nd$ ratios are relative to the value of 0.511860 for the La Jolla standard. Pb was separated using the ion–exchange technique with

Bio–Rad 1x8. Pb isotope compositions were analyzed on Finnigan MAT–261 multicollector mass spectrometer. The measured Pb isotope ratios were corrected for mass fractionation calculated from replicate measurements of Pb isotope composition in the National Bureau of Standards SRM – 982 standards. External reproducibility of lead isotope ratios – $^{206}Pb/^{204}Pb$ =0.1%, $^{207}Pb/^{204}Pb$=0.1%, $^{208}Pb/^{204}Pb$=0.2% – on the 2σ level has been demonstrated through multiple analyses of standard BCR–1.

6. Geochemistry

We report below on the geochemistry of the representative samples of oceanic basaltic rocks in the Ankara Mélange, as well as the lamprophyric dikes, a syeno–dioritic pluton, and alkaline lavas that crosscut and/or cover the blocks of volcanic and volcaniclastic rocks, serpentinite, radiolarian chert, and shale in the Ankara Mélange.

6.1. Oceanic Basaltic Rocks

The Na_2O+K_2O values of basaltic blocks of the Neotethyan oceanic crust range from 1 wt% to 4.28 wt%, with the K_2O values much lower than those of Na_2O (Table 5). The Na enhancement of two samples (CE.07, CE.08) may be a result of spilitization caused by low–grade hydrothermal ocean floor metamorphism. Similarly, the total alkali values from the seamount volcanic blocks vary between 4.72 and 8.14 wt%, with the Na_2O values (3.78–6.79 wt%) much higher than that of oceanic crust (Table 6).

On the total alkali vs. silica (TAS) diagram the tholeiitic–calcalkaline volcanic and isolated dike rocks from the Tethyan oceanic crust fall in the field of basalt and basaltic andesite, whereas the samples of seamount alkaline rocks plot in the basanite, tephrite (SiO_2 = 39.77–46.36 wt%), trachyte (SiO_2 = 68.47 wt%), trachybasalt (SiO_2 = 50.15 wt%) and foidite (SiO_2 = 39.77 wt%) fields (Fig. 13a and b). The oceanic basalt samples have lower TiO_2 values (0.26–1.74 wt%) in comparison to the alkaline, seamount volcanic rocks (1.64–2.46 wt%), except for a volcanic sample with tholeiitic OIB (Ocean–Island basalt) characteristics. On a Ti–Zr–Y discrimination diagram (Pearce and Cann, 1973), the oceanic basalt samples plot in the MORB (mid–ocean ridge basalt) and island arc tholeiite (IAT) fields, whereas the seamount volcanic rocks generally fall in the within–plate alkali basalt field (except a trachyte sample; Fig. 13c). On a Ti–V diagram (Shervais, 1982), the samples of oceanic basaltic rocks mostly plot in the MORB field (Ti/V = 22.6–28.9), whereas four samples have island arc tholeiite to boninitic affinities (Ti/V = 5.4–25.55) (Fig. 13d). The samples of silica–undersaturated, seamount volcanic rocks display an OIB–character with high Ti/V ratios (62.6–261.2).

The N–MORB normalized multi–element diagrams of the representative samples of basalts of oceanic crust and seamount volcanic rocks are shown in Fig. 13e. Basaltic samples of both MORB and SSZ (suprasubduction zone) affinities show enrichment in their LILE (the large ion lithophile elements: Rb, Ba, K, Sr, Cs, Th) contents. The HFSE (high field strength elements: Nb, Ta, Zr, Hf, Ti, Y) and REE (rare earth elements) contents of the MORB–type basaltic rocks display a slight increase, whereas the SSZ–related basaltic rocks (four samples) exhibit depletion in HFSE and REE. The LILE, HFSE, LREE (light–REE) contents of the seamount volcanic rocks are extremely enriched relative to the HREE (heavy–REE) values. Also, the Th/Yb (2.8–5.6) and Nb/Yb (27.6–54.8) values of the seamount volcanic rocks are high in comparison to those of the Neotethyan oceanic basalt samples (Th/Yb=0.2–1.1; Nb/Yb=0.7–2.7). However, the alkaline lava samples have the ratios of Nb/Y>1.5 and Zr/Nb<6 that are typical for within–plate basalts (Edwards et al., 1991). The seamount volcanic rocks have Nb/Y ratios of 2.3–3.1 and Zr/Nb ratios of 3.1–4.1, indicating OIB–like geochemical characteristics, whereas the oceanic crust basalt samples have Nb/Y (0.1–0.4) and Zr/Nb (8.1–32) values.

6.2. Island Arc Rocks

A small syeno–diorite pluton, a suite of volcanic rocks, and lamprophyric dikes in the Kalecik (Ankara) area collectively represent the products of island arc magmatism. These arc rocks mostly plot in the alkaline field on a TAS diagram (Fig. 14a and b).The alkaline rock samples with medium to high Al_2O_3 contents (10–19 wt%) represent both silica–saturated and silica–undersaturated rock units (Tables, 7, 8 and 9). The lamprophyric dikes have picrobasalt, trachybasalt, trachyandesite, tephrite and phonotephrite compositions, whereas the volcanic rocks display basalt, basanite, tephrite, leucite tephrite and foidite compositions. The samples from small alkaline intrusions fall into the syeno–diorite field in the TAS diagram (Fig. 14b; Cox et al., 1979). The Late Cretaceous–Early Paleocene volcanic rocks (andesite, dacite, rhyolite), found nearly 60 km SW of Kalecik, show subalkaline (tholeiitic and calc–alkaline) compositions, except for a few trachytbasalt and trachyandesite samples (Fig. 14a, c and d; Dönmez et al., 2009).

The alkaline volcanic rocks mostly display high–K shoshonitic compositions in the K_2O vs. SiO_2 diagram (Fig. 14d; Peccerillo and Taylor, 1976). Some volcanic and dike rocks also plot in the fields of medium– high–K, calc–alkaline series. Although some alkaline volcanic rocks show medium–K calc–alkaline characteristics as a result of hydrotermal alteration (LOI/loss on ignition>2wt%), they have high–K shoshonitic affinity since the leucite bearing, silica–undersaturated alkaline rocks experienced analcimization resulting in low K_2O values in favor

of Na_2O values. On the Hastie et al. (2007), and Pearce (1982) diagrams, which utilize the immobile elements and the ratios of immobile elements (Th vs. Co, and Ce/Yb vs. Ta/Yb), the arc–related plutonic, volcanic and dike rocks generally display high–K (K_2O/Na_2O = 1.5–3.4) and shoshonitic characteristics (Fig. 14e and f). However, seven samples from the volcanic rocks and lamprophyre dikes contain high K_2O/Na_2O ratios (18.16–24.52) showing ultrapotassic (K_2O/Na_2O>3) characteristics.

When plotted on MgO vs. major element diagrams, the analyzed samples mainly exhibit negative correlations, except on the Fe_2O_3 and TiO_2 plots, which show positive correlations (Fig. 15). Based on the MgO vs. trace element variation diagrams (Fig. 15), Co shows a positive trend while Ba, Rb, Sr, Th and Zr all exhibit negative trends. These major and trace element trends can be explained by fractionation of clinopyroxene, feldspar, black mica (biotite, phlogopite), Fe–Ti oxides and apatite. However, the scatter in Fig. 15 may also be caused by the alteration of the arc rocks and/or the involvement of subducted sediments in their melt regime. The rock samples from the small syeno–diorite pluton with metaluminous characteristics plot in the VAG (volcanic arc granites) field (Fig. 16a, b and c). The Ti–Zr–Y and Ti–V diagrams (Pearce and Cann, 1973; Shervais, 1982) show that the alkaline basic samples and the subalkaline volcanic rocks (Dönmez et al., 2009) from the southwestern part of the study area all plot in the arc field (Fig. 16d and e), whereas the TiO_2–Al_2O_3 and Y–Zr diagrams (Muller et al., 1992) show that these samples fall into the arc field (Fig. 16f and g). The analyzed alkaline rocks display shoshonitic characteristics in the Th/Yb vs. Nb/Yb diagram (Pearce, 2008), and their Hf/Th ratios are rather low ranging from 0.11 to 0.57, consistent with their shoshonitic affinity. The island–arc tholeiitic (IAT) basaltic rocks have Hf/Th>3, whereas the calc–alkaline volcanic rocks have Hf/Th<3 (Wood, 1980). Their Th enrichment and increased Th/Yb ratios along the mantle metasomatism trend indicate the influence of subduction–derived fluids in their magma source (Fig. 16h; Pearce, 2008). The samples derived from the blocks of N–MORB–, SSZ– and OIB–like oceanic basalts in the Ankara Mélange typically plot within the MORB–OIB mantle array (Fig. 16h).

The primitive mantle–normalized, multi–element diagrams of the representative samples from the high–K shoshonitic arc rocks around Kalecik (Ankara), Yapraklı (Çankırı) and Laloğlu (Çorum) are plotted in Fig. 17a. The trace element patterns of all the analyzed alkaline rocks display strong enrichment of the LILE, LREE and also Pb, U in comparison to HFSE (Nb, Ta, Zr, Hf, Ti, Y), which show negative anomalies indicating subduction zone influence (Kempton et al., 1991). The high Ba/Ta (>450) and Ba/Nb (>28) ratios are characteristic features of subduction–related magmas (Fitton et al., 1988). The very high ratios of Ba/Ta (383–5255), Ba/Nb (64–538), and relatively high Zr/Nb (5–22), Th/Yb (2–14),

Zr/Y (3–7) and La/Yb (9–36) have been attributed to a mantle source, which was enriched by a subduction component (Frey et al., 1978; Fitton et al., 1988; Maury et al., 1992; Schiano et al., 1995). However, some of the lamprophyre dike samples (DM.2, DM.6, DM.8, DM.9, DM.10) contain La/Yb ratios of 30, indicating highly undersaturated magmas for their origin. Also, the alkaline rocks with Mg# <61, except for one sample (Mg# = 71), [MgO/(MgO + 0.8*FeO total)], imply that none of these shoshonitic rocks represents primary mantle-derived subduction-related magmas. However, their chondrite–normalized REE patterns (Fig. 17b) show LREE enrichment, flat HREE (La/Sm_n=2.18–5.71; Gd/Lu_n=1.69–4.14; La/Lu_n=6.57–24.72), and minor negative Eu anomalies (Eu/Eu*=0.77–0.95). These geochemical characteristics are compatible with those defining subduction–related, arc volcanic assemblages (Tatsumi et al., 1986; Kelemen et al., 1993; Hawkesworth et al., 1993; Pearce and Peate, 1995).

The high–K shoshonitic lamprophyric dikes are characterized by intermediate $^{143}Nd/^{144}Nd$ (0.512674–0,512690) and $^{87}Sr/^{86}Sr$ (0.704697–0.704892) isotopic compositions. The initial ε_{Nd} values range from +1.3 to +1.7, whereas the modern ε_{Nd} values vary between +0.7 and +1.0 indicating a relatively enriched mantle source. Their Pb isotope ratios range from 19.332 to 19.939 for $^{206}Pb/^{204}Pb$, 15.655 to 15.691 for $^{207}Pb/^{204}Pb$, and 39.192 to 39.612 for $^{208}Pb/^{204}Pb$. The high $^{206}Pb/^{204}Pb$, and relatively high $^{143}Nd/^{144}Nd$ and $^{87}Sr/^{86}Sr$ ratios seem to be compatible with a mantle source that is enriched by slab–derived fluids and/or subducted pelagic sediments. Rock (1977; 1984) described shoshonitic lamprophyres (minette, kersantite, vogesite, spessartite) as mildly potassic alkaline rocks (Na<K; SiO_2 =~53 wt%), indicating their magma source to be hybrids between basic magma and granitic residua or crustal sediments. Also, alkaline lamprophyres (camptonite, monchiquite, sannaite) with mantle-type $^{87}Sr/^{86}Sr$ ratios derived from a lamprophyre magma by hydrous crystallization of basaltic magma (Rock, 1977).

7. Discussion

7.1. Source Characteristics

The subduction–accretion complex represented by the Ankara Mélange contains blocks of oceanic lithosphere showing geochemical affinities ranging from MORB to IAT and calc–alkaline. The SSZ–type ophiolite assemblages in the melange display both IAT–like and boninitic geochemical signatures. The ophiolitic units with an IAT–like chemistry are the manifestation of partial melting of the upper mantle peridotites, which were modified by incompatible element–enriched hydrous fluids (or melt) released from the subducting

441 Tethyan oceanic slab. The ophiolitic units with MORB–like signatures represent the products
442 of a depleted mantle source. Some of the samples with MORB–like chemistry plot within or
443 near the IAT field (Figs.13c and 16h) indicating that their magmas were influenced by
444 subduction–derived fluids. These ophiolitic rocks are the oldest units as constrained by the
445 volcanic stratigraphy and crosscutting relationships. Some doleritic dikes and basaltic rocks
446 in the ophiolites show boninitic affinities, consistent with their formation in a forearc setting
447 (Dilek and Furnes, 2011; Sarifakioglu et al., 2011). Collectively, the ophiolitic units in the
448 Ankara mélange display a geochemical progression that is typical of the development of
449 forearc oceanic crust in the early stages of subduction–induced magmatism, as also
450 documented from other Tethyan ophiolites (Dilek and Furnes, 2009, 2011; Dilek and Thy,
451 2009; Pearce and Robinson, 2010; Saccani et al., 2011; Moghadam et al., 2013).

452 Seamount volcanic rocks occurring in the Ankara mélange have OIB–like geochemical
453 features, showing tholeiitic to alkaline affinities (Fig. 13e) with enrichment in incompatible
454 elements and LREEs. The tholeiitic OIB affinity of some of the seamount volcanic rocks may
455 have resulted from the interaction of plume–derived melts with MORB–type melts near a
456 seafloor spreading system. The depletion of the OIB–type volcanic rocks in immobile
457 elements (especially Ti) suggests mixing of the plume and MORB–type melts during
458 seamount evolution.

459 The high–K alkaline rocks exhibit LILE and HFSE enrichments and negative Nb, Ta, Hf, Zr,
460 Ti anomalies, indicating strong subduction influence in their melt evolution (Fig. 17a). The
461 high ratios of LILE/HFSE (Ba/Nb = 64–538; Ba/Ta = 383–5255; Rb/Nb = ~2–20),
462 LREE/HFSE (La/Nb = 1.8–7.2; La/Ta=48–188; La/Sm_n~4), LILE/LREE (Th/La=0.16–0.49)
463 and Zr/Nb (5–22), and the large negative Nb–Ta anomaly in the multi–element diagrams all
464 point to a melt source affected by subduction–generated fluids and/or crustally contaminated
465 magmas. The observed high Ba/Nb (64–538), La/Yb (9–36), Sr/Nd (14–45) and Ce/Yb (20–
466 73) ratios, and low Nb/U (2–7), Ba/La (20.02–59.83), U/Th (0.13–0.50) and Ce/Pb (~2–20)
467 values indicate that the mantle melt source may have been modified by some melts derived
468 from relatively incompatible element–rich, subducted pelagic and/or terrigenous sediments.
469 In contrast, the high Ce/Pb (25+5) and Nb/U (47+10) ratios observed in the OIB–type
470 seamount volcanic rocks indicate that the magmas of these rocks were not modified by
471 subducted sediments (Hoffman et al., 1986).

472 Enrichments in Cs, Rb, Ba, Th, U, K, La, Ce and Pb of the alkaline rocks suggest that their
473 melt source was modified by subducted slab metarial (mainly fluids, and pelagic and/or
474 terrigenous sediments). Slab–derived fluids helped to form hydrous and K–rich minerals,

such as amphibole, apatite and phlogopite with high Rb/Sr (0.04–0.71) and K/Ti (3.77–16.62) ratios relative to MORB– and OIB–like magmas, and resulted in a positive correlation between Ba/Nb and La/Nb ratios (Fig. 18a). Also, the high La (18.4–69.2 ppm) contents and La/Yb ratios (9.5–34.6) reflect that the high–K magmas may have been produced by small degrees of partial melting of a subduction–metasomatised mantle source (Fig. 18b).

As illustrated in the $^{143}Nd/^{144}Nd$ vs. $^{87}Sr/^{86}Sr$ diagram (Fig. 19a), six lamprophyre samples plot on the mantle array defining a subduction component during the evolution of their magmas. We also show in this diagram, for comparison, the Late Cretaceous–Early Tertiary volcanic rocks from the southern part of Central Anatolia and the Eastern Pontides, and the Cenozoic volcanic units in Western Anatolia (Alpaslan et al., 2004; 2006; Eyüboğlu, 2010; Altunkaynak and Dilek, 2006 and references therein). The relatively high Pb (up to 34 ppm in some samples) and $^{87}Sr/^{86}Sr$ contents, and the Rb/Sr ratios (0.02–0.71) of the lamprophyre rocks also indicate the effects of subducted oceanic sediments added to the mantle melt source (Pearce and Peate, 1995). In the $^{206}Pb/^{204}Pb$ vs. $^{208}Pb/^{204}Pb$, $^{206}Pb/^{204}Pb$ vs. $^{207}Pb/^{204}Pb$, $^{87}Sr/^{86}Sr$ vs. $^{206}Pb/^{204}Pb$ and $^{143}Nd/^{144}Nd$ vs. $^{206}Pb/^{204}Pb$ variation diagrams, the data points lie above the Northern Hemisphere Reference Line (NHRL), and the radiogenic isotope data fall close to the fields of MORB, enriched lithospheric mantle source (EMII) and oceanic sediments. These features collectively suggest that the magmas of the lamprophyre rocks were derived from a MORB–like mantle source that was enriched by subducted terrigenous and carbonate sediments (Fig. 19b–e). However, the post–collisional Late Cretaceous–Early Tertiary volcanic rocks in the Ulukisla basin in the southern part of Central Anatolia have higher $^{87}Sr/^{86}Sr$ and lower $^{143}Nd/^{144}Nd$ ratios than those of the lamprophyres in the Ankara Mélange, indicating an EMII with recycled, continent–derived material. The late Cretaceous high–K volcanic rocks representing active continental margin arc units in the Eastern Pontides with low $^{87}Sr/^{86}Sr$ reflect a mantle source enriched by continental crustal rocks. The $^{143}Nd/^{144}Nd$, $^{87}Sr/^{86}Sr$, $^{206}Pb/^{204}Pb$, $^{208}Pb/^{204}Pb$ and $^{207}Pb/^{204}Pb$ values reflecting subduction enrichment and crustal contamination of the source of the post–collisional, Middle Eocene volcanic units in Central Anatolia and the Tertiary volcanic suites in western Anatolia have been explained by slab breakoff–induced asthenospheric upwelling and associated partial melting of the orogenic lithospheric mantle (Alpaslan et al., 2004, 2006; Altunkaynak and Dilek, 2006, 2013; Dilek and Altunkaynak, 2007; Keskin et al., 2008; Gündoğdu–Atakay, 2009; Sarifakioglu et al., 2013).

The depletion of HFSE with respect to LREE enrichment, and high LILE/HFSE and radiogenic isotope ratios suggest that the high–K shoshonitic rocks are likely to have formed

by small degrees of partial melting of a lithospheric mantle modified by slab–derived hydrous fluids.

7.2. Tectonic Model

The Ankara Mélange displays a heterogeneous structural architecture containing oceanic and crustal rocks with different internal structure, stratigraphy and geochemical compositions. The oldest ophiolitic rocks in the Ankara Mélange appear to have formed in a SSZ setting within the Northern Tethys around 180 Ma (Dilek and Thy, 2006; Sarifakioglu et al., 2011). The ~80 Ma (80.3±7.6 Ma) ophiolitic rocks in the same mélange also indicate that oceanic crust formation in the Northern Tethys was still in operation in the Late Cretaceous (Table 1).

We obtained Middle–Upper Triassic biostratigraphic age data from the neritic limestones that are spatially associated with the seamount volcanic rocks, indicating that an oceanic lithosphere of the Late Triassic and older ages must have existed in this ocean to make up the substratum of the seamounts. Thus, we know that the northern branch of Neotethys was already a wide–open ocean with its MORB–type oceanic lithosphere between the Pontide block to the north and the Anatolide–Tauride micro–continent to the south in the Early Triassic (or even before). The ophiolitic mélange units in the Kırıkkale–Ankara–Çankırı–Çorum area are uncomformably overlain by basal volcanic conglomerates of an arc origin. The overlying volcanosedimentary units contain clayey– and sandy–limestone, limey sandstone, and sandstone–claystone alternating with volcaniclastic rocks. These rock types and their internal stratigraphy suggest their deposition in a frontal arc–forearc basin. The clayey limestones are intruded by dikes and sills and have Late Santonian, and Campanian–Maastrichtian ages based on their fossil contents (Sarifakioglu, unpublished data). The radiometric age data from an alkaline basaltic rock (YK.4) and a syeno–diorite intrusion (YK.438) give ages of 67.8±4.9 Ma and 75.9±1.3 Ma, respectively (Table 4a and d), constraining the timing of intra–oceanic arc magmatism as the Latest Cretaceous.

In general, subalkaline (tholeiitic and calcalkaline) volcanic arc rocks occur in the northern part of the study area, whereas the younger alkaline volcanic and plutonic rocks in the south. We interpret this spatial and temporal relationship to have resulted from a southward progression of the arc magmatism from subalkaline to alkaline affinities through time due to arc rifting above the southward retreating Tethyan subduction system (Fig. 20). We, therefore, think that the arc–related late alkaline dikes and plutons were emplaced on and

across the evolving subduction–accretion complex above the north–dipping, southward rolling Tethyan slab.

The high–K and shoshonitic Eocene dikes and lavas in the Ankara mélange formed from melts derived from partial melting of the metasomatized arc mantle that was triggered by the influx of slab breakoff–induced asthenospheric flow.This slab breakoff was a result of an arc–continent (Central Anatolian Crystalline Complex – CACC) collision, followed by the continent–continent collision (Sakarya and CACC) in the Early to Middle Eocene.

8. Conclusions

1. Blocks of Middle–Late Triassic seamount and Upper Permian metamorphic rocks occurring in the Ankara Mélange represent an intra–oceanic subduction–accretion complex that developed in the Northern Tethys during the late Paleozoic through Cretaceous.

2. Thrust sheets and/or megablocks containing SSZ ophiolite units with Liassic and Cretaceous ages were incorporated into this subduction–accretion complex during the early Late Cretaceous.

3. The Late Cretaceous tholeiitic to calc–alkaline volcanic rocks are the products of an intra–oceanic island arc system. The tholeiitic and calc-alkaline arc rocks show enrichment in incompatible elements due to the influence of slab-derived fluids. The shoshonitic arc rocks representing the latest stage of island arc magmatism were produced by partial melting of a subduction–enriched mantle source.

Acknowledgements

This study was supported by a grant from the General Directorate of Mineral Research and Exploration of Turkey (MTA, Ankara; Project no: 2007–2008.30.1601.d–f). We thank Dr. Yakov Kapusta (ACTLabs, Canada) for the radiometric and isotopic analyses of our rock samples in a timely fashion, and for his help with the interpretation of the obtained data. We extend our appreciation to the refrees, Dr. Ibrahim Uysal (Blacksea Technical University, Turkey), Dr. Ryo Anma (University of Tsukuba) and Prof. Dr. Harald Furnes (Bergen University, Norway). Special thanks are due to Dr. Francesca Funiciello and Prof. Dr. Shuhai Xiao for editorial suggestions, which improved the manuscript. We would like to acknowledge the Head of the Geological Research Department, Dr. Erol Timur, in MTA-Ankara for his continued support of our *Ophiolite Inventory Project* in Turkey over the last two years.

572 **References**

573 Akyürek, B., Bilginer, E., Akbaş, B., Hepşen, N., Pehlivan, Ş., Sunu, O., Soysal, T., Dağer,
574 Z., Çatal, E., Sözeri, B., Yıldırım, H. and Hakyemez, Y.: Fundamental geological
575 characteristics of Ankara–Elmadağ–Kalecik area. Journal of Geological Engineering
576 (Jeoloji Mühendisligi Dergisi), Chamber of Geological Engineers of Turkey (TMMOB
577 Jeoloji Mühendisleri Odasi), 20, 31–46, 1984 (in Turkish with English abstract).

578 Alpaslan, M., Boztug, D., Frei, R., Temel, A. and Kurt, M.A.: Geochemical and Pb–Sr–Nd
579 isotopic composition of the ultrapotassic volcanic rocks from the extension–related
580 Çamardı–Ulukisla basin, Nigde Province, Central Anatolia, Turkey. Journal of Asian
581 Earth Sciences 27, 613–627, 2006.

582 Alpaslan, M., Frei, R., Boztug, D., Kurt, M.A. and Temel, A.: Geochemical and Pb–Sr–Nd
583 isotopic constraints indicating an enriched–mantle source for Late Cretaceous to Early
584 Tertiary volcanism, Central Anatolia, Turkey. International Geology Review 46, 1023–
585 1041, 2004.

586 Altunkaynak, S¸. and Dilek, Y.: Timing and nature of postcollisional volcanism in Western
587 Anatolia and geodynamic implications, in:Postcollisional Tectonics and Magmatism in
588 the MediterraneanRegion and Asia, edited by: Dilek, Y. and Pavlides, S., Geological
589 Society of America Special Paper 409, 321–351, 2006.

590 Altunkaynak, Ş. and Dilek, Y.: Eocene mafic volcanism in northern Anatolia: its causes and
591 mantle sources in the absence of active subduction. International Geology Review 55
592 (13), 1641-1659, 2013.

593 Bailey, E.B. and McCallien, W.S.: The Ankara Mélange in Central Anatolia. Bulletine of
594 Mineral Research and Exploration Institute, Maden Tetkik ve Arama Enstitüsü, Ankara,
595 Turkey, 40, 12-22, 1950.

596 Bailey, E.B. and McCallien, W.S.: The Ankara Mélange and Anatolia Thrust. Nature 166,
597 938–941, 1953.

598 Bingöl, E., Akyürek, B. and Korkmazer, B.: Geology of Biga Peninsula and characteristics of
599 Karakaya formation. Geoscience Congress of 50th Anniversary of the Turkish Republic,
600 Ankara, 1975, the Publications of MTA General Directorate, 70–77 (in Turkish with
601 English abstract), 1975.

602 Boztug, D.: S–I–A type intrusive associations: geodynamic significance of synchronism
603 between metamorphism and magmatism in Central Anatolia, Turkey, in: Tectonics and
604 Magmatism in Turkey and the Surrounding Area, edited by: Bozkurt, E., Winchester, J.
605 A., and 10 Piper, J. D. A., Geological Society of London Special Publication, 173, 441–
606 458, 2000.

607 Çelik, Ö.F., Marzoli, A., Marschik, R., Chiaradia, M., Neubauer, F. and Öz, İ.: Early–Middle
608 Jurassic intra-oceanic subduction in the İzmir-Ankara-Erzincan Ocean, Northern
609 Turkey. Tectonophysics, 509, 120–134, 2011.

610 Çoğulu, E., Delaloye, M. and Chessex, R.: Sur l'age de quelques roches plutoniques acides
611 dans region d'Eskisehir, Turquie, Archives des Sciences, Genève, 18, 692–699, 1965.

612 Cox, K.G., Bell, J.D. and Pankhurst, R.J.: The interpretation of ignous rocks. Allen and
613 Unwin, London, 450p, 1979.

614 Dangerfield, A., Harris, R. Sarifakioglu, E. and Dilek, Y.: Tectonic evolution of the Ankara
615 Mélange and associated Eldivan ophiolite near Hançili, Central Turkey. Geological
616 Society of America Special Paper 480, 143–169, 2011.

617 Delaloye, M. and Bingöl, E.: Granitoids from western and Northwestern Anatolia:
618 Geochemistry and modelling of geodynamic evolution. International Geology Review
619 42, p. 241–268, doi:10.1080/00206810009465081, 2000.

620 Dilek, Y. and Altunkaynak, Ş.: Cenozoic Crustal Evolution and Mantle Dynamics of Post–
621 Collisional Magmatism in Western Anatolia. International Geology Review 49, 431–
622 453, 2007.

623 Dilek, Y. and Thy, P.: Age and petrogenesis of plagiogranite intrusions in the Ankara
624 Mélange, central Turkey. Island Arc 15, 44–57, 2006.

625 Dilek, Y. and Furnes, H.: Ophiolite genesis and global tectonics: Geochemical and tectonic
626 fingerprinting of ancient oceanic lithosphere. Geological Society of America Bulletin
627 123, 387–411, doi: 10.1130/B30446.1, 2011.

628 Dilek, Y. and Furnes, H.: Structure and geochemistry of Tethyan ophiolites and their
629 petrogenesis in subduction rollback systems. Lithos 113, 1–20, 2009.

630 Dilek, Y. and Thy, P.: Island arc tholeiite to boninitic melt evolution of the Cretaceous Kizildag
631 (Turkey) ophiolite: Model for multi–stage early arc–forearc magmatism in Tethyan
632 subduction factories. Lithos 113, 68–87, 2009.

633 Dönmez, M., Akçay, A.E., Türkecan, A., Evcimen, Ö., Atakay, E. and Görmüş, T.: Tertiary
634 Volcanites in Ankara surrroundings. Mineral Research and Exploration Institute of
635 Turkey (MTA) Report, No. 11164, 116 pp., Ankara, Turkey, 2009 (in Turkish,
636 unpublished).

637 Eyüboğlu, Y.: Late cretaceous high–K volcanism in the eastern pontide orogenic belt:
638 implications for the geodynamic evolution of NE Turkey. International Geology Review
639 52(2-3), 142-186, 2010.

640 Festa, A., Pini, A., Dilek, Y. and Codegone, G.: Mélanges and mélanges-forming processes:
641 a historical overview and new concepts. International Geology Review, 52, 1040-1105,
642 2010.

643 Fitton, J.G., James, D., Kempton, P.D., Ormerod, D.S. and Leeman, W.P.: The role of
644 lithospheric mantle in the generation of Late Cenozoic basic magmas in the Western
645 United States. Journal of Petrology, Special Lithosphere Issue, 331–349, 1988.

646 Frey, F.A., Green, D.H. and Roy, S.D.: Integrated models of basalt petrogenesis: A study of
647 Quartz tholeiite to olivine melililites from southeastern Australia utilizing geochemical
648 and experimental data. Journal of Petrology 19, 463–513, 1978.

649 Göncüoğlu, M.C., Tekin, U.K. and Turhan, N.: Late Carnian radiolarite-bearing basalt blocks
650 within the Late Cretaceous Central Sakarya Ophiolitic Mélange, NW Anatolia:
651 Geological constrains. 54th Geological Congress of Turkey, Proceedings CD-format,
652 54-61, 2001.

653 Güleç, N.: Rb–Sr isotope data from the Agacoren granitoid (East of Tuz Gölü):
654 Geochronological and genetical implications. Turkish Journal of Earth Sciences 3, 39–
655 43, 1994.

656 Gündoğdu–Atakay, E.: Geological and petrological characteristics of volcanic rocks at
657 soutwest of Çorum and geoarc heological studies at Alaca höyük excavation site. PhD
658 Thesis, Ankara University, Ankara, Turkey, 194pp., 2009.

659 Hakyemez, Y., Barkurt, M.Y., Bilginer, E., Pehlivan, Ş., Can, B., Dağer, Z. and Sözeri, B.:
660 The geology of Yapraklı–Ilgaz–Çankırı–Çandır surroundings. Mineral Research and
661 Exploration Institute of Turkey (MTA) Report, No. 7966, Ankara, Turkey, 1986 (in
662 Turkish, unpublished).

663 Hastie, A.R., Kerr, A.C., Pearce, J.A. and Mitchell, S.F.: Classification of Altered Volcanic
664 Island Arc Rocks using Immobile Trace Elements: Development of the Th–Co
665 Discrimination Diagram. Journal of Petrology 48 (12), 2341–2357, 2007.

666 Hawkesworth, C.J., Gallagher, K., Hergt, J.M. and McDermott, F.: Mantle and slab
667 contributions in arc magmas. Annual Review of Earth and Planetary Sciences 21, 175–
668 204, 1993.

669 Hoffman, A.W., Jochum, K.P., Seufert, M. and White, W.M.: Nb and Pb in oceanic basalts:
670 New constraints on mantle evolution. Earth and Planetary Science Letters 90, 421–
671 436, 1986.

672 Ilbeyli, N., Pearce, J.A., Thirwall, M.F. and Mitchell, J.G.: Petrogenesis of collision–related
673 plutonics in Central Anatolia, Turkey. Lithos 72, 163–182, 2004.

674 Irvine, T.N. and Baragar, W.R.A.: A guide to the chemical classification of the common
675 volcanic rocks. Canadian Journal of Earth Sciences, 8, 523–548, doi:10.1139/e71-055,
676 1971.

677 Kadıoglu, Y.K., Dilek, Y. and Foland, K.A.: Slab breakoff and syncollisional origin of the Late
678 Cretaceous magmatism in the Central Anatolian Crystalline Complex, Turkey, in Dilek,
679 Y., and Pavlides, S., eds., Postcollisional tectonics and magmatism in the
680 Mediterranean Region and Asia. Geological Society of America, Special Paper 409,
681 381–415, doi:10.1130/2006/2409(19), 2006.

682 Kadıoglu, Y.K., Dilek, Y., Güleç, N. and Foland, K.A.: Tectonomagmatic evolution of bimodal
683 plutons in the Central Anatolian Crystalline Complex, Turkey. Journal of Geology 111,
684 671–690, 2003.

685 Kelemen, P.B., Shimizu, N. and Dunn, T.: Relative depletion of niobium in some arc magmas
686 and the continental crust: partitioning of K, Nb, La and Ce during melt/rock reaction in
687 the upper mantle. Earth and Plenetary Science Letters 120, 111–134, 1993.

688 Kempton, P.D., Fitton, J.G., Hawkesworth, C.J. and Ormerod, D.S.: Isotopic and trace
689 element contraints on the composition and evolution of the lithosphere beneath the
690 southern United State. Journal of Geophysics Reseach 96, 13713–13735, 1991.

691 Keskin, M., Genç, C.Ş. and Tüysüz, O.: Petrology and geochemistry of post–collisional
692 Middle Eocene volcanic units in North–Central Turkey: Evidence for magma generation
693 by slab breakoff following the closure of the Northern Noetethys Ocean. Lithos 104,
694 267–305, 2008.

695 Koçyiğit, A.: An example of an accretionary forearc basin from northern Central Anatolia and
696 its implications for the history of the Neo–Tethys in Turkey. Geological Society of
697 America, Special Paper 103, 22–36, 1991.

698 Le Bas, M.J., Le Maitre, R.W., Streckeisen, A. and Zanettin, B.: Achemical classification of
699 volcanic rocks based on total Alcali–Silica content. Journal of Petrology 27, 745–750,
700 1986.

701 Maury, R.C., Defant, M.J. and Joron, J.L.: Metasomatism of arc mantle inferred from trace
702 elements in Philippine xenoliths. Nature 360, 661–663, doi: 10.1038/360661a0, 1992.

703 Moghadam, H. S., Stern R.J., Chiaradia, M. and Rahgoshay, M.: Geochemistry and tectonic
704 evolution of the Late Cretaceous Gogher-Baft ophiolite, Central Iran. Lithos, 168, 33–
705 47, doi:10.1016/j.lithos.2013.01.013, 2013.

706 MTA: The geological map of Turkey, 1/500 000 scaled, Geological Survey of Turkey, The
707 General Directorate of Mineral Research and Exploration, Ankara, Turkey, 2001.

708 Muller, D., Rock, N.M.S. and Groves, D.I.: Geochemical discrimination between shoshonitic
709 and potassic volcanic rocks in different tectonic settings: a pilot study. Mineralogy and
710 Petrology 46, 259–289, 1992.

711 Norman, T.N.: The role of the Ankara Melange in the development of Anatolia (Turkey), in:
712 The Geological Evolution of the Eastern Mediterranean, edited by: Dixon, J. E., and
713 Robertson, A. H. F., Geological Society of London Special Publication, 17, 441–447,
714 1984.

715 Nzegge, O. M., Satır, M., Siebel, W. and Taubald, H.: Geochemical and isotopic constraints
716 on the genesis of the Late Palaeozoic Deliktaş, and Sivrikaya granites from the

717 Kastamonu granitoid belt (Central Pontides, Turkey). Neues Jahrbuch Mineralogische
718 Abhandlungen 183, p. 27–40, 2006.

719 Okay, A.I. and Göncüoğlu, M.C.: Karakaya Complex: A review of data and concepts. Turkish
720 Journal of Earth Sciences 13, p. 77–95, 2004.

721 Okay, A.I., Monod, O. and Monié, P.: Triassic blueschists and eclogites from northwest
722 Turkey: vestiges of the Paleo–Tethyan subduction. Lithos 64, 155–178, 2002.

723 Okay, A.I., Tüysüz, O., Satır, M., Özkan–Altıner, S., Altıner, D., Sherlock, S. and Eren, R.H.:
724 Cretaceous and Triassic subduction–accretion HP–LT metamorphism and continental
725 growth in the Central Pontides, Turkey. Geological Society of America Bulletin 118, p.
726 1247–1269, doi:10.1130/B25938.1, 2006.

727 Pearce, J.A.: Trace element characteristics of lavas from destructive plate boundaries. In:
728 Thorpe, R.S. (ed), Andesites: orogenic andesites and related rocks. John Wiley &
729 Sons, Chichester, 525–548, 1982.

730 Pearce, J.A.: Geochemical fingerprinting of oceanic basalts with applications to ophiolite
731 classification and the search for Archean oceanic crust. Lithos 100, 14–48, 2008.

732 Pearce, J.A. and Cann, J.R.: Tectonic setting of basic volcanic rocks determined using trace
733 element analyses. Earth and Planetary Scientific Letters 19, 290–300, 1973.

734 Pearce, J.A. and Peate, D.W.: Tectonic implications of the composition of volcanic arc
735 magmas. Annual Review of Earth and Planetary Sciences 23, 251–285, doi:
736 10.1146/annurev.ea.23.050195.001343, 1995.

737 Pearce, J. A. and Robinson, P.T.: The Troodos ophiolitic complex probably formed in a
738 subduction initiation, slab edge setting. Gondwana Research 18 60–81.
739 10.1016/j.gr.2009.12.003, 2010.

740 Pearce, J.A., Harris, B.W., and Tindle, A.G.: Trace element discrimination diagrams for the
741 tectonic interpretation of granitic rocks. Journal of Petrology 25, 956-983, 1984.

742 Peccerillo, A. and Taylor, S.R.: Geochemistry of Eocene calc–alkaline volcanic rocks from
743 the Kastamonu area, northern Turkey. Contributions to Mineralogy and Petrology 58,
744 63–81, 1976.

745 Plechov, P.Y., Tsai, A.E., Shcherbakov, V.D. and Dirksen, O.V.: Opacitization conditions of
746 hornblende in Bezymyannyi volcano andesites (March 30, 1956 eruption). Petrology 1,
747 19–35, 2008.

748 Rock, N.M.S.: The nature and origin of lamprophyres: some definitions, distinctions, and
749 derivations. Earth-Science Reviews 13, 123-169, 1977.

750 Rock, N.M.S.: The nature and origin of calc-alkaline lamprophyres: minettes, vogesites,
751 kersantites and spessartites. Transactions of the Royal Society of Edinburgh: Earth
752 Sciences 74 (04), 193-227, 1984.

753 Rojay, B. and Süzen, L.: Tectonostratigraphic evolution of the Cretaceous dynamic basins on
754 accretionary ophiolitic melange prism, SW of Ankara Region. Turkish Association of
755 Petroleum Geologists Bulletin 9, 1–12, 1997.

756 Rojay, B., Altıner, D., Altıner Özkan, S., Önen, A.P., James, S. and Thirlwall, M.F.:
757 Geodynamic significance of the Cretaceous pillow basalts from North Anatolian
758 Ophiolitic Mélange (Central Anatolia, Turkey): geochemical and paleontological
759 constraints. Geodinamica Acta 17/5, 349–361, 2004.

760 Saccani, E., Beccaluva, L., Photiades, A. and Zeda, O.: Petrogenesis and tectono–magmatic
761 significance of basalts and mantle peridotites from the Albanian–Greek ophiolites and
762 sub–ophiolitic mélanges. New constraints for the Triassic–Jurassic evolution of the
763 Neo–tethys in the Dinaride sector. Lithos 124, 227–242, 2011.

764 Sarıfakıoğlu, E., Dilek, Y. and Winchester, J.A.: Late Cretaceous Subduction Initiation and
765 Paleocene–Eocene Slab Breakoff Magmatism in South–Central Anatolia, Turkey,
766 International Geology Review 55 (1), 66–87, 2013.

767 Sarifakioglu, E., Sevin, M., Esirtgen, E., Bilgiç, T., Duran, S., Parlak, O., Karabalık, N.,
768 Alemdar, S., Dilek, Y. and Uysal, I.: The geology of ophiolitic rocks around Çankırı–
769 Çorum Basen: petrogenesis, tectonics and ore deposits, Mineral Research and
770 Exploration Institute of Turkey (MTA) Report, No. 11449, 196 pp., 2011 (in Turkish,
771 unpublished).

772 Schiano, P., Clocchiatti, R., Shimizu, N., Mury, R.C., Johum, K.P. and Hofmann, A.W.:
773 Hydrous, silica rich melts in the subarc mantle and their relationship with erupted arc
774 lavas. Nature 377, 595–600, doi:10.1038/377595a0, 1995.

775 Shand, S.J.: Eruptive Rocks: London: Thomas Murby & Co, p. 1–360, 1927.

776 Shervais, J.W.: Ti–V plots and the petrogenesis of modern and ophiolitic lavas. Earth and
777 Planetary Scientific Letters 59, 101–118, 1982.

778 Sun, S.S. and McDonough, W.F.: Chemical and isotopic systematics of oceanic basalts:
779 Implications for mantle composition and processes. In: Saunders, A.D. and Norry, M.J.
780 (eds.), Magmatism in the ocean basins. Geological Society of London Special
781 Publication 42, 313–345, 1989.

782 Tankut, A., Dilek, Y. and Önen, P.: Petrology and geochemistry of the Neo–Tethyan
783 volcanism as revealed in the Ankara melange, Turkey. Journal of Volcanology and
784 Geothermal Research 85, 265–284, 1998.

785 Tatsumi, Y., Hamilton, D. and Nesbitt, R.W.: Chemical characteristics of fluid phase released
786 from a subducted lithosphere and origin of arc magmas. Evidence from high pressure
787 experiments and natural rocks. Journal of Volcanology and Geothermal Research 29,
788 293–309, 1986.

789 Tekeli, O.: Subduction complex of pre–Jurassic age, northern Anatolia, Turkey. Geology 9,
790 68–72, 1981.

791 Tekin, U.K. and Göncüoğlu, M.C.: Discovery of the oldest (Upper Ladinian to Middle Carnian)
792 radiolarian assemblages from the Bornova Flysch Zone in western Turkey: implications
793 fort he evolution of the Neotethyan Izmir-Ankara Ocean. Ofioliti 32 (2), 131-150, 2007.

794 Topuz, G., Altherr, R., Satır, M. and Schwarz, M.: Low grade metamorphic rocks from the
795 Pulur complex, NE Turkey: Implications for pre–Liassic evolution of the Eastern
796 Pontides. International Journal of Earth Sciences 93, p. 72–91, doi:10.1007/s00531–
797 003–0372–5, 2004.

798 Topuz, G., Okay, A.I., Altherr, R., Meyer, H.P. and Nasdala, L.: Partial high–pressure
799 aragonitization of micritic limestones in an accretionary complex, Tavşanlı Zone, NW
800 Turkey. Journal of Metamorphic Geology 24, p. 603–613, 2006.

801 Tüysüz, O., Dellaloğlu, A.A. and Terzioğlu, N.: A magmatic belt within the Neo–tethyan
802 suture zone and its role in the tectonic evolution of northern Turkey. Tectonophysics
803 243, 173–191, 1995.

804 Uğuz, M. F., Sevin, M. and Duru, M.: 1/500 000 scale geological maps of Turkey, Sinop
805 Quadrangle (MTA General Directorate, Ankara), 2002.

806 White, W.M.: Sources of oceanic basalts: radiogenic isotopic evidence. Geology 13, 115–
807 118, 1985.

808 Whitney, D.L. and Dilek, Y.: Metamorphism during crustal thickening and extension in central
809 Anatolia: The Nigde metamorphic core complex. Journal of Petrology 39, 1385–1403,
810 1998.

811 Wood, D.A.: The application of a Th–Hf–Ta diagram to problems of tectonomagmatic
812 classification and to establishing the nature of crustal contamination of basaltic lavas of
813 the British Tertiary Volcanic Province. Earth and Planet Scientific Letters 56, 11–30,
814 1980.

815 Zindler, A. and Hart, S.R.: Chemical geodynamics. Annual Review of Earth and Planet
816 Science Letters 14, 493–571, 1986.

FIGURE CAPTIONS

Figure 1. Simplified ophiolite map of Turkey showing the distribution of the suture zones and some of the major tectonic entities in Turkey (from MTA, 2001). Pontide tectonic belt including the Sakarya Continent. The inset box refers to the map area in Fig. 2.

Figure 2. Geological map of the Çankırı–Çorum area along the IAESZ in north-central Turkey (modified after Uğuz et al., 2002). NAF: North Anatolian Fault.

Figure 3a. Geological map of the Kalecik area, east of Ankara, showing the distribution of the ophiolitic, turbiditic and island-arc rock units in the Ankara Mélange in north-central Turkey.

Figure 3b. The generalized tectonostratigraphic columnar section showing the igneous pseudostratigraphy and internal structure of the Eldivan ophiolite, the Ankara Mélange and the island-arc magmatic rocks, their tectonic basement, and sedimentary cover.

Figure 4. Geological map of the northern part of the Kalecik area (modified after Hakyemez et al., 1986).

Figure 5. View of the Ankara Mélange and the Karakaya Complex (Sakarya Continent). Key to lettering: AOM = Ankara Mélange, β = basalt, KC = Karakaya Complex, ms = mudstone, pg = plagiogranite, sp = serpentinized peridotites.

Figure 6. Simplified geological map of the Yapraklı–Çankırı area, showing the distribution of the ~180 Ma Neotethyan ophiolitic units, ophiolitic mélange and island-arc rocks.

Figure 7. Geological map of the Laloglu (Çorum) area, showing the Neotethyan Eldivan ophiolite and the island-arc rock units.

Figure 8. (a) Neritic limestone covering the seamount volcanic-volcaniclastic rocks in the Ankara Mélange. (b) Seamount pillow lavas in the Ankara Mélange. NL= neritic limestone.

Figure 9. (a) Limestone-volcanic sandstone intercalation in the island-arc sequence. (b) A mafic dike (island-arc origin) crosscutting the pelagic limestone rocks. (c) Alkaline basaltic rocks with columnar joint structures. (d) Arc volcaniclastic rocks intruded by basaltic to andesitic dikes.

Figure 10. (a) Upper Cretaceous reefal limestone with rudist fossils unconformably overlying the arc volcanic rocks. (b) Reefal limestone underlain by volcanic sandstone. (c) Alkaline

pillow lavas overlain by volcanic sandstone-pebblestone. (d) Alkaline pillow lavas with radial joint structures. All rocks in *a* through *d* represent the island-arc units.

Figure 11. Lamprophyric dikes crosscutting various lithological units in the Ankara Mélange.

Figure 12. Photomicrographs of (a) A seamount alkaline basalt sample. (b) Doleritic dike rock of the 180 Ma Neotethyan oceanic crust. (c) Island-arc alkaline basalt sample in cross-polarized light. (d) Island-arc alkaline basalt sample in plane-polarized light. (e) Island-arc basaltic andesite dike, showing a glomeroporphyritic texture. (f) Lamprophyric dike rock with small prismatic cpx (diopside) in a feldspar + phlogopite groundmass (plane-polarized light). (g). Lamprophyric dike rock with small prismatic cpx (diopside and phlogopite). (h) Syeno-dioritic pluton rock with plagioclase (altered to clay minerals) and biotite + hornblende and minor cpx (cross-polarized light).

Figure 13. Geochemical classification of ophiolitic and seamount volcanic rocks. (a) Total alkali vs. SiO_2 diagram (Le Bas et al., 1986). (b) AFM diagram (Irvine and Baragar, 1971). (c) Ti–Zr–Y discrimination diagram (Pearce and Cann, 1973). (d) Ti–V diagram (Shervais, 1982). (e) N-MORB-normalized multi-element diagrams of the most representative samples (normalization values from Sun and McDonough, 1989). Key to lettering: A = andesite, B = basalt, BA = basaltic andesite, BS = basanite, BTA = basaltic trachyandesite, D = dacite, F = foidite, PC = picrobasalt, PH = phonolite, PHTP = phonotephrite, TPPH = Tephriphonolite, R = rhyolite, T = trachyte, TA = trachyandesite, TB = trachybasalt, TD = trachydacite, TP = tephrite. lB = alkali–subalkali subdivision from Irvine and Baragar (1971).

Figure 14. Geochemical classification of island-arc rocks. (a) Total alkali vs. SiO_2 diagram (Le Bas et al., 1986). (b) TAS diagram (Cox et al., 1979) for syeno-dioritic pluton rocks. (c) Alk–MgO–FeO_t diagram (Irvine and Baragar, 1971) of the subalkaline arc volcanic units (Dönmez et al., 2009, and this study). (d) K_2O vs. SiO_2 diagram (Peccerillo and Taylor, 1976). (e) Th vs. Co diagram (Hastie et al., 2007). Ce/Yb vs. Ta/Yb diagram (Pearce, 1982).

Figure 15. Major oxides and trace elements vs. MgO variation diagrams for various alkaline island-arc units.

Figure 16. (a) A/CNK, molar $Al_2O3/(CaO+Na_2O+K_2O)$ vs. A/NK, molar $Al_2O_3/(Na_2O+K_2O)$ diagram (Shand, 1927). (b, c) trace element discrimination diagrams (Nb–Y and Rb vs. Y+Nb) for syenodioritic pluton rocks (fields from Pearce et al., 1984; VAG = volcanic arc granites, WPG = within-plate granites, ORG = ocean ridge granites. SYN-COLG = syn-collisional granites. (d) Ti–Zr–Y diagram. (e) Ti–V diagram. (f) TiO_2 vs. Al_2O_3 diagram. (g) Y

vs. Zr diagram. (h) Th/Yb vs. Nb/Yb diagram (fields after Pearce and Cann, 1973; Shervais, 1982; Muller et al., 1992; Pearce, 2008).

Figure 17. (a) Primitive mantle-normalized multi-element diagrams for the high-K shoshonitic arc rocks (normalization values from Sun & McDonough, 1989). (b) Chondrite-normalized REE patterns of the same rocks (normalization values from Sun & McDonough, 1989).

Figure 18. (a) Ba/Nb vs. La/Nb diagram for the high-K island arc rocks. The data for N-MORB, OIB and PM are from Sun & McDonough (1989). (b) La/Yb vs. La diagram for the island-arc rock units, illustrating the effects of partial melting and fractionation in their melt evolution.

Figure 19. Isotope variation diagrams for the Upper Cretaceous–Lower Paleocene high-K island-arc rocks. (a) $^{143}Nd/^{144}Nd$ vs. $^{87}Sr/^{86}Sr$ diagram. (b) $^{206}Pb/^{204}Pb$ vs. $^{208}Pb/^{204}Pb$ diagram. (c) $^{206}Pb/^{204}Pb$ vs. $^{207}Pb/^{204}Pb$ diagram. (d) $^{87}Sr/^{86}Sr$ vs. $^{206}Pb/^{204}Pb$ diagram. (e) $^{143}Nd/^{144}Nd$ vs. $^{206}Pb/^{204}Pb$ diagram. Compositional fields for the upper and lower crust, MORB (mid-ocean ridge basalt), HIMU (enriched mantle in U and Th relative to Pb), OIB (ocean island basalt), EMI (enriched mantle I) and EMII (enriched mantle II) are from Zindler and Hart (1986). The field for *Oceanic Islands* is from White (1985). NHRL = Northern Hemisphere Reference Line.

Figure 20. Sequential tectonic diagrams depicting the intra-oceanic magmatic evolution of the Ankara Mélange in the Northern Neotethys during the Jurassic – Paleocene. A. Suprasubduction zone generation of the oldest Neotethyan oceanic crust (~180 Ma) in the upper plate of a North-dipping intra-oceanic subduction zone, and seamount construction (SM1 and SM2) in the downgoing oceanic plate. High-grade metamorphic rock blocks and turbiditic sandstone-mudstone sequences in the Ankara Mélange formed in the subduction channel (blue in color) and the accretionary prism, respectively. B. Accretion of Seamount-1 into the accretionary complex and related deformation in the subduction-accretion system. C. Slab rollback and associated extension and SSZ oceanic crust formation (~85-80 Ma) in the upper plate. Accretion of Seamount-2 into the accretionary complex, and the lateral growth and deformation in the subduction-accretion system. D. Island arc construction and magmatism on and across the pre-existing SSZ oceanic lithosphere and the subduction-accretion complex (i.e. Ankara Mélange units). With continued slab retreat, arc magmatism shifts southward following the migrating trench, and becomes more alkaline in time, producing lamprophyric and syeno-dioritic intrusions. See text for further explanation.

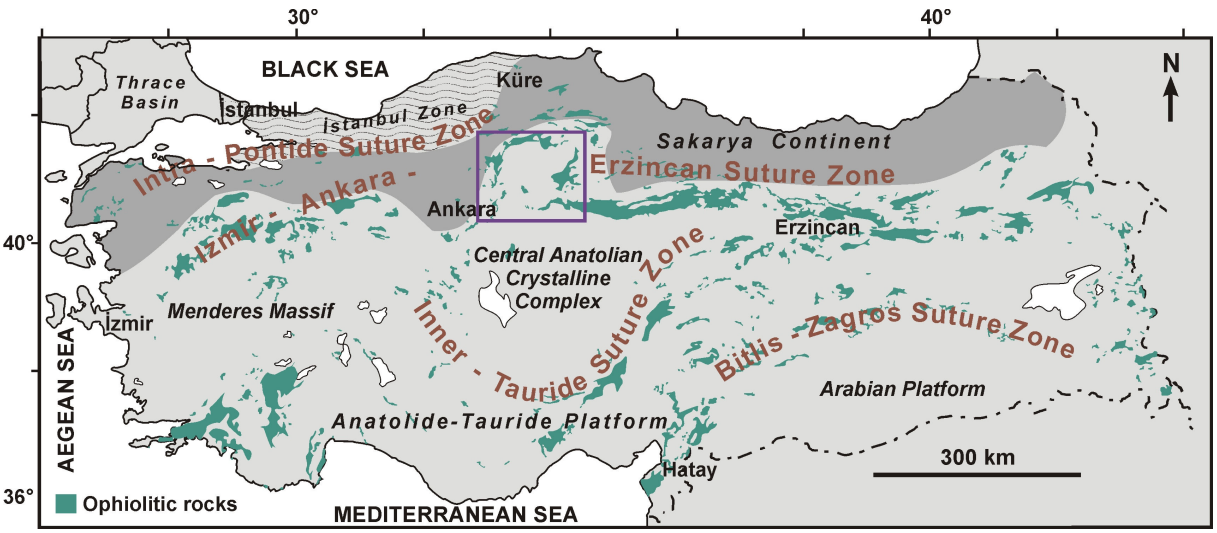

910

911 **Figure 1.**

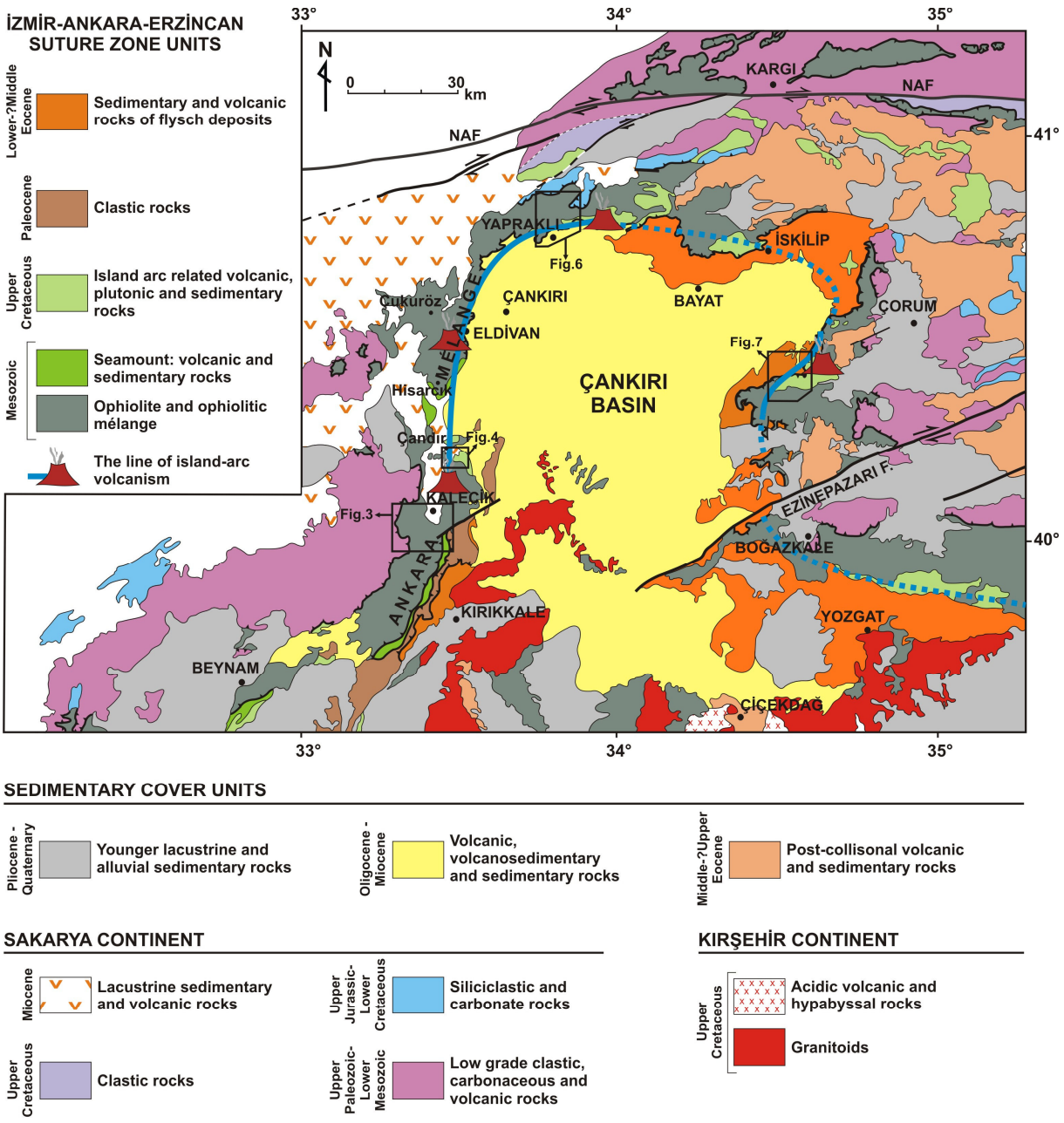
İZMİR-ANKARA-ERZİNCAN SUTURE ZONE UNITS
Lower-?Middle Eocene
Sedimentary and volcanic rocks of flysch deposits
Paleocene
Clastic rocks
Upper Cretaceous
Island arc related volcanic, plutonic and sedimentary rocks
Mesozoic
Seamount: volcanic and sedimentary rocks
Ophiolite and ophiolitic mélange
The line of island-arc volcanism
33°
34°
35°
41°
40°
N
0
30
km
KARGI
NAF
YAPRAKLI
Fig.6
İSKİLİP
ÇANKIRI
BAYAT
ÇORUM
Çukuröz
ELDİVAN
Fig.7
ÇANKIRI BASIN
Hisarcık
Çandır
Fig.4
KALECİK
Fig.3
EZİNEPAZARI F.
BOĞAZKALE
ANKARA MÉLANGE
KIRIKKALE
YOZGAT
BEYNAM
ÇİÇEKDAĞ
SEDIMENTARY COVER UNITS
Pliocene - Quaternary
Younger lacustrine and alluvial sedimentary rocks
Oligocene - Miocene
Volcanic, volcanosedimentary and sedimentary rocks
Middle-?Upper Eocene
Post-collisonal volcanic and sedimentary rocks
SAKARYA CONTINENT
Miocene
Lacustrine sedimentary and volcanic rocks
Upper Cretaceous
Clastic rocks
Upper Jurassic-Lower Cretaceous
Siliciclastic and carbonate rocks
Upper Paleozoic-Lower Mesozoic
Low grade clastic, carbonaceous and volcanic rocks
KIRŞEHİR CONTINENT
Upper Cretaceous
Acidic volcanic and hypabyssal rocks
Granitoids

Figure 2.

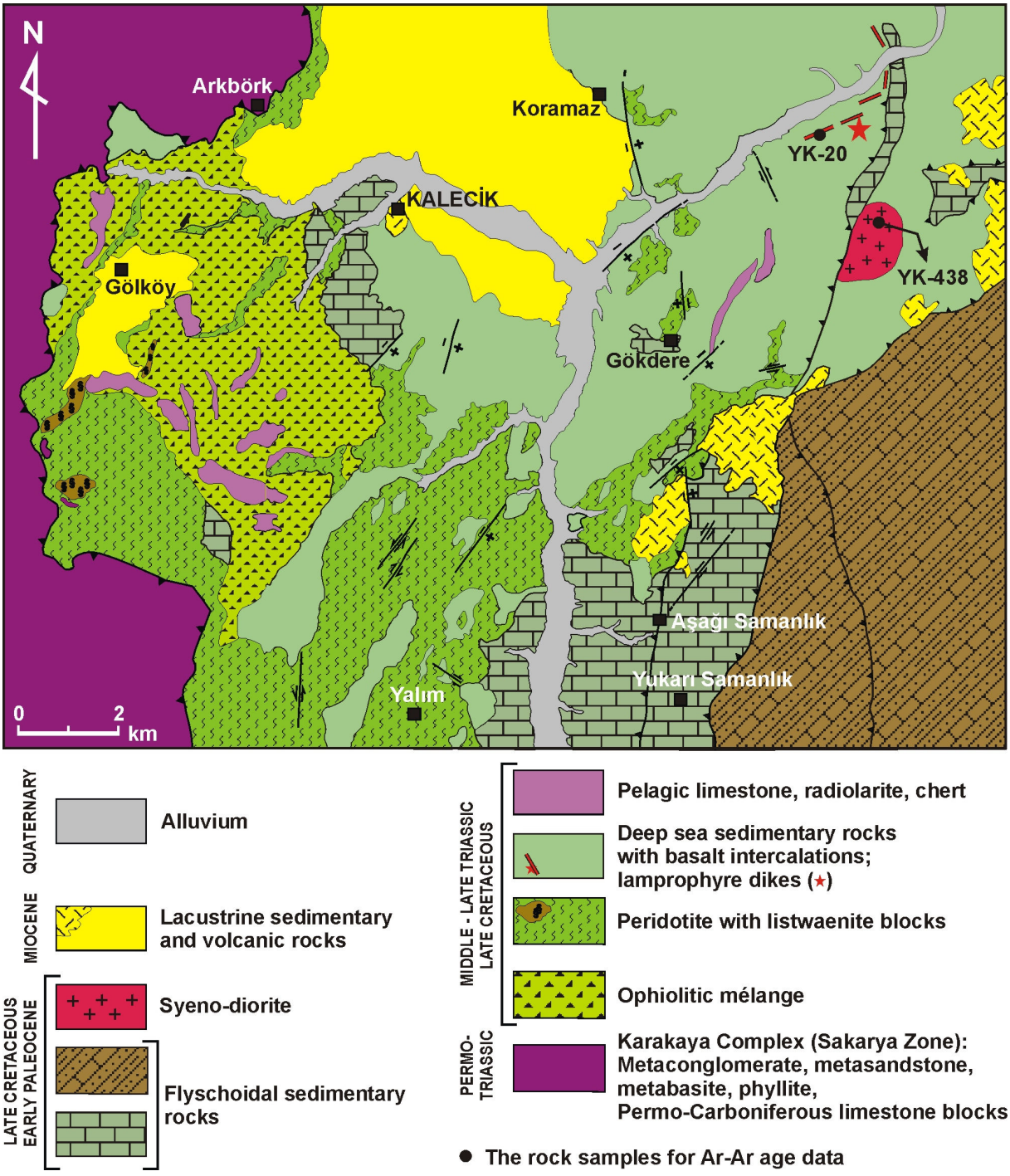

914

915 **Figure 3a.**

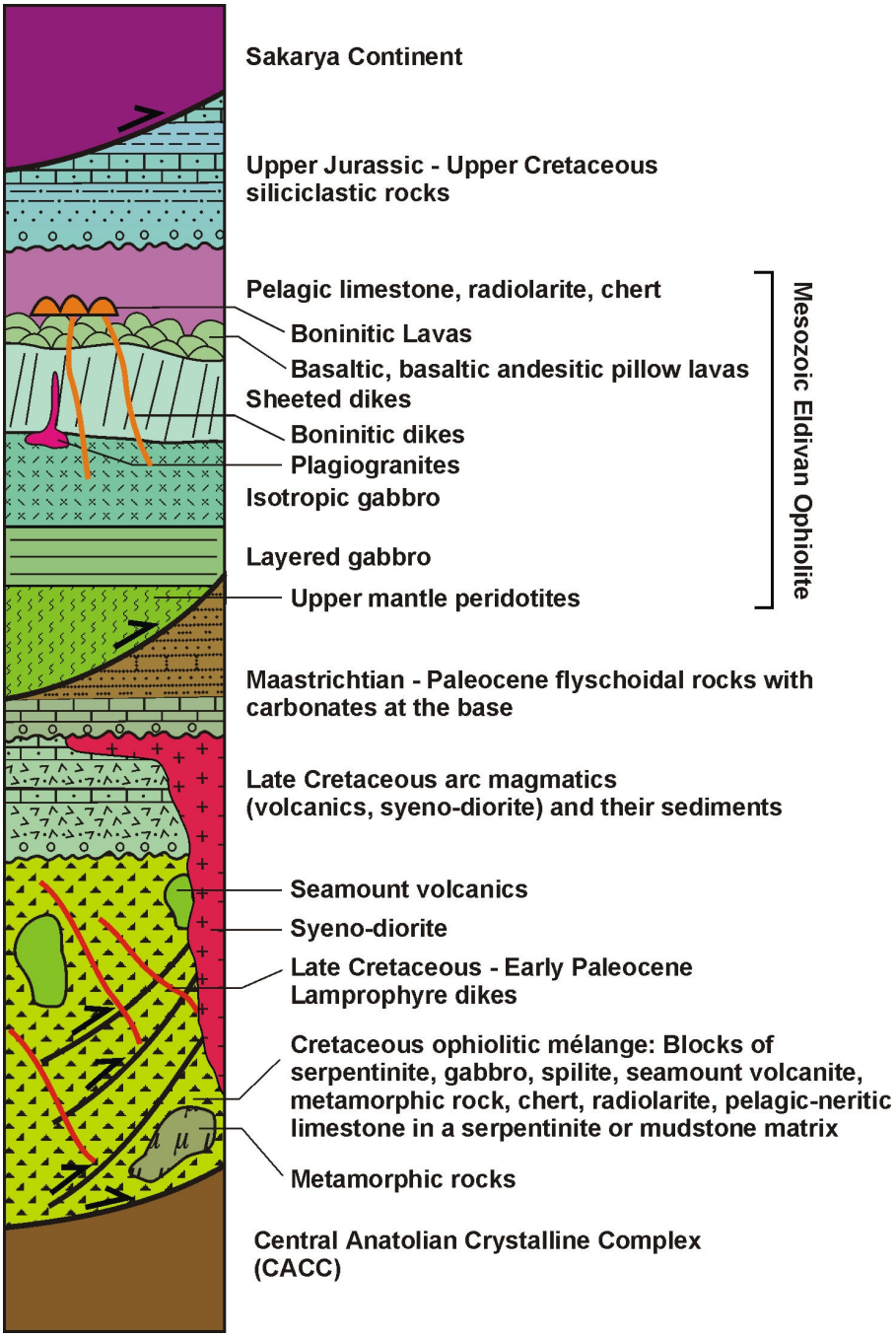

916

917 **Figure 3b.**

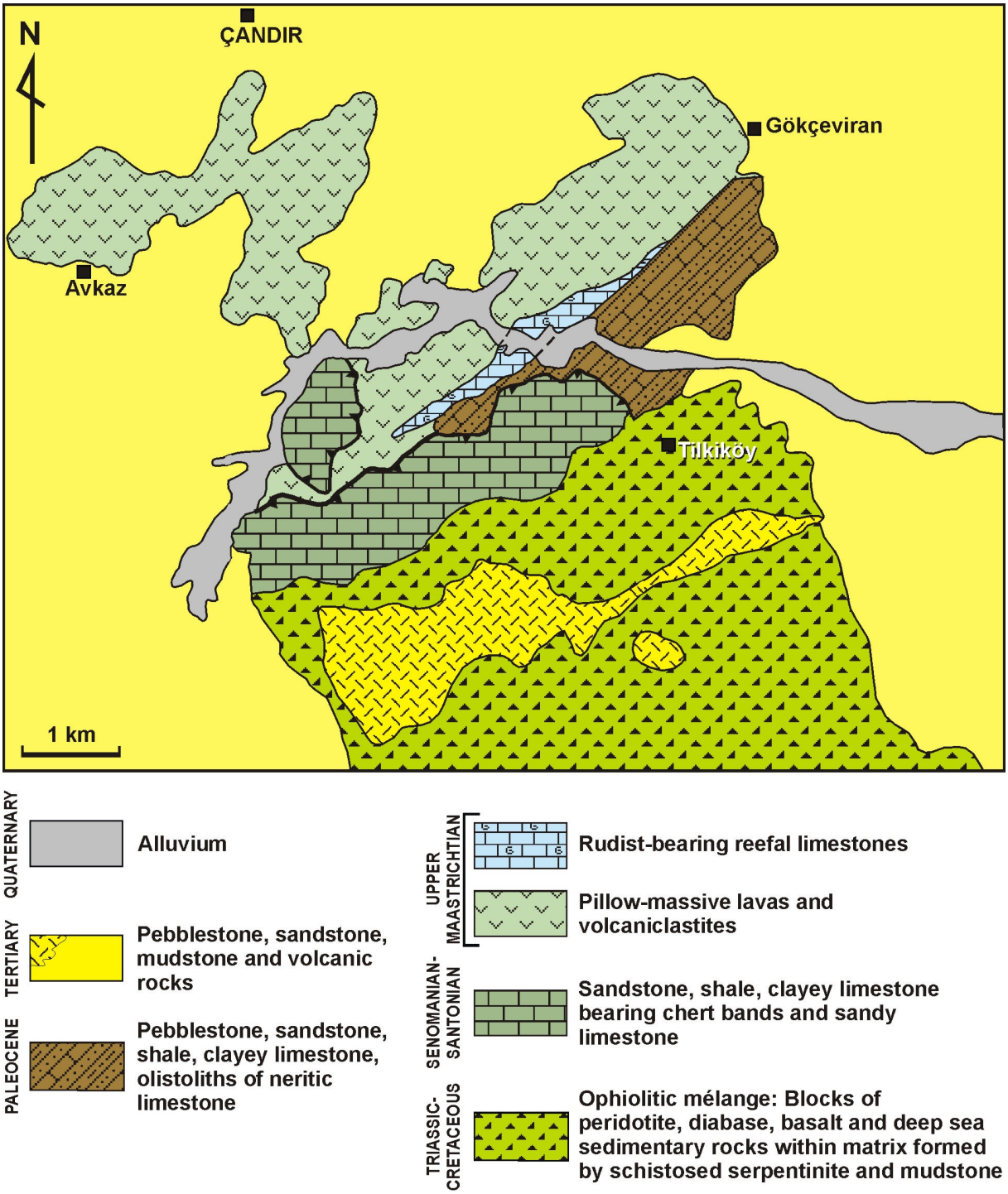
N
ÇANDIR
Gökçeviran
Avkaz
Tilkiköy
1 km
QUATERNARY
Alluvium
TERTIARY
Pebblestone, sandstone, mudstone and volcanic rocks
PALEOCENE
Pebblestone, sandstone, shale, clayey limestone, olistoliths of neritic limestone
UPPER MAASTRICHTIAN
Rudist-bearing reefal limestones
Pillow-massive lavas and volcaniclastites
SENOMANIAN-SANTONIAN
Sandstone, shale, clayey limestone bearing chert bands and sandy limestone
TRIASSIC-CRETACEOUS
Ophiolitic mélange: Blocks of peridotite, diabase, basalt and deep sea sedimentary rocks within matrix formed by schistosed serpentinite and mudstone

Figure 4.

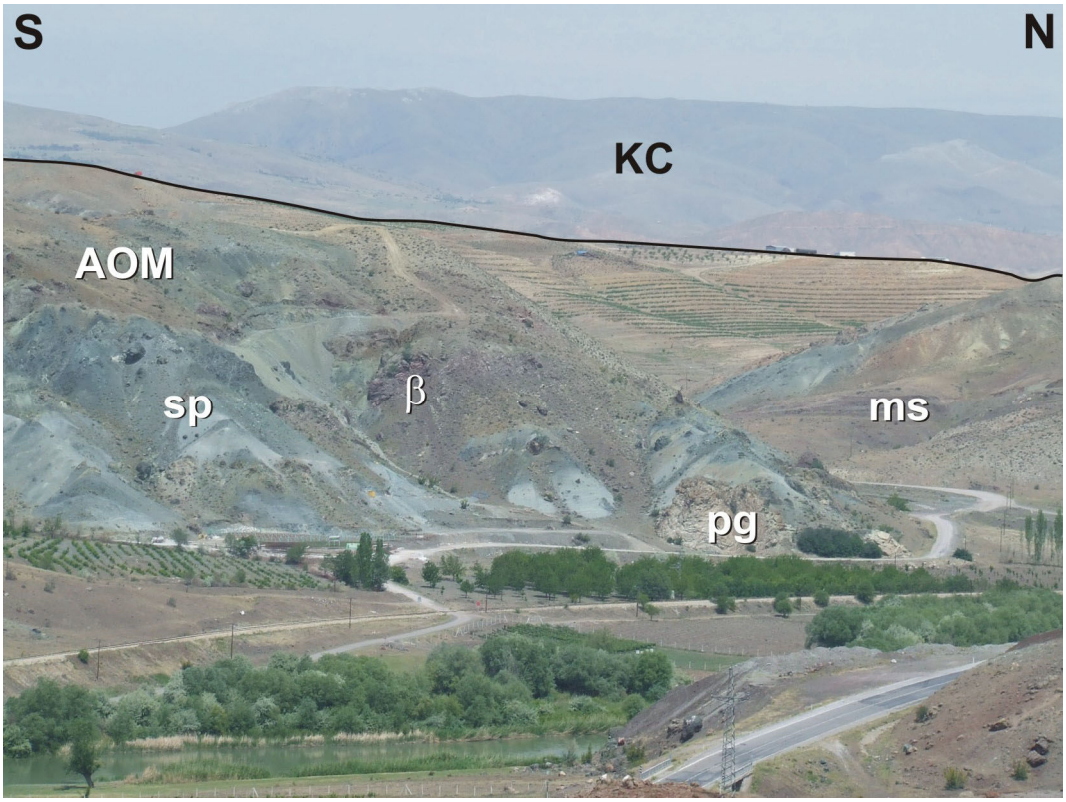

Figure 5.

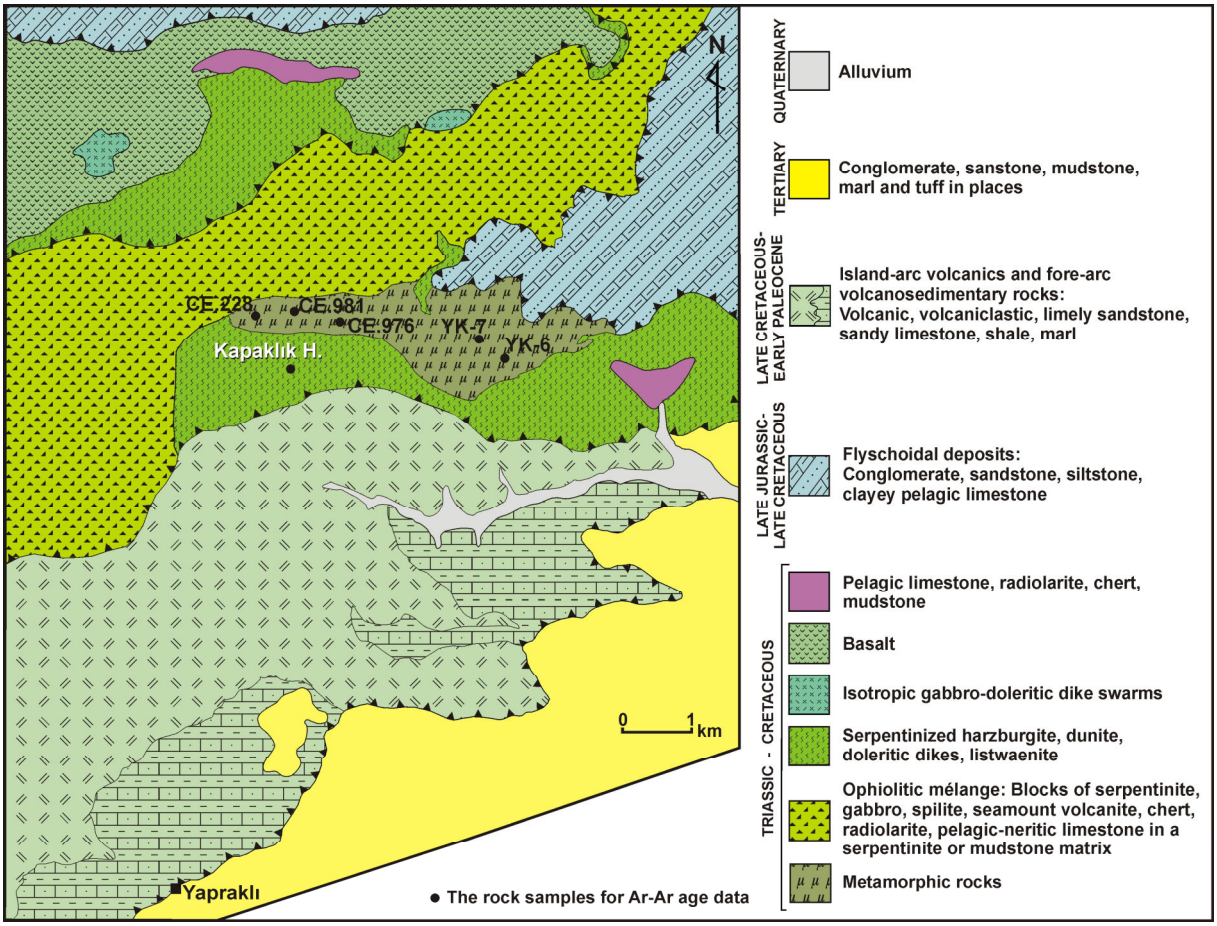
N
CE.228
CE.981
CE.976
YK-7
YK-6
Kapaklık H.
0
1
km
Yapraklı
● The rock samples for Ar-Ar age data
QUATERNARY
Alluvium
TERTIARY
Conglomerate, sanstone, mudstone, marl and tuff in places
LATE CRETACEOUS-EARLY PALEOCENE
Island-arc volcanics and fore-arc volcanosedimentary rocks: Volcanic, volcaniclastic, limely sandstone, sandy limestone, shale, marl
LATE JURASSIC-LATE CRETACEOUS
Flyschoidal deposits: Conglomerate, sandstone, siltstone, clayey pelagic limestone
TRIASSIC - CRETACEOUS
Pelagic limestone, radiolarite, chert, mudstone
Basalt
Isotropic gabbro-doleritic dike swarms
Serpentinized harzburgite, dunite, doleritic dikes, listwaenite
Ophiolitic mélange: Blocks of serpentinite, gabbro, spilite, seamount volcanite, chert, radiolarite, pelagic-neritic limestone in a serpentinite or mudstone matrix
Metamorphic rocks

Figure 6.

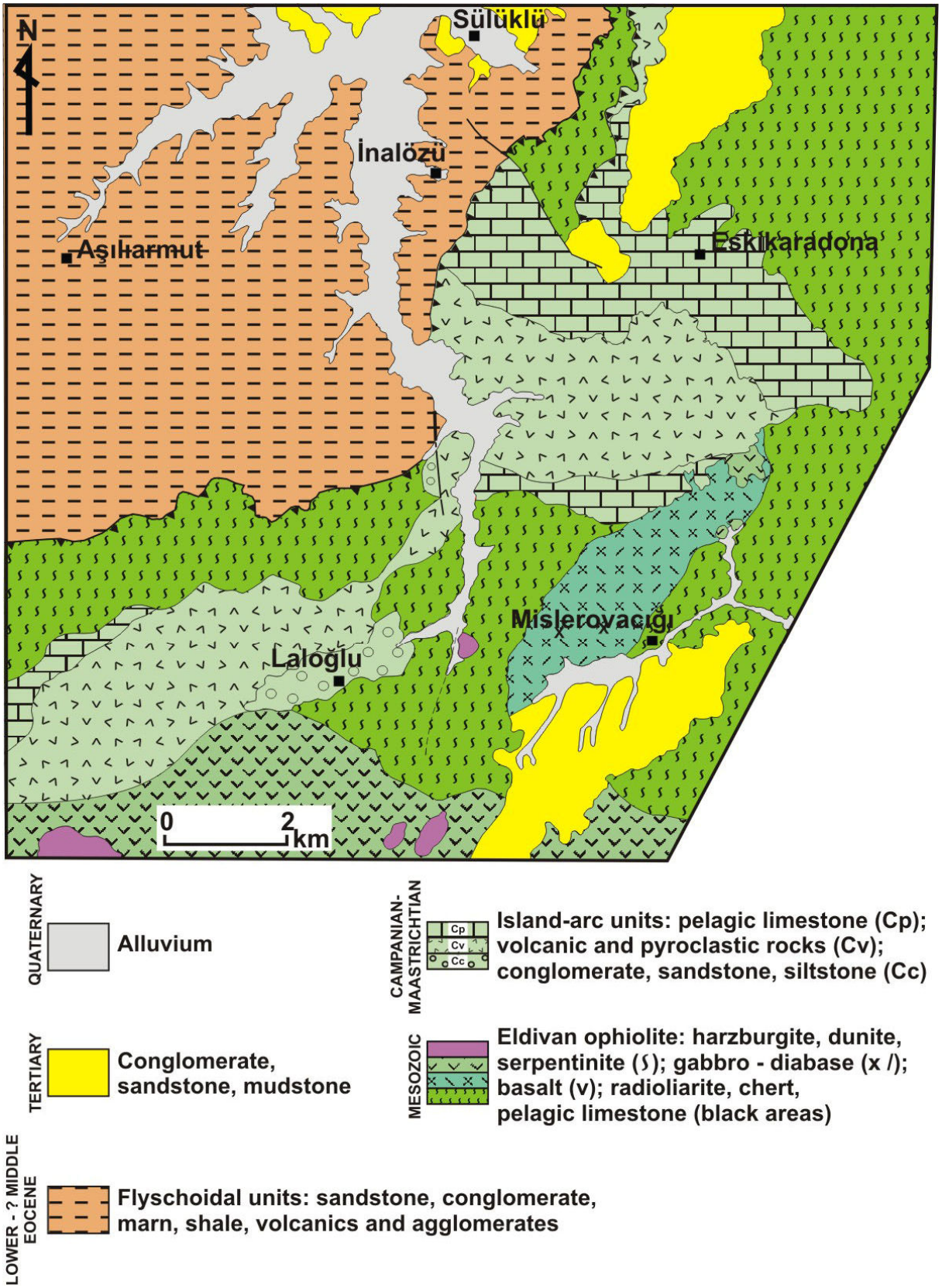
N
Sülüklü
İnalözü
Aşılıarmut
Eskikaradona
Mislerovacığı
Laloğlu
0
2
km
QUATERNARY
Alluvium
TERTIARY
Conglomerate, sandstone, mudstone
LOWER - ? MIDDLE EOCENE
Flyschoidal units: sandstone, conglomerate, marn, shale, volcanics and agglomerates
CAMPANIAN-MAASTRICHTIAN
Cp
Cv
Cc
Island-arc units: pelagic limestone (Cp); volcanic and pyroclastic rocks (Cv); conglomerate, sandstone, siltstone (Cc)
MESOZOIC
Eldivan ophiolite: harzburgite, dunite, serpentinite (ʃ); gabbro - diabase (x /); basalt (v); radioliarite, chert, pelagic limestone (black areas)

Figure 7.

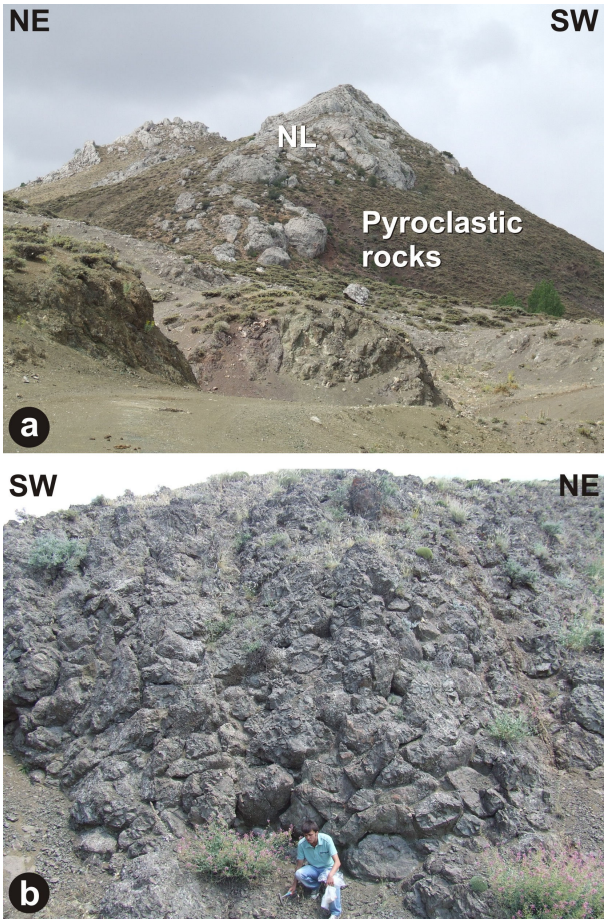

Figure 8.

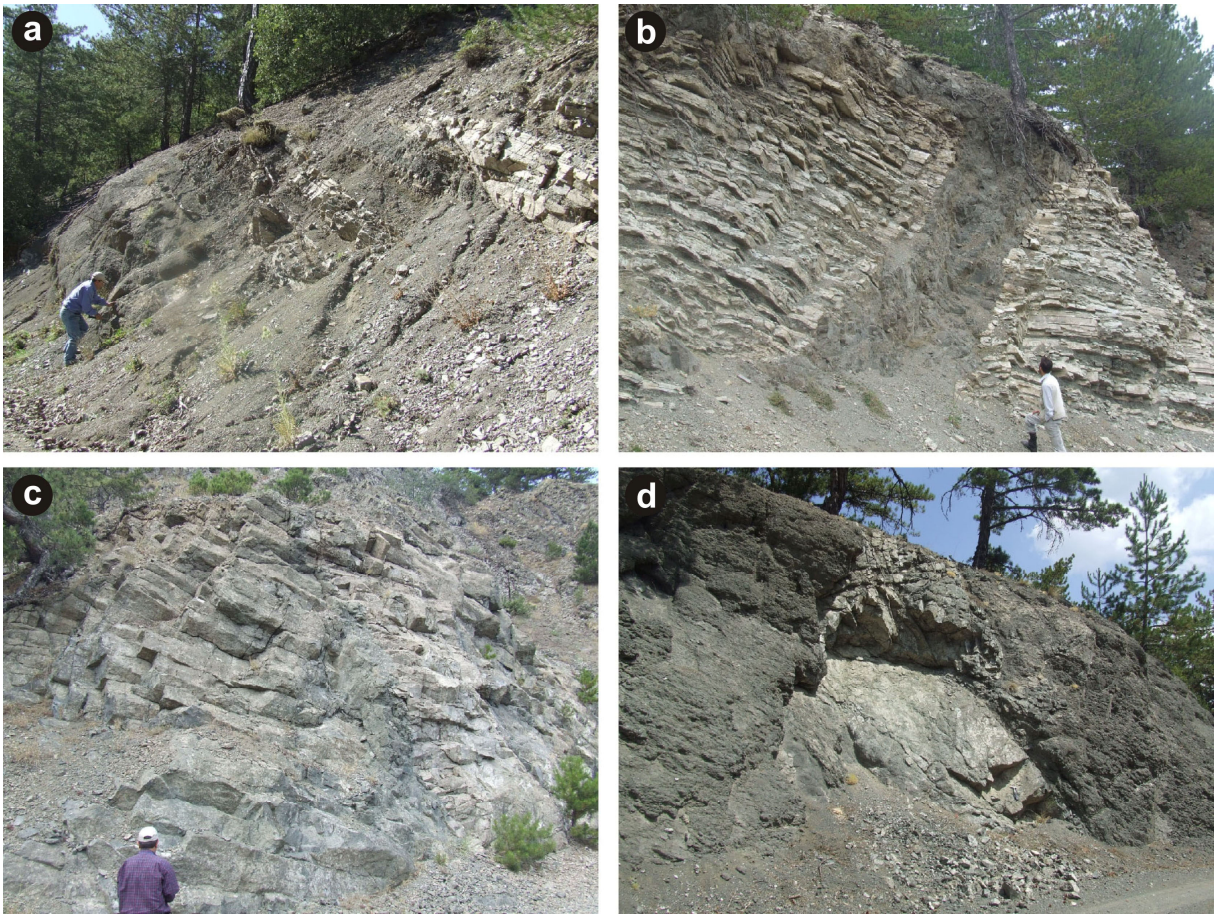

Figure 9.

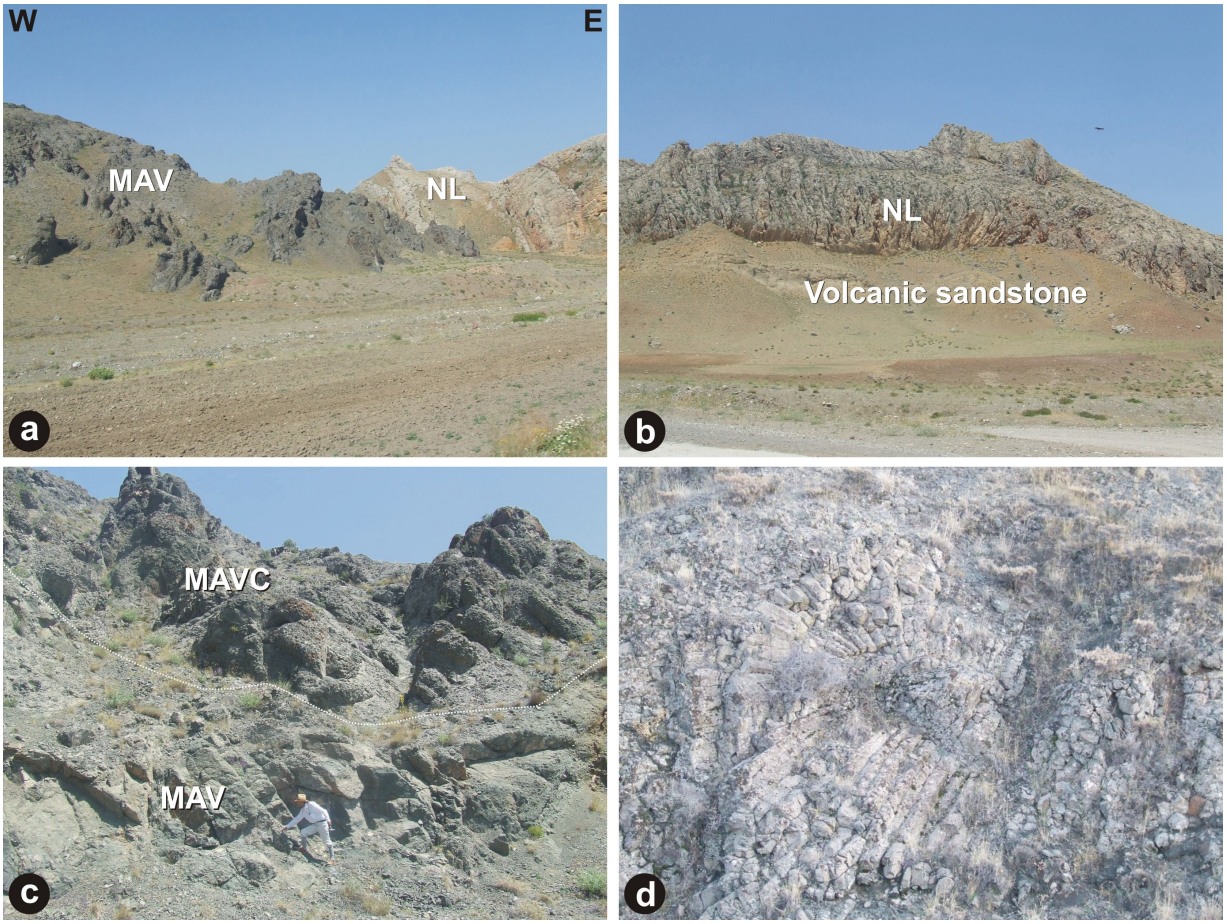

930

931 **Figure 10.**

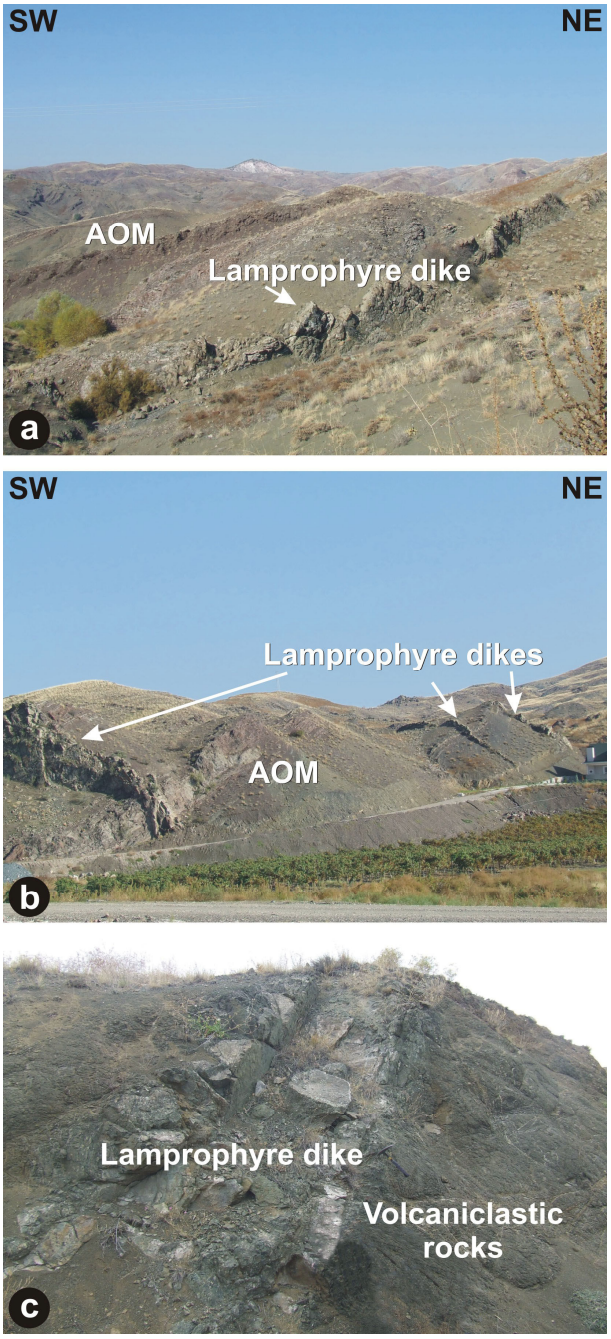
SW
NE
AOM
Lamprophyre dike
a
SW
NE
Lamprophyre dikes
AOM
b
Lamprophyre dike
Volcaniclastic rocks
c

Figure 11.

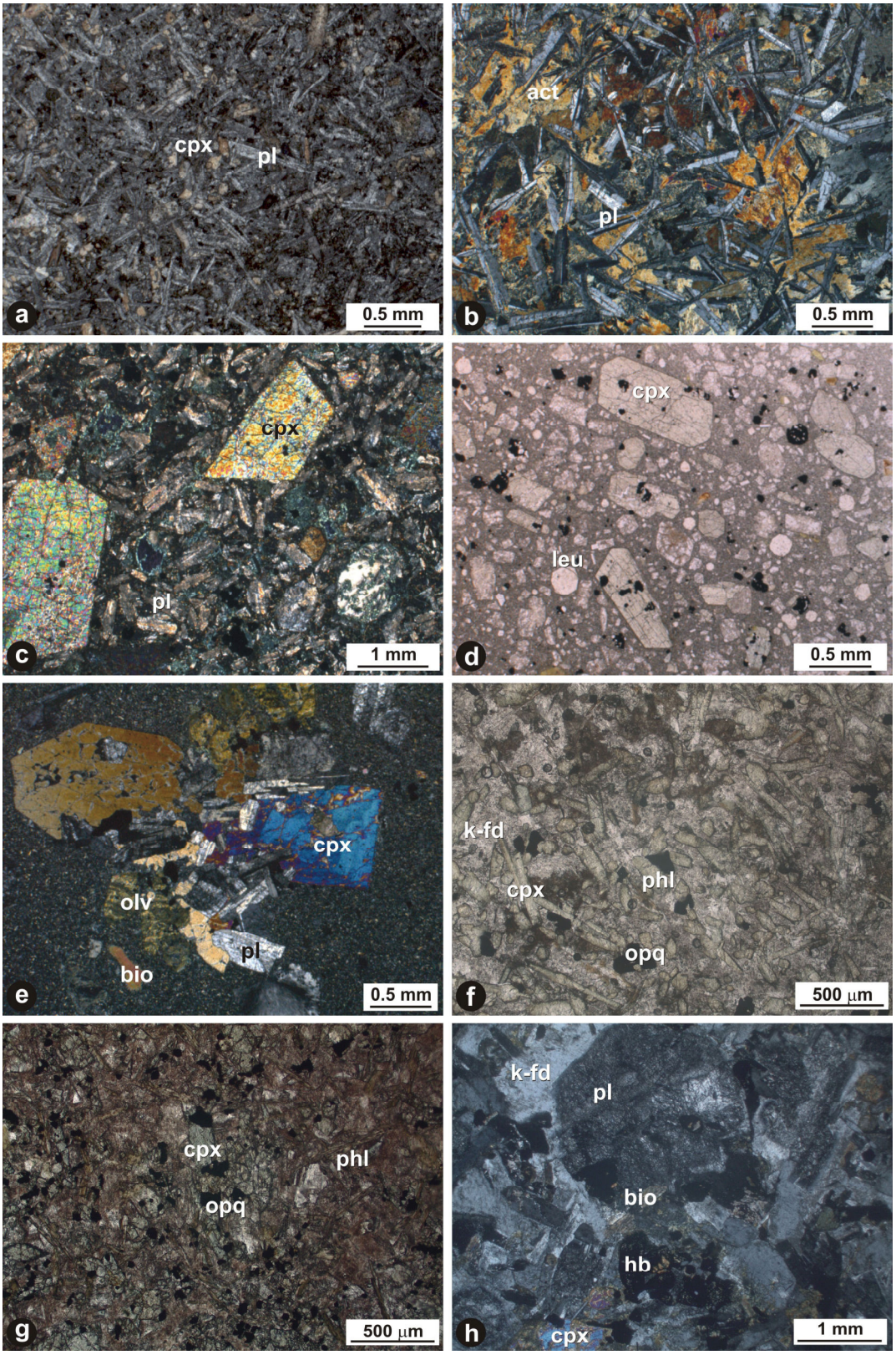

934

935 **Figure 12.**

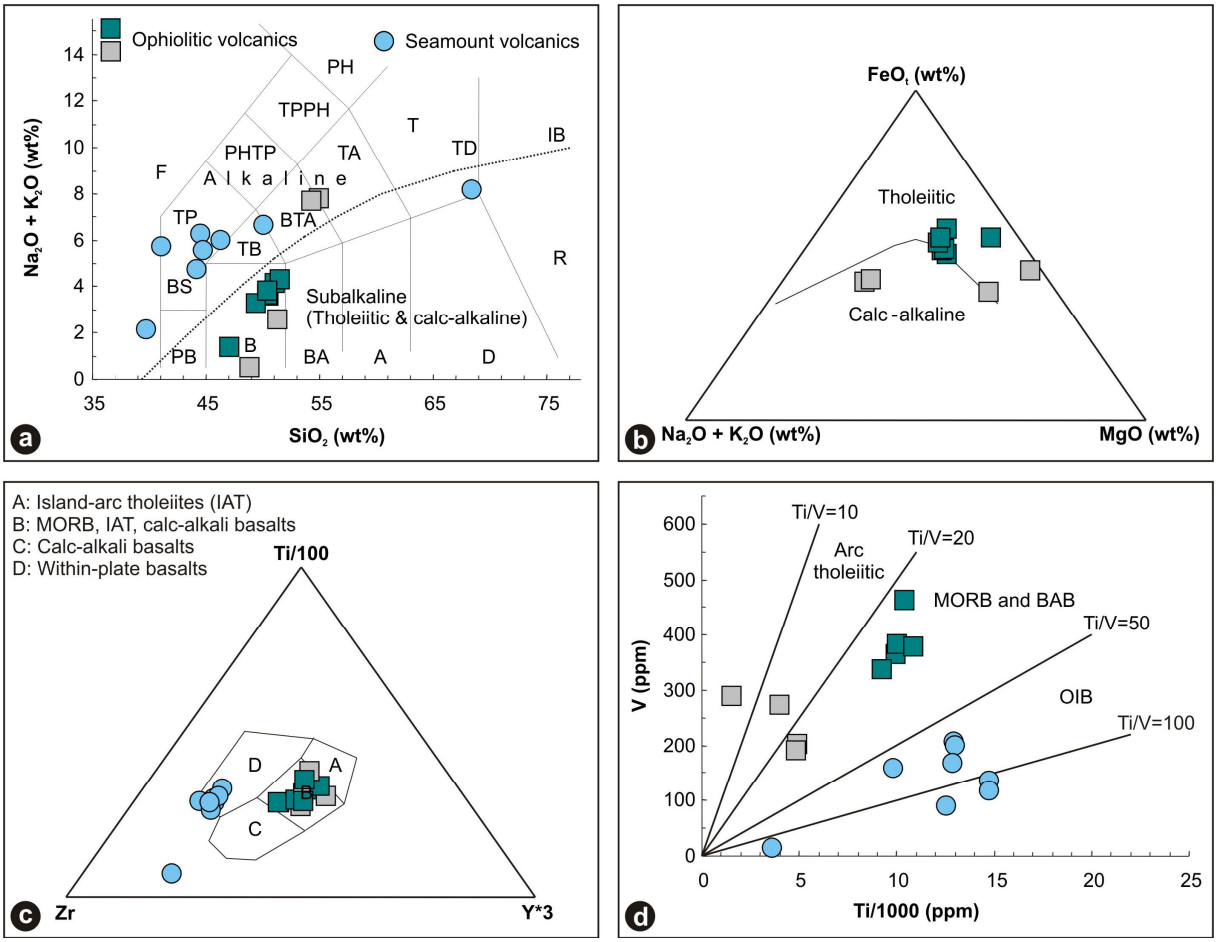
Ophiolitic volcanics
Seamount volcanics
PH
TPPH
T
IB
PHTP
TA
TD
F
A l k a l i n e
TP
BTA
TB
R
BS
Subalkaline
(Tholeiitic & calc-alkaline)
PB
B
BA
A
D
Na2O + K2O (wt%)
SiO2 (wt%)
a
FeOt (wt%)
Tholeiitic
Calc - alkaline
Na2O + K2O (wt%)
MgO (wt%)
b
A: Island-arc tholeiites (IAT)
B: MORB, IAT, calc-alkali basalts
C: Calc-alkali basalts
D: Within-plate basalts
Ti/100
Zr
Y*3
c
Ti/V=10
Arc
tholeiitic
Ti/V=20
MORB and BAB
Ti/V=50
OIB
Ti/V=100
V (ppm)
Ti/1000 (ppm)
d
IAB
OIB
Rock/N-MORB
Cs Rb Ba Th U Nb Ta K La Ce Pb Pr Sr Nd Zr Hf Sm Eu Ti Gd Tb Dy Y Ho Er Tm Yb Lu
e

Figure 13.

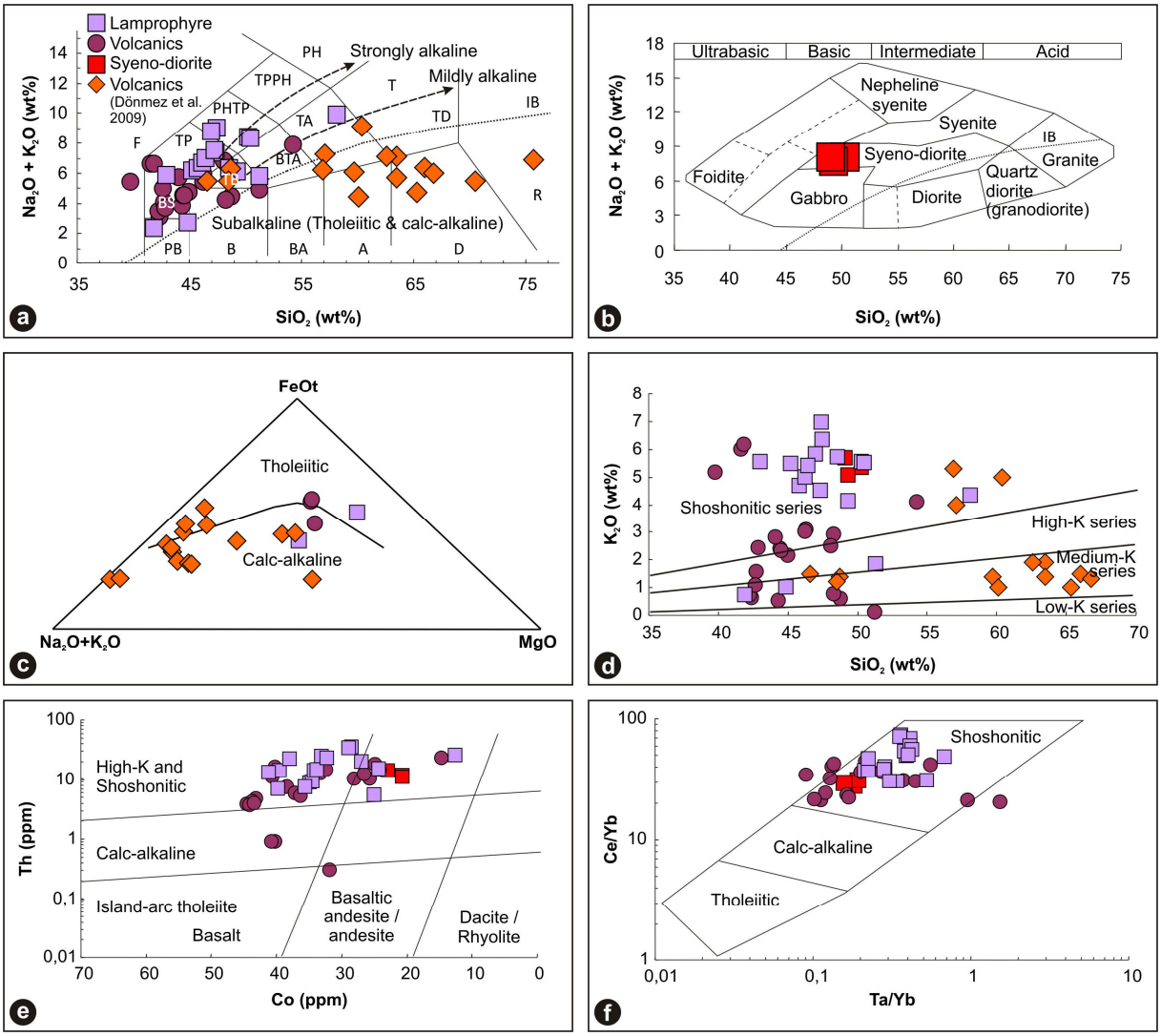
Lamprophyre
Volcanics
Syeno-diorite
Volcanics
(Dönmez et al. 2009)
Strongly alkaline
Mildly alkaline
Subalkaline (Tholeiitic & calc-alkaline)
Na2O + K2O (wt%)
SiO2 (wt%)
a
Ultrabasic
Basic
Intermediate
Acid
Nepheline syenite
Syenite
Syeno-diorite
Foidite
Gabbro
Diorite
Quartz diorite (granodiorite)
Granite
b
FeOt
Tholeiitic
Calc-alkaline
Na2O+K2O
MgO
c
K2O (wt%)
Shoshonitic series
High-K series
Medium-K series
Low-K series
d
Th (ppm)
High-K and Shoshonitic
Calc-alkaline
Island-arc tholeiite
Basalt
Basaltic andesite / andesite
Dacite / Rhyolite
Co (ppm)
e
Ce/Yb
Shoshonitic
Calc-alkaline
Tholeiitic
Ta/Yb
f

Figure 14.

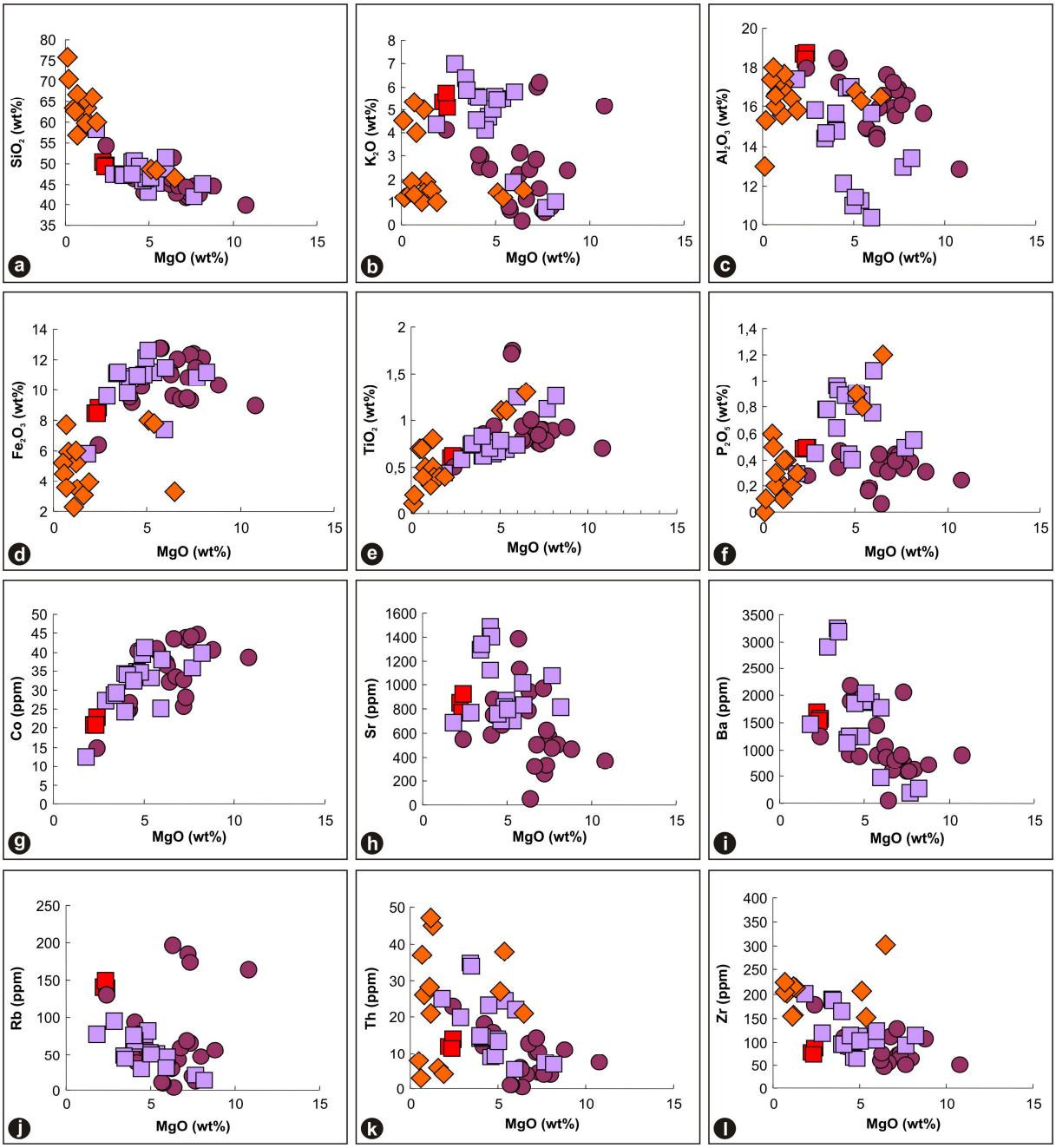
a
SiO2 (wt%)
MgO (wt%)
b
K2O (wt%)
MgO (wt%)
c
Al2O3 (wt%)
MgO (wt%)
d
Fe2O3 (wt%)
MgO (wt%)
e
TiO2 (wt%)
MgO (wt%)
f
P2O5 (wt%)
MgO (wt%)
g
Co (ppm)
MgO (wt%)
h
Sr (ppm)
MgO (wt%)
i
Ba (ppm)
MgO (wt%)
j
Rb (ppm)
MgO (wt%)
k
Th (ppm)
MgO (wt%)
l
Zr (ppm)
MgO (wt%)

Figure 15.

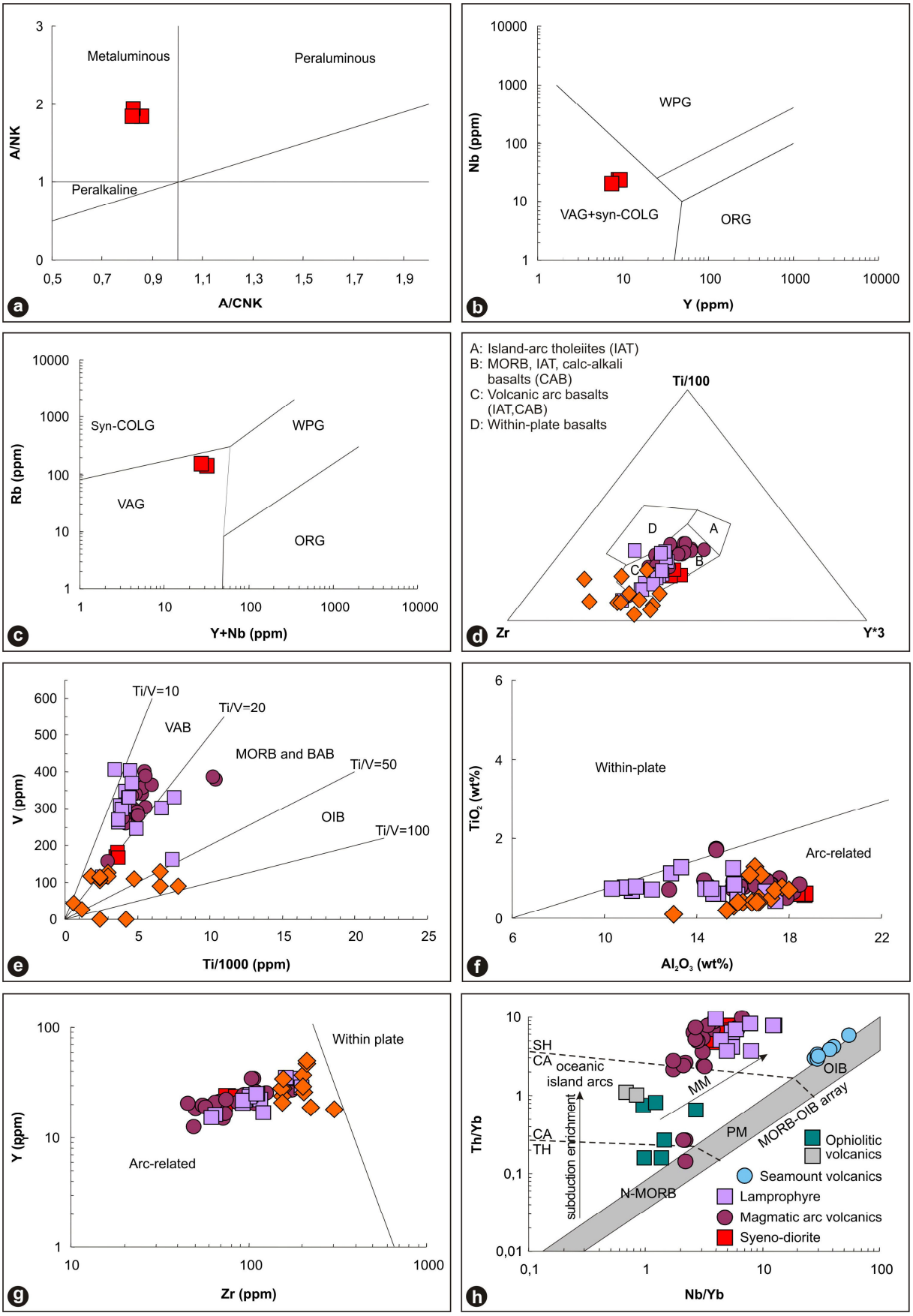
Metaluminous
Peraluminous
Peralkaline
A/NK
A/CNK
a
WPG
VAG+syn-COLG
ORG
Nb (ppm)
Y (ppm)
b
Syn-COLG
WPG
VAG
ORG
Rb (ppm)
Y+Nb (ppm)
c
A: Island-arc tholeiites (IAT)
B: MORB, IAT, calc-alkali basalts (CAB)
C: Volcanic arc basalts (IAT,CAB)
D: Within-plate basalts
Ti/100
Zr
Y*3
d
Ti/V=10
Ti/V=20
VAB
MORB and BAB
Ti/V=50
OIB
Ti/V=100
V (ppm)
Ti/1000 (ppm)
e
Within-plate
Arc-related
TiO2 (wt%)
Al2O3 (wt%)
f
Within plate
Arc-related
Y (ppm)
Zr (ppm)
g
SH
CA
oceanic island arcs
MM
OIB
CA
TH
subduction enrichment
PM
MORB-OIB array
N-MORB
Ophiolitic volcanics
Seamount volcanics
Lamprophyre
Magmatic arc volcanics
Syeno-diorite
Th/Yb
Nb/Yb
h

Figure 16.

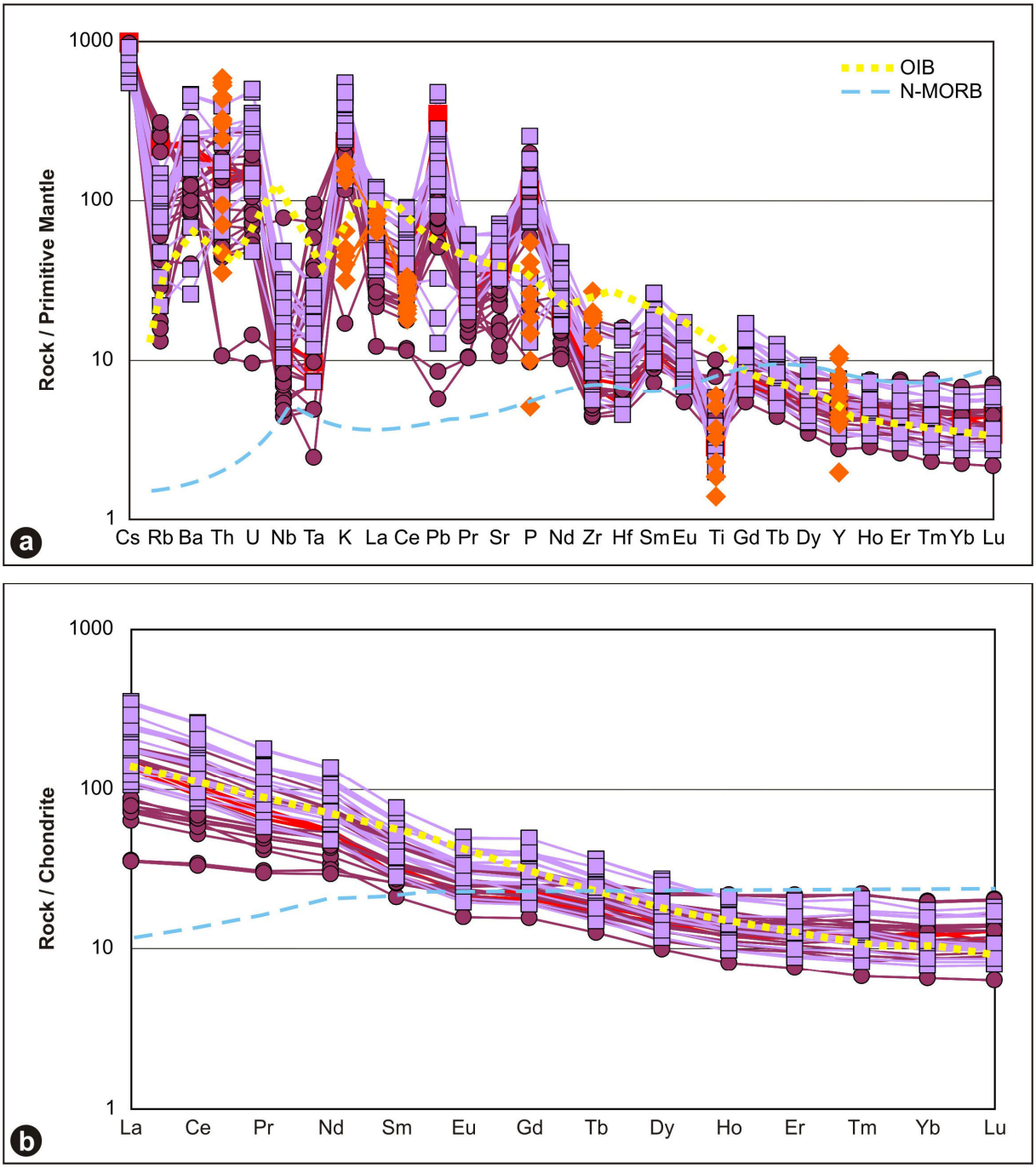
1000
100
10
1
Rock / Primitive Mantle
OIB
N-MORB
Cs Rb Ba Th U Nb Ta K La Ce Pb Pr Sr P Nd Zr Hf Sm Eu Ti Gd Tb Dy Y Ho Er Tm Yb Lu
a
1000
100
10
1
Rock / Chondrite
La Ce Pr Nd Sm Eu Gd Tb Dy Ho Er Tm Yb Lu
b

Figure 17.

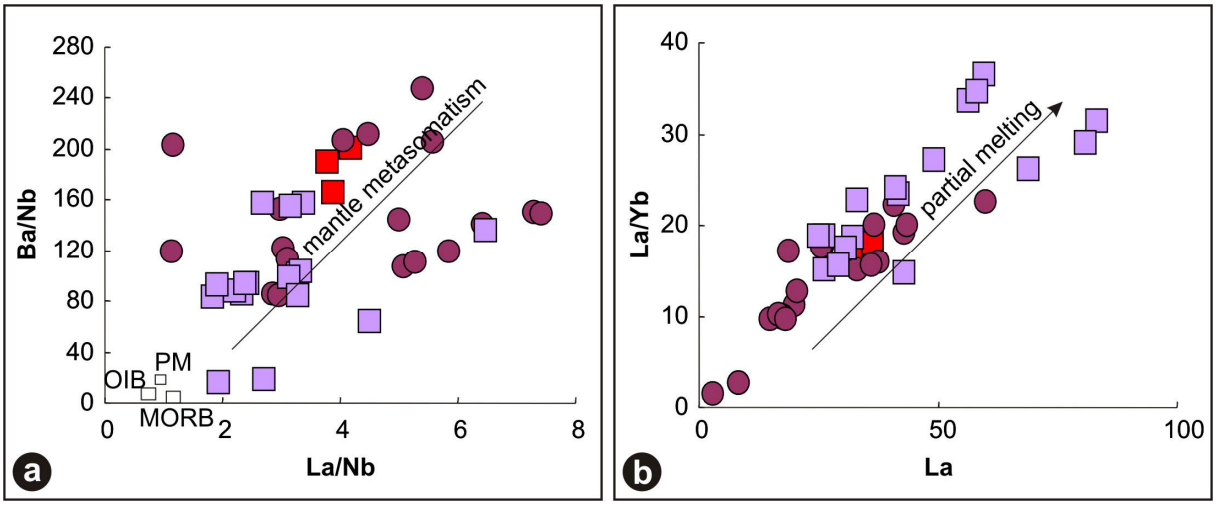

946

947 **Figure 18.**

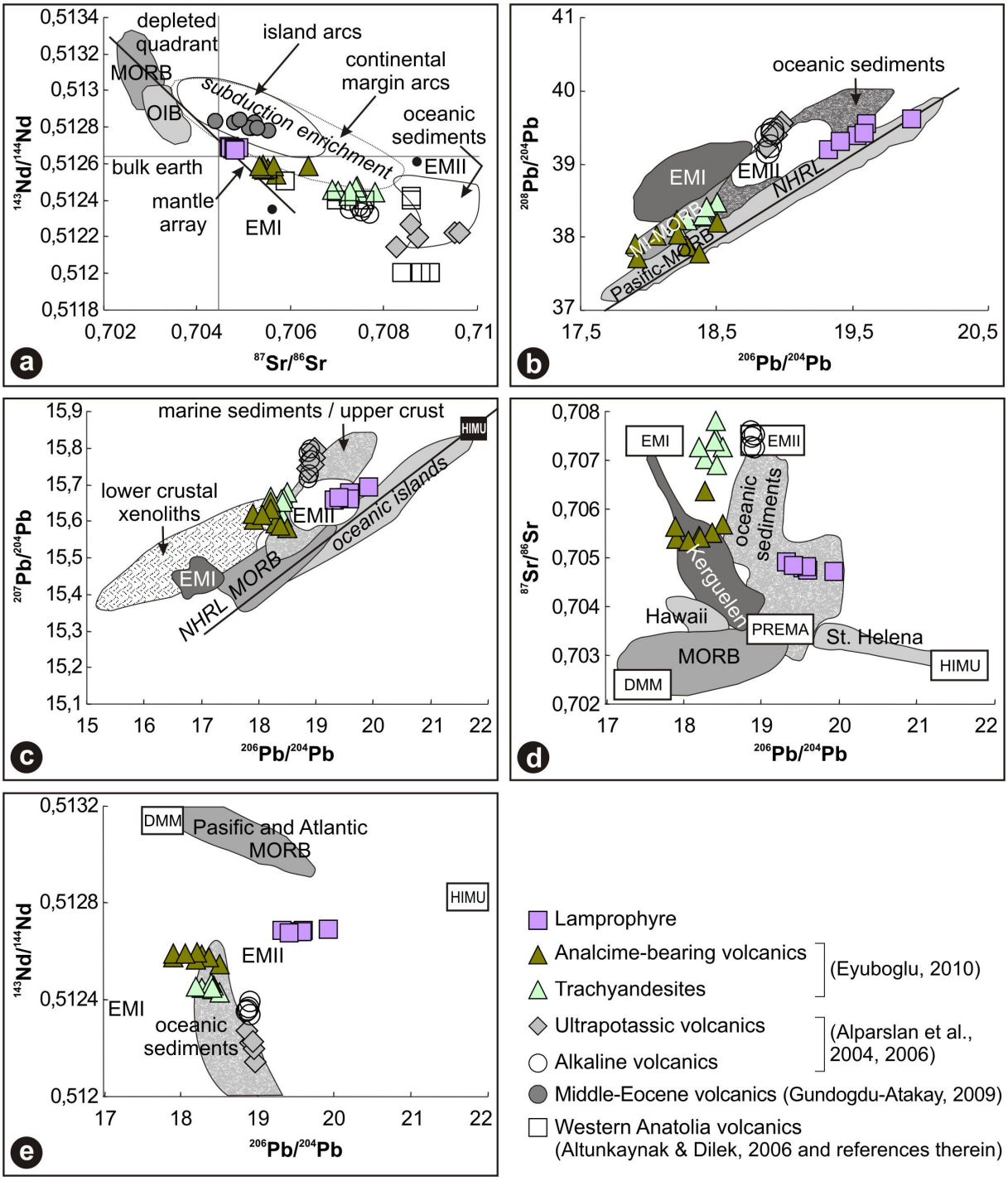
a
depleted quadrant
MORB
OIB
island arcs
continental margin arcs
subduction enrichment
oceanic sediments
EMII
bulk earth
mantle array
EMI
$^{143}Nd/^{144}Nd$
$^{87}Sr/^{86}Sr$
b
oceanic sediments
EMI
EMII
NHRL
M-MORB
Pasific-MORB
$^{208}Pb/^{204}Pb$
$^{206}Pb/^{204}Pb$
c
marine sediments / upper crust
HIMU
lower crustal xenoliths
EMII
oceanic islands
EMI
NHRL MORB
$^{207}Pb/^{204}Pb$
$^{206}Pb/^{204}Pb$
d
EMI
EMII
oceanic sediments
Kerguelen
Hawaii
PREMA
St. Helena
MORB
DMM
HIMU
$^{87}Sr/^{86}Sr$
$^{206}Pb/^{204}Pb$
e
DMM
Pasific and Atlantic MORB
HIMU
EMII
EMI
oceanic sediments
$^{143}Nd/^{144}Nd$
$^{206}Pb/^{204}Pb$
Lamprophyre
Analcime-bearing volcanics
Trachyandesites
(Eyuboglu, 2010)
Ultrapotassic volcanics
Alkaline volcanics
(Alparslan et al., 2004, 2006)
Middle-Eocene volcanics (Gundogdu-Atakay, 2009)
Western Anatolia volcanics
(Altunkaynak & Dilek, 2006 and references therein)

Figure 19.

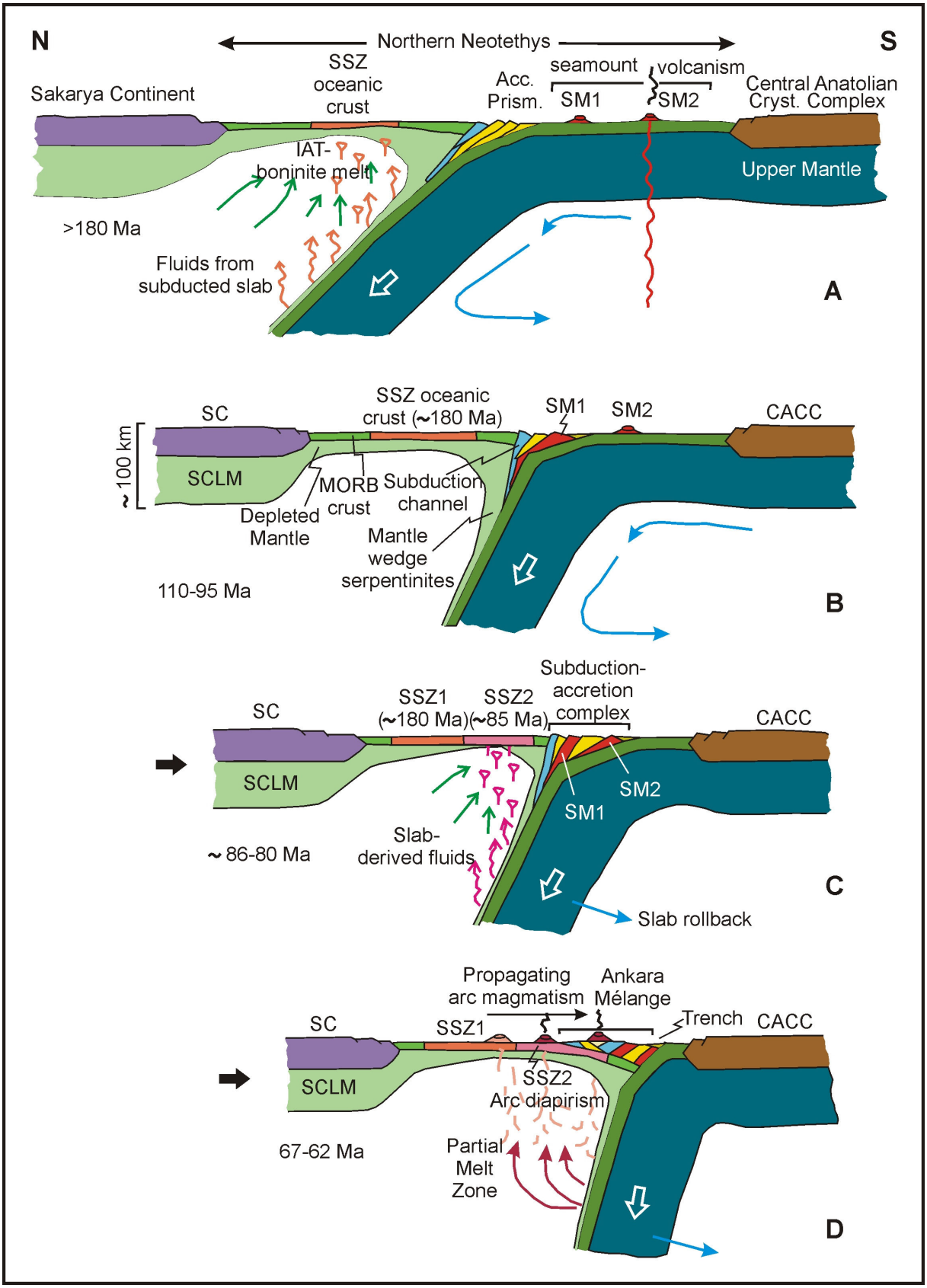

950

951 **Figure 20.**

952 **TABLES**

953 **Table 1.** Whole-rock $^{40}Ar/^{39}Ar$ age data for a basaltic rock sample (YK-11) from the youngest SSZ ophiolite in the Ankara Mélange, Turkey.

Sample: YK-11 (whole rock): Basalt, J=0.004426±0.000051

T°C	$^{40}Arcc(STP)$	$^{40}Ar/^{39}Ar$	±1σ	$^{38}Ar/^{39}Ar$	±1σ	$^{37}Ar/^{39}Ar$	±1σ	$^{36}Ar/^{39}Ar$	±1σ	Ca/K	$\Sigma^{39}Ar$ (%)	Age (Ma) ±1σ	±1σ
500	20.81×10^{-9}	29.6	0.1	0.0418	0.0029	0.479	0.011	0.0620	0.0049	1.72	40.5	88.0	11.0
600	9.45×10^{-9}	22.5	0.1	0.0364	0.0037	0.584	0.011	0.0438	0.0033	2.10	64.8	74.4	7.6
700	12.18×10^{-9}	79.8	0.6	0.0733	0.0129	0.627	0.036	0.2306	0.0075	2.26	73.6	90.6	16.5
800	9.18×10^{-9}	184.7	9.4	0.1457	0.0530	0.751	0.145	0.5966	0.0347	2.70	76.5	65.7	38.7
1000	9.00×10^{-9}	58.5	0.7	0.0714	0.0153	1.630	0.046	0.1440	0.0125	5.87	85.3	123.2	27.4
1130	8.12×10^{-9}	32.0	0.2	0.0332	0.0070	1.131	0.019	0.0811	0.0055	4.07	100.0	62.9	12.6

Age Spectrum: The sample yielded age spectrum with well behaved plateau, characterized by 73.6% of ^{39}Ar, Age value of 80.3 ± 7.6 Ma. On the Inverse Isochrone Plot points form linear regression characterized by age value of 75.8 ± 7.4 and $(^{40}Ar/^{36}Ar)_0$ = 300 ± 8

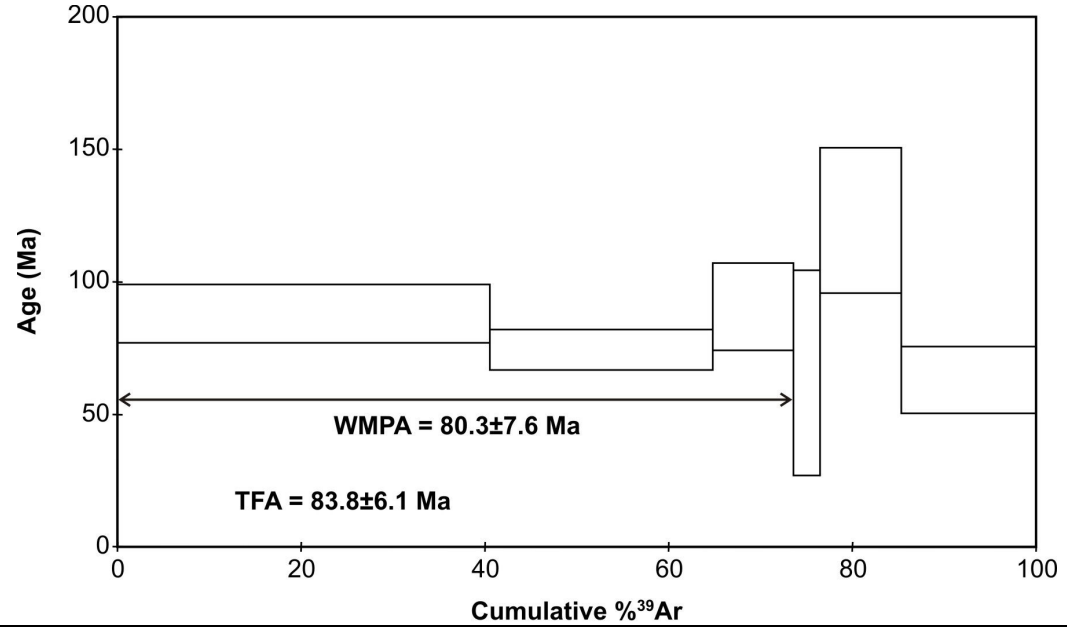

954 **Table 2a.** Whole-rock $^{40}Ar/^{39}Ar$ age data for an epidote-glaucophane schist rock from a metamorphic block in the Ankara Mélange, Turkey.

Sample: YK-6: epidote-glaucophane schist, J=0.004420±0.000051

T°C	$^{40}Arcc$ (STP)	$^{40}Ar/^{39}Ar$	±1σ	$^{38}Ar/^{39}Ar$	±1σ	$^{37}Ar/^{39}Ar$	±1σ	$^{36}Ar/^{39}Ar$	±1σ	Ca/K	$\sum^{39}Ar$ (%)	Age (Ma) ±1σ	±1σ
500	35.70×10^{-9}	48.05	0.1	0.0463	0.003	1.5385	0.0082	0.1299	0.002	5.54	6.4	75.4	4.6
600	32.83×10^{-9}	18.75	0.02	0.0257	0.0005	1.221	0.0031	0.0274	0.0012	4.4	21.5	83.1	2.9
700	38.21×10^{-9}	17.65	0.01	0.0255	0.0007	0.5962	0.0014	0.0229	0.0006	2.15	40.1	84.7	1.7
800	40.74×10^{-9}	19.89	0.02	0.0236	0.001	1.3996	0.0017	0.027	0.0008	5.04	57.8	92.7	2.1
900	21.78×10^{-9}	19.32	0.03	0.0277	0.0008	10.821	0.0144	0.0325	0.0012	38.96	67.5	75.8	2.9
1000	16.15×10^{-9}	14.81	0.03	0.0253	0.0016	12.5237	0.0228	0.0168	0.0017	45.09	76.9	76.8	4
1130	35.36×10^{-9}	13.2	0.01	0.0244	0.0004	9.9743	0.0097	0.0145	0.0009	35.91	100	69.8	2.2

Age Spectrum: The sample yielded age spectrum with two 3 steps plateaus, characterized accordingly by 40.1% of ^{39}Ar, Age value of 83.5 ± 1.7 Ma and 42.2 % of ^{39}Ar, Age value of 72.2 ± 2.2 Ma. On the Inverse Isochrone Plot points form two linear regression characterized by age value of 87.8 ± 2.5 and $(^{40}Ar/^{36}Ar)_0$ = 285 ± 5. The presence of two age plateaus evidence to isotope heterogeneity of YK 6.

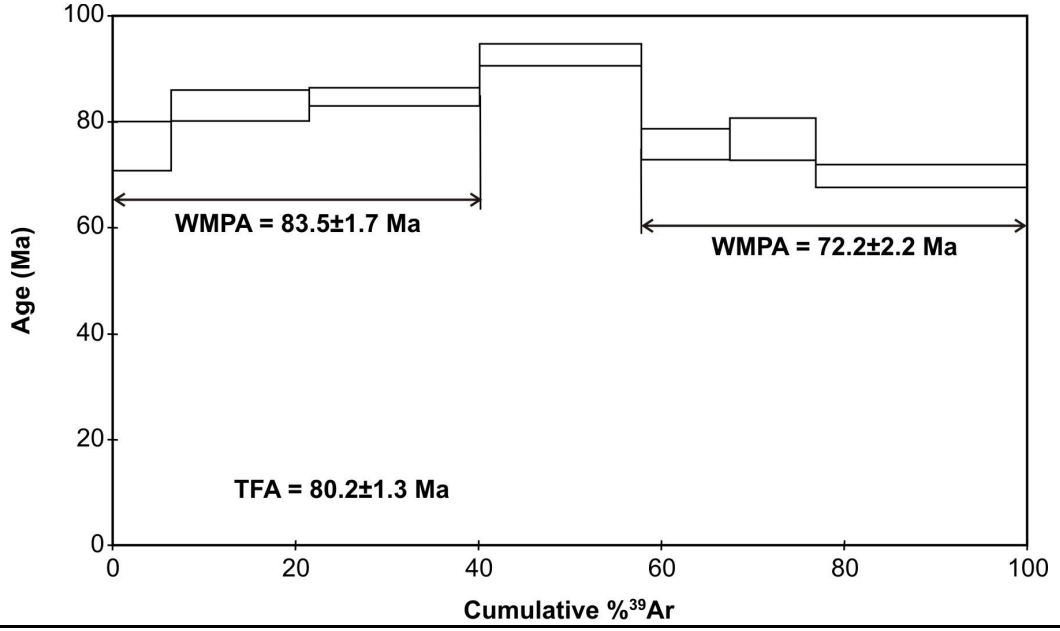

Table 2b. Whole-rock $^{40}Ar/^{39}Ar$ age data for an epidote-chlorite schist rock from a metamorphic block in the Ankara Mélange, Turkey.

Sample: YK-7: epidote-chlorite schist, J=0.004121±0.000044

T°C	$^{40}Arcc$ (STP)	$^{40}Ar/^{39}Ar$	±1σ	$^{38}Ar/^{39}Ar$	±1σ	$^{37}Ar/^{39}Ar$	±1σ	$^{36}Ar/^{39}Ar$	±1σ	Ca/K	$\sum^{39}Ar$ (%)	Age (Ma) ±1σ	±1σ
500	33.53×10^{-9}	57.6	0.2	0.051	0.0027	4.4795	0.0134	0.1488	0.0027	16.13	16.1	98.8	5.7
600	31.15×10^{-9}	38.4	0.1	0.0304	0.0018	3.5391	0.0081	0.0525	0.0019	12.74	38.7	162.5	4.2
700	42.75×10^{-9}	44.5	0.1	0.0355	0.0018	5.4612	0.0142	0.0761	0.0023	19.66	65.3	156.8	4.9
800	19.66×10^{-9}	31	0.1	0.0271	0.0028	1.8875	0.0089	0.0323	0.0027	6.8	82.9	153.1	5.8
900	12.92×10^{-9}	50.5	0.4	0.0507	0.0062	3.436	0.0365	0.1139	0.0087	12.37	90	121	17.9
1000	6.24×10^{-9}	60.7	1	0.0518	0.0203	11.168	0.1806	0.1419	0.0162	40.2	92.8	134.7	32.7
1130	22.81×10^{-9}	88.4	0.5	0.0743	0.0064	56.2813	0.3389	0.2421	0.0062	202.61	100	121.4	12.4

Age Spectrum: The sample yielded age spectrum with 3 steps plateau, characterized by 66.7% of ^{39}Ar, Age value of 158.4 ± 4.2 Ma. On the Inverse Isochrone Plot points form linear regression characterized by age value of 166.9 ± 5.9 and $(^{40}Ar/^{36}Ar)_0$ = 272 ± 8.

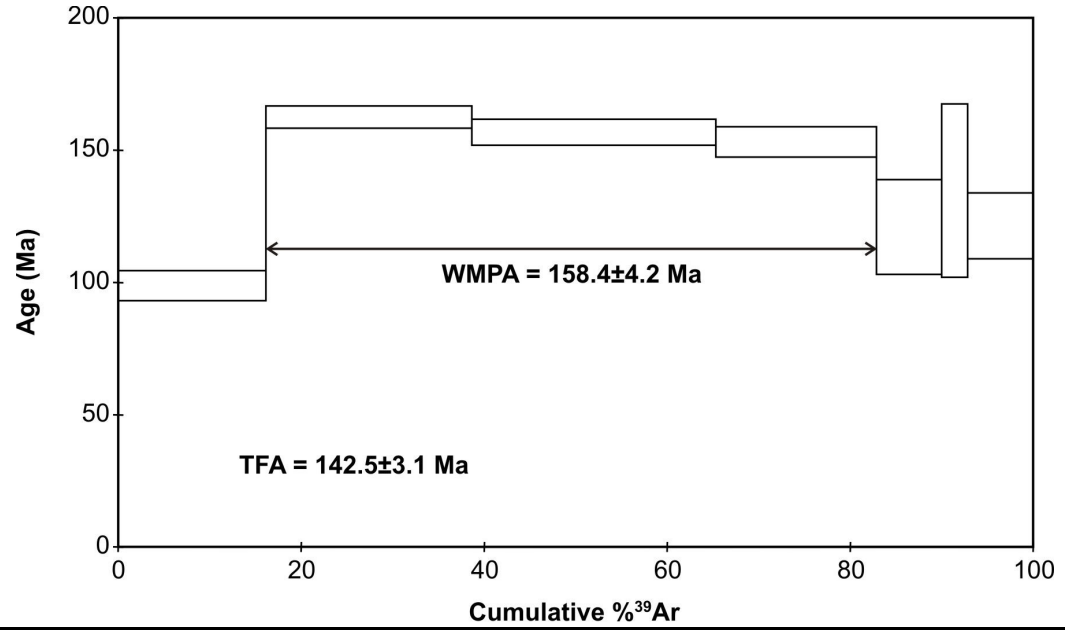

Table 2c. Whole-rock $^{40}Ar/^{39}Ar$ age data for an epidote-actinolite schist rock from a metamorphic block in the Ankara Mélange, Turkey.

Sample: YK-1: epidote-actinolite schist, J=0.004428±0.000051

T°C	$^{40}Arcc$ (STP)	$^{40}Ar/^{39}Ar$	±1σ	$^{38}Ar/^{39}Ar$	±1σ	$^{37}Ar/^{39}Ar$	±1σ	$^{36}Ar/^{39}Ar$	±1σ	Ca/K	$\sum^{39}Ar$ (%)	Age (Ma) ±1σ	±1σ
500	28.20×10^{-9}	195.111	1.614	0.1185	0.0072	8.7082	0.0754	0.5725	0.0095	31.35	4.1	196.1	17.7
600	35.22×10^{-9}	109.08	0.736	0.0809	0.0035	12.8319	0.0878	0.2835	0.007	46.19	13.2	191.6	14.5
700	46.14×10^{-9}	52.526	0.083	0.0345	0.0021	5.2249	0.0101	0.0848	0.0016	18.81	38.1	207	4
800	22.10×10^{-9}	43.305	0.132	0.032	0.0025	3.3143	0.0128	0.0652	0.003	11.93	52.5	182.5	6.8
900	28.97×10^{-9}	56.607	0.158	0.0384	0.0023	16.1294	0.0458	0.1083	0.0028	58.07	67	186.6	6.3
1000	30.80×10^{-9}	41.871	0.112	0.0328	0.0018	21.4028	0.0573	0.0558	0.0027	77.05	87.8	192.1	6
1130	30.24×10^{-9}	69.813	0.261	0.0523	0.0025	34.5698	0.1292	0.1345	0.0038	124.45	100	225.6	8.2

Age Spectrum: The sample yielded age spectrum with 3 steps plateau, characterized by 50% of ^{39}Ar, Age value of 187.4 ± 3.7 Ma. On the Inverse Isochrone Plot one can observe linear regression characterized by age value of 166.1 ± 12.3.

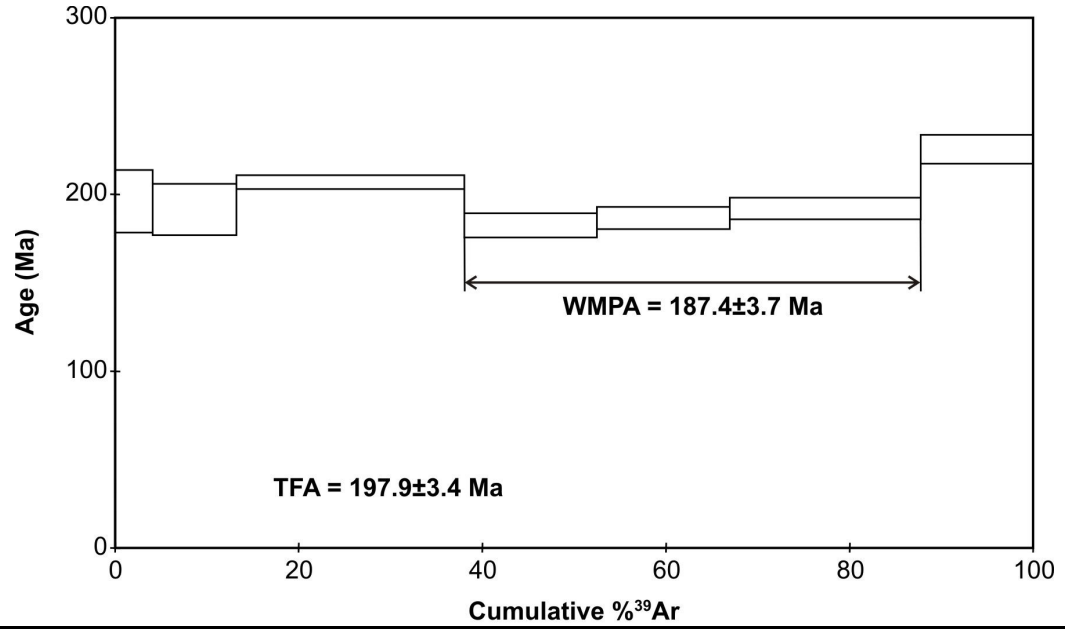

959 **Table 3.** Whole-rock K/Ar age data from metamorphic rock blocks in the Ankara Mélange, Turkey.

Sample no.	Rock	%K	40Ar/36Ar	$^{40}Ar_{rad}$, nl/g	% $^{40}Ar_{air}$	error	Age, Ma
CE.981	Phyllite	1.68	883.2	7.932	33.5	4.5	119.8±3.3
CE.228	Actinolite schist	0.36	347.8	2.558	85.1	0.6	177.4±5.8
CE.976	Amphibole-epidote schist	0.22	405.9	2.316	72.9	1.3	256.9±8.0

960

961 **Table 4a.** Whole-rock $^{40}Ar/^{39}Ar$ age data for an island-arc basaltic rock (Sample No. YK-4) in the Ankara Mélange, Turkey.

Sample: YK-4 (whole rock): Basalt, J=0.004353±0.000050

T°C	$^{40}Arcc$ (STP)	$^{40}Ar/^{39}Ar$	±1σ	$^{38}Ar/^{39}Ar$	±1σ	$^{37}Ar/^{39}Ar$	±1σ	$^{36}Ar/^{39}Ar$	±1σ	Ca/K	$\Sigma^{39}Ar$ (%)	Age (Ma) ±1σ	±1σ
500	44.60×10^{-9}	168.69	0.97	0.1269	0.007	7.5932	0.0458	0.539	0.0065	27.34	6.9	72.4	12.8
600	14.83×10^{-9}	32.9	0.17	0.0413	0.0033	10.1845	0.0528	0.0795	0.0051	36.66	18.7	72.4	11.4
700	13.82×10^{-9}	26.82	0.1	0.0333	0.0048	4.2753	0.017	0.0621	0.0036	15.39	32.2	65.2	8
800	24.70×10^{-9}	26.65	0.08	0.0331	0.0022	1.935	0.0067	0.0635	0.0029	6.97	56.5	60.8	6.6
900	18.59×10^{-9}	18.29	0.04	0.021	0.0013	1.3887	0.0051	0.0299	0.0022	5	83.1	72.8	4.9
1000	7.83×10^{-9}	31.49	0.17	0.0381	0.0053	1.4804	0.0211	0.0611	0.0055	5.33	89.7	102.6	12.1
1130	11.68×10^{-9}	29.58	0.12	0.0279	0.0033	3.5167	0.016	0.054	0.0041	12.66	100	104	9.2

Age Spectrum: The sample yielded age spectrum with 3 steps plateau, characterized by 64.4% of ^{39}Ar, Age value of 67.8 ± 4.9 Ma. On the Inverse Isochrone Plot points form linear regression characterized by age value of 68.1 ± 4.4 and $(^{40}Ar/^{36}Ar)_0$ = 296.1 ± 3.5.

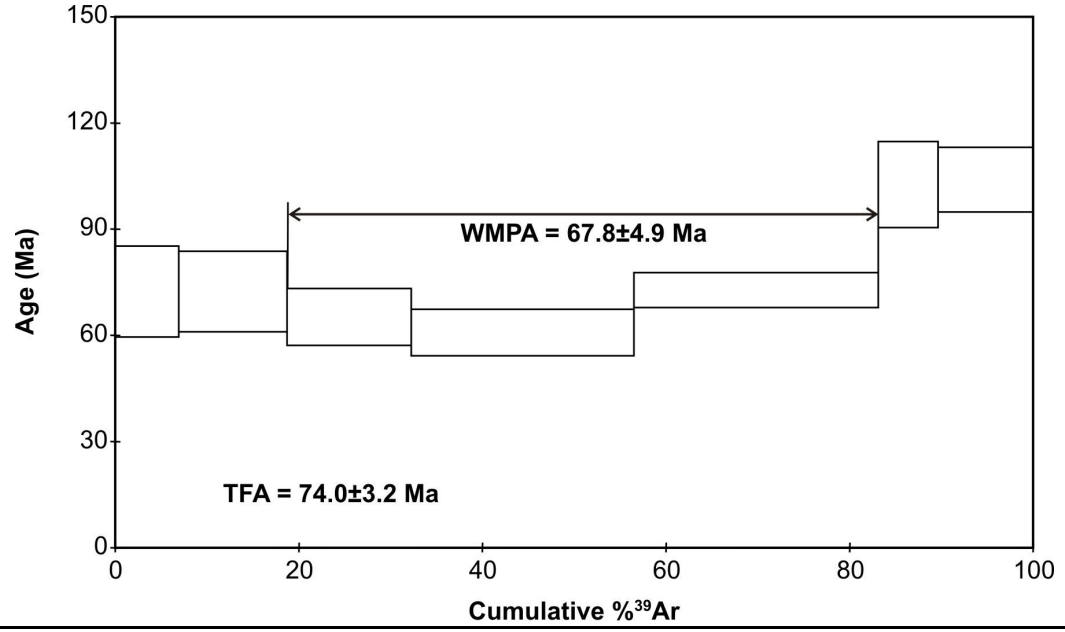

962

963 **Table 4b.** $^{40}Ar/^{39}Ar$ biotite age data for a lamprophyre dike (Sample No. YK-19) from the island-arc unit in the Ankara Mélange, Turkey.

Sample: YK-19 (biotite): Lamprophyre, J=0.007143 ± 0.000133

T°C	$^{40}Arcc$ (STP)	$^{40}Ar/^{39}Ar$	±1σ	$^{38}Ar/^{39}Ar$	±1σ	$^{37}Ar/^{39}Ar$	±1σ	$^{36}Ar/^{39}Ar$	±1σ	Ca/K	$\sum^{39}Ar$ (%)	Age (Ma) ±1σ	±1σ
500	3.9×10^{-9}	92.802	0.0393	0.015480	0.004274	0.61970	0.05770	0.028643	0.001314	22.30	0.6	10.50	5.0
625	7.7×10^{-9}	83.584	0.0116	0.015744	0.001217	0.31455	0.01480	0.015871	0.001284	1.13	2.0	46.7	4.80
750	37.9×10^{-9}	69.914	0.0044	0.013301	0.000117	0.05874	0.00360	0.008418	0.000210	0.21	10.40	57.1	1.30
850	45.7×10^{-9}	64.526	0.0017	0.013498	0.000076	0.04725	0.00102	0.004948	0.000237	0.17	21.20	63.2	1.40
950	51.6×10^{-9}	65.506	0.0033	0.013393	0.000248	0.08738	0.00394	0.004805	0.000142	0.31	33.3	64.9	1.30
1050	112.6×10^{-9}	62.462	0.0035	0.013738	0.000060	0.07037	0.00091	0.004305	0.000083	0.25	61.0	63.0	1.20
1130	156.9×10^{-9}	61.778	0.0020	0.013593	0.000030	0.07395	0.00067	0.003986	0.000051	0.27	100.0	63.3	1.20

Age Spectrum: The sample yielded age spectrum with four steps Plateau characterized by 89.6% of ^{39}Ar, Age value of 63.6 ± 1.2 Ma. On the Inverse Isochrone Plot plateau points form linear trend, characterized by age value of 57.5 ± 4.1 Ma, MSWD = 1.5

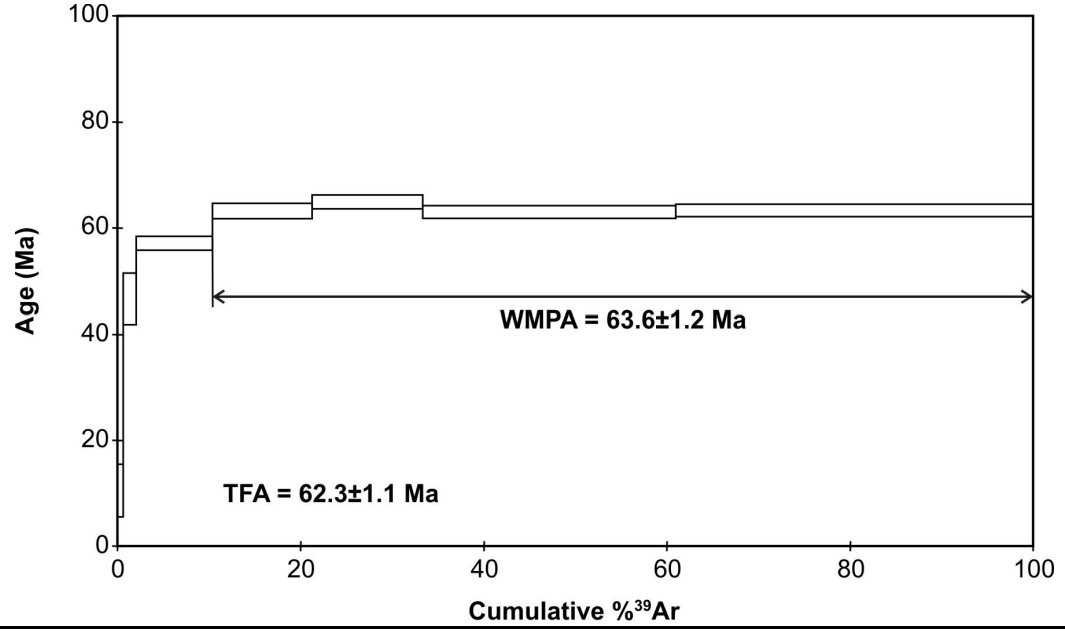

964

965 **Table 4c.** Whole-rock $^{40}Ar/^{39}Ar$ age data for a lamprophyre dike (Sample No. YK-20) from the island-arc unit in the Ankara Mélange, Turkey.

Sample: YK-20 (whole rock): Lamprophyre, J=0.007258 ± 0.000137

T°C	$^{40}Arcc$ (STP)	$^{40}Ar/^{39}Ar$	±1σ	$^{38}Ar/^{39}Ar$	±1σ	$^{37}Ar/^{39}Ar$	±1σ	$^{36}Ar/^{39}Ar$	±1σ	Ca/K	$\sum^{39}Ar$ (%)	Age (Ma) ±1σ	±1σ
550	114.7×10^{-9}	48.724	0.0048	0.014063	0.000040	0.28860	0.00023	0.004714	0.000071	1.04	16.20	45.0	0.9
625	78.3×10^{-9}	71.168	0.0064	0.014657	0.000137	128.516	0.00083	0.006715	0.000045	4.63	23.70	66.0	1.20
700	73.1×10^{-9}	63.482	0.0041	0.014148	0.000062	115.422	0.00187	0.003713	0.000142	4.16	31.70	67.5	1.40
775	85.2×10^{-9}	62.554	0.0032	0.013660	0.000068	0.51460	0.00080	0.003174	0.000096	1.85	41.0	68.3	1.30
850	68.1×10^{-9}	59.659	0.0028	0.013744	0.000112	0.19993	0.00023	0.004958	0.000090	0.72	48.9	58.0	1.10
950	54.6×10^{-9}	58.431	0.0024	0.014092	0.000162	0.29838	0.00075	0.004897	0.000152	1.07	55.3	56.7	1.20
1050	210.7×10^{-9}	50.825	0.0020	0.013886	0.000024	0.61827	0.00022	0.005145	0.000055	2.23	83.8	46.0	0.9
1130	121.2×10^{-9}	51.432	0.0013	0.014028	0.000073	144.061	0.00118	0.005433	0.000056	5.19	100.0	45.7	0.9

Age Spectrum: The sample yielded complex age spectrum with noticeable hump after low temperature step containing three steps intermediate plateau followed by high temperature two steps intermediate Plateau. Intermediate plateaus are characterized accordingly by 24.8% of ^{39}Ar, Age value of 67.2 ± 1.2 Ma and 44.7% of ^{39}Ar, Age value of 45.9 ± 0.9 Ma.

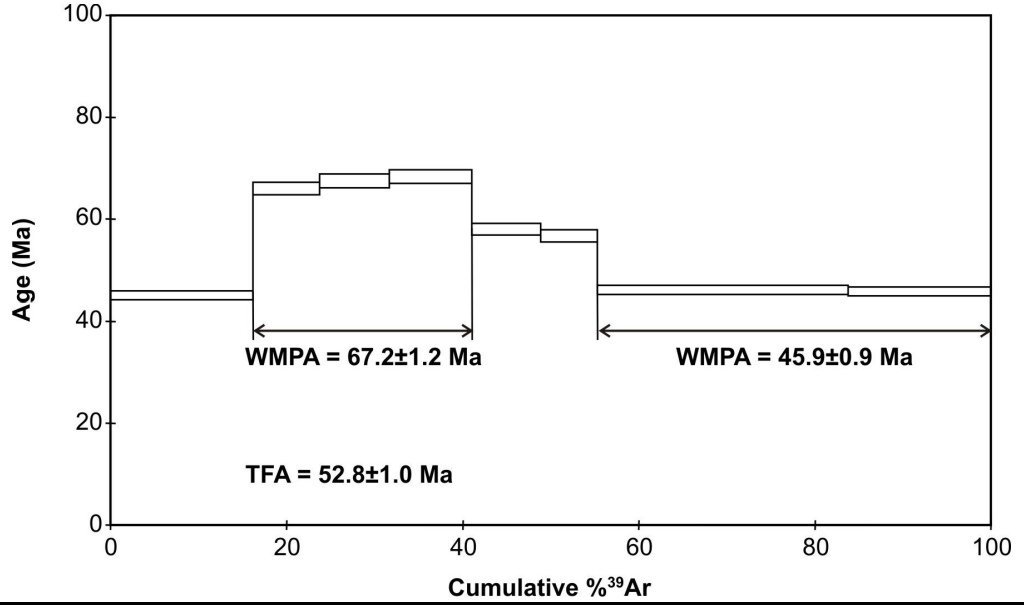

966 **Table 4d.** $^{40}Ar/^{39}Ar$ biotite age data for a syeno-diorite plutonic rock (Sample No. YK-438) from the island-arc unit in the Ankara Mélange, Turkey.

Sample: YK-438 (biotite): Syeno-diorite, J=0.004553 ± 0.000054

T°C	$^{40}Arcc$ (STP)	$^{40}Ar/^{39}Ar$	±1σ	$^{38}Ar/^{39}Ar$	±1σ	$^{37}Ar/^{39}Ar$	±1σ	$^{36}Ar/^{39}Ar$	±1σ	Ca/K	$\sum^{39}Ar$ (%)	Age (Ma) ±1σ	±1σ
500	10.2×10^{-9}	61.084	0.0090	0.01989	0.00107	0.7800	0.0026	0.01226	0.00144	2.81	9.0	20.30	3.46
600	14.4×10^{-9}	82.535	0.0136	0.01627	0.00075	15.022	0.0075	0.00992	0.00159	5.41	18.4	43.20	3.79
700	17.3×10^{-9}	121.050	0.0098	0.00960	0.00130	21.617	0.0064	0.01488	0.00069	7.78	26.1	62.22	1.78
800	25.9×10^{-9}	128.671	0.0263	0.01743	0.00152	0.9964	0.0146	0.00617	0.00198	3.59	37.0	88.51	4.68
900	39.8×10^{-9}	126.457	0.0087	0.01645	0.00019	0.8052	0.0025	0.00343	0.00027	2.9	53.9	93.11	1.25
1000	48.8×10^{-9}	126.405	0.0147	0.01668	0.00067	0.4739	0.0055	0.00371	0.00111	1.71	74.8	92.41	2.77
1130	52.0×10^{-9}	111.241	0.0102	0.01900	0.00068	21.389	0.0021	0.00361	0.00065	7.7	100.0	80.77	1.78

Age Spectrum: The sample yielded age spectrum with three steps plateau characterized by 48.6% of ^{39}Ar, Age value of 92.7 ± 1.2 Ma. On the Inverse Isochrone Plot points don't form linear regression.

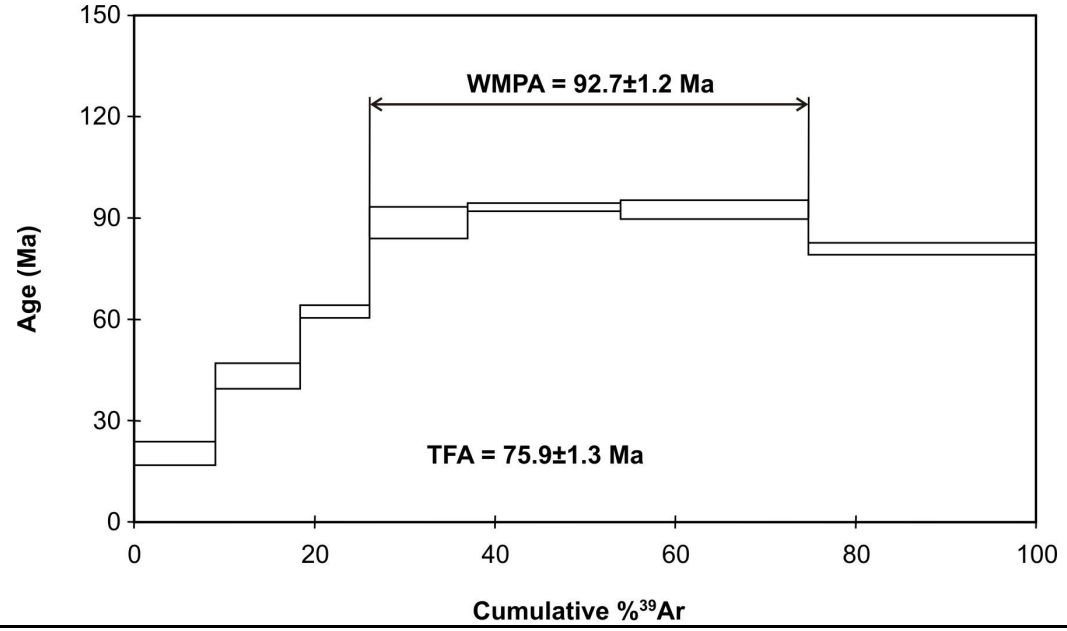

Table 5. Major, trace element and REE data for a selected group of volcanic and dike rocks from the Neotethyan ophiolitic units in the Ankara Mélange (first nine samples from Tankut et al., 1998).

Sample no	BM1	BM3	BM5	95GK4	95GK6	95GKE4	96GKE51	96GKE57	96GKE58B	CE.07	CE.08
Rock-type	**Basalt**	**Basaltic andesite**	**Basalt**	**Dolerite**	**Dolerite**	**Dolerite**	**Dolerite**	**Dolerite**	**Dolerite**	**Basalt**	**Basalt**
Oxide, wt %											
SiO_2	50.53	51.34	50.47	51.08	49.45	51.53	48.93	50.45	47.08	55.50	54.94
TiO_2	1.12	0.26	1.13	1.66	1.68	1.82	0.67	1.74	1.55	0.82	0.81
Al_2O_3	15.96	17.16	15.93	13.45	13.52	12.53	11.00	12.97	11.18	18.43	18.66
Fe_2O_3	10.01	6.80	9.99	11.91	13.23	12.69	9.07	12.31	12.21	8.12	8.47
MnO	0.14	0.12	0.14	0.23	0.22	0.23	0.18	0.23	0.22	0.60	0.63
MgO	6.32	8.17	5.89	7.04	6.41	6.67	10.54	6.30	8.67	3.54	3.81
CaO	4.88	11.07	5.33	9.18	10.91	7.93	15.30	8.66	13.11	1.27	1.17
Na_2O	3.31	2.30	3.34	3.79	2.89	3.89	0.43	3.41	1.22	7.62	7.50
K_2O	0.28	0.28	0.29	0.34	0.36	0.39	0.07	0.37	0.12	0.17	0.19
P_2O_5	0.13	0.07	0.12	0.17	0.21	0.22	0.06	0.21	0.23	0.09	0.10
LOI	6.81	2.05	6.94	1.2	1.04	0.85	3.12	1.69	3.06	3.70	3.50
Total	99.49	99.62	99.57	100.05	99.92	99.75	99.35	98.34	98.65	99.85	99.84
Trace, ppm											
Cr	53.00	166.00	36.00	70.00	84.00	130.00	624.00	134.00	103.00	27.40	20.55
Ni	10.00	101.00	8.00	21.00	25.00	48.00	91.00	59.00	37.00	13.20	11.70
Co										27.90	26.10
Sc				35	38	32	41	35	45		
Rb	11.00	9.00	12.00	4.00	4.00	5.00	2.00	7.00	0.00	2.10	2.40
Ba	242.00		270.00	60.00	503.00	188.00	22.00	185.00	52.00	130.00	110.00
Sr	441.00	100.00	420.00	174.00	510.00	402.00	24.00	208.00	71.00	472.80	494.80
Cs							0.64	24.94	3.91	0.40	0.50
Th	0.47	0.60	0.44	0.00	1.00	3.00	2.00	4.00	3.00	0.60	0.60
U				0.21	0.26	0.29	0.14	0.28	0.28	0.30	0.30
Nb	3.00	2.60	4.00	3.70	5.70	4.00	1.30	3.40	4.80	1.30	1.40
Ta	0.00	0.00	0.00	0.24	0.29	0.25	0.15	0.18	0.29	0.10	0.10
Zr	96.00	21.00	98.00	101.00	126.00	119.00	39.00	91.00	113.00	37.90	43.60
Hf	1.70	0.30	2.20	2.77	3.10	3.14	1.16	2.64	3.13	1.40	1.40
Y	25.00	7.00	25.00	37.00	40.00	41.00	18.00	39.00	39.00	14.50	15.50
V		288		363	383	378	273	462	337	202.00	190.00
Pb					1		1		3	5.9	5.3
REE, ppm											
La	3.90	2.90	4.30	7.42	9.25	9.17	3.03	8.19	9.66	4.00	2.90
Ce	10.70	3.70	8.20	16.67	20.29	19.96	6.18	17.66	21.46	8.30	6.90
Pr				2.31	2.81	2.73	0.83	2.43	2.90	1.31	1.05
Nd	5.70	2.20	6.90	11.64	13.66	13.37	4.44	12.10	14.01	5.90	5.90
Sm	2.90	0.50	3.00	4.07	4.64	4.71	1.67	4.41	4.75	1.71	1.53
Eu	0.90	0.18	1.00	1.43	1.59	1.29	0.70	1.42	1.52	0.49	0.46
Gd				5.14	5.71	5.73	2.31	5.85	6.04	2.08	2.00
Tb	0.60	0.15	0.70	1.02	1.13	1.13	0.46	1.10	1.13	0.41	0.40
Dy				6.78	7.42	7.42	3.12	7.39	7.34	2.54	2.59
Ho				1.47	1.60	1.63	0.70	1.62	1.58	0.57	0.61
Er				4.30	4.59	4.78	2.03	4.58	4.39	1.77	1.84
Tm				0.61	0.65	0.68	0.30	0.67	0.65	0.29	0.31
Yb	3.10	0.96	2.90	3.71	3.94	4.18	1.89	4.09	3.90	1.80	1.90
Lu	0.49	0.16	0.50	0.58	0.63	0.65	0.30	0.63	0.61	0.28	0.32

971 **Table 6.** Major, trace element and REE data for a selected group of seamount volcanic rocks
972 from the Ankara Mélange.

Sample no	2007KM327	DM19	KM24	KM27	KM28	KM121	KM126	CM38
Rock-type	**Foidite**	**Trachybasalt**	**Basanite**	**Basanite**	**Trachyte**	**Tephrrite**	**Tephyrite**	**Basanite**
Oxide, wt %								
SiO_2	39.77	50.15	41.08	44.55	68.47	46.36	44.83	44.26
TiO_2	2.16	2.46	1.64	2.17	0.61	2.10	2.46	2.15
Al_2O_3	15.84	15.90	13.21	15.83	15.16	16.70	15.78	15.75
Fe_2O_3	11.67	9.10	7.75	10.41	3.17	12.04	12.27	10.54
MnO	0.33	0.19	0.12	0.16	0.04	0.18	0.18	0.30
MgO	8.10	3.43	3.91	4.91	0.54	3.12	3.93	9.48
CaO	13.95	5.64	13.78	7.8	1.48	8.59	9.60	4.63
Na_2O	0.57	4.74	5.25	4.15	6.79	4.18	3.78	3.98
K_2O	1.56	1.91	0.45	2.1	1.35	1.81	1.78	0.74
P_2O_5	0.51	0.77	0.464	0.653	0.484	0.89	0.84	0.68
LOI	5.3	5.5	11.8	7.1	1.7	3.8	4.3	7.1
Total	99.81	99.77	99.46	99.84	99.77	99.73	99.72	99.61
Trace, ppm								
Cr	342.45	13.70	232.87	198.62	13.70	13.70	20.55	219.17
Ni	128.00	21	113	106	20	20	20	130.70
Co	40.10	24.3	30.6	36.4	2.2	26.10	32.50	39.30
Sc	25.00	15	18	20	3	5	7	21
Rb	26.80	39.8	7.7	43.5	33.4	18.7	18.1	13.50
Ba	280	135	151	251	379	426	401	371.00
Sr	223.30	368.6	529.6	588.4	294.3	577.9	547.0	740.00
Cs	0.20	1.00	0.1	1.00	0.7	0.10	0.10	0.30
Th	5.90	7.6	4.9	5.8	10.5	8.8	8.0	6.30
U	1.40	1.6	1.5	1.2	1.4	1.9	1.6	1.60
Nb	55.40	74.5	47.2	60.5	96	88.3	82.0	62.40
Ta	3.00	4.5	2.8	3.6	6	5.1	5.2	3.70
Zr	200.40	291.3	187.2	240	389.5	273.4	257.0	252.10
Hf	4.90	6.9	4.6	6.2	10.2	5.7	5.9	6.50
Y	22.70	24.3	20.6	25	34	29.2	29.0	25.60
V	207	136	157	199	14	90	117	168
Pb	4	1.5	5.6	4.9	7.2	5	7.9	1.8
REE, ppm								
La	37.00	54.4	33	43.4	60.7	63.4	61.1	42.30
Ce	73.00	122.0	64.8	83.5	114.7	128.8	122.9	84.90
Pr	8.80	13.61	7.8	9.71	14.25	13.73	13.57	9.87
Nd	34.30	54.0	29.1	37.3	49	50.7	51.0	39.90
Sm	6.11	9.76	5.21	6.56	8.05	9.06	9.04	6.64
Eu	2.03	3.17	1.74	2.11	2.19	2.84	2.99	2.16
Gd	5.78	8.46	4.65	5.81	6.67	8.33	8.33	6.21
Tb	0.88	1.17	0.76	0.93	1.15	1.18	1.21	0.93
Dy	4.49	5.56	4.01	4.89	6.34	5.88	5.90	4.72
Ho	0.82	0.87	0.76	0.93	1.21	1.07	1.06	0.91
Er	2.11	1.94	2	2.48	3.42	2.72	2.63	2.68
Tm	0.33	0.25	0.29	0.36	0.51	0.36	0.36	0.38
Yb	1.85	1.36	1.71	2.07	3.27	2.18	2.17	2.10
Lu	0.28	0.17	0.25	0.31	0.47	0.30	0.30	0.33

973

974 **Table 7.** Major, trace element and REE data for a selected group of island-arc volcanic and
975 syeno-diorite rocks from the Ankara Mélange.

Sample no	04.NAM	05.NAM	06.NAM	DM35	DM 36	DM37	CE960	08CM01	08CM07	KM54
Rock-type	Syeno-diyorite	Syeno-diyorite	Syeno-diyorite	Tephrite	Tephrite	Foidite	Basanite	Leucite Tephrite	Basanite	Basanite
Oxide, wt %										
SiO_2	50.31	49.35	49.11	41.65	41.86	39.81	42.41	48.29	45.00	46.34
TiO_2	0.59	0.61	0.62	0.76	0.74	0.70	0.89	0.67	0.79	0.93
Al_2O_3	18.69	18.75	18.39	15.90	15.55	12.84	16.89	18.21	14.57	14.36
Fe_2O_3	8.45	8.77	8.42	10.82	9.31	8.90	12.38	9.15	11.21	11.03
MnO	0.17	0.19	0.19	0.15	0.15	0.14	0.25	0.25	0.21	0.18
MgO	2.25	2.45	2.39	7.23	7.35	10.81	7.5	4.23	6.28	6.33
CaO	6.38	7.14	6.82	3.51	4.08	5.36	11.17	7.91	12.22	9.64
Na_2O	2.68	2.57	2.35	0.57	0.46	0.21	2.48	3.78	2.56	2.79
K_2O	5.32	5.07	5.68	5.99	6.15	5.15	0.62	2.91	2.15	3.09
P_2O_5	0.48	0.49	0.49	0.44	0.41	0.24	0.42	0.46	0.33	0.44
LOI	4.30	4.20	5.10	12.7	13.6	15.4	4.7	3.7	4.2	4.5
Total	99.61	99.58	99.63	99.69	99.68	99.61	99.71	99.56	99.52	99.67
Trace, ppm										
Cr	47.94	82.19	47.94	13.70	20.55	342.45	21	14.00	130.00	61.64
Ni	20	20	20	23	41	156	43	5.00	24.50	39.00
Co	20.60	22.80	20.70	25.7	28.0	38.4	43.1	24.80	37.10	36.20
Sc	11	11	11	20	21	37	30	20.00	48.00	39.00
Rb	140.2	138.5	148.2	184.1	172.6	162.6	18.3	52.50	29.40	195.80
Ba	1685	1557	1520	783	739	887	577	1883	1051	840
Sr	845.2	915.3	759.4	257.5	331.3	362.2	563.5	742.60	779.80	934.80
Cs	1.1	2.1	3.5	6	4.5	3.4	0.9	3.10	1.20	1.50
Th	11.9	13.9	11.1	10.1	10.3	7.5	4.7	18.00	5.90	5.30
U	3.2	3.1	3.0	3.3	3.7	1.8	1.5	2.40	1.70	2.20
Nb	8.9	9.4	7.6	9.1	8.7	4.2	4	12.30	5.10	3.40
Ta	0.4	0.4	0.3	0.3	0.4	0.1	0.3	0.50	0.20	0.20
Zr	76.1	86.0	72.9	72.8	74.4	49.2	68.9	87.80	57.70	75.20
Hf	1.6	2.2	2.0	2.0	1.7	1.4	2	2.50	1.60	2.00
Y	23.6	23.0	20.3	14.8	16.5	12.5	21.4	20.90	18.70	22.00
V	169	182	166	279	275	260	339	273	301	302
Pb	4	21.8	24.9	3.9	7.4	6.1	5.2	7.3	5.5	9
REE, ppm										
La	33.7	36.6	31.9	26.0	25.7	18.8	20	36.70	20.70	18.40
Ce	60.0	63.7	55.4	53.2	53.5	37.7	42.6	66.70	40.00	41.90
Pr	6.72	7.12	6.20	5.85	5.63	3.93	5.52	7.87	4.89	5.51
Nd	25.3	25.7	24.9	23.0	22.5	15.7	25	32.80	20.70	22.90
Sm	4.91	4.88	4.41	4.42	4.29	3.21	5.27	5.81	4.18	5.12
Eu	1.32	1.31	1.24	1.18	1.21	0.91	1.57	1.53	1.33	1.47
Gd	4.70	4.51	4.18	3.89	4.02	3.21	5.12	5.23	4.31	5.17
Tb	0.70	0.71	0.64	0.57	0.60	0.47	0.79	0.76	0.66	0.80
Dy	3.89	4.11	3.73	2.83	3.28	2.52	4.03	3.88	3.54	4.34
Ho	0.72	0.75	0.67	0.56	0.60	0.46	0.76	0.73	0.69	0.81
Er	2.02	2.14	1.92	1.60	1.61	1.24	2.07	2.05	2.00	2.14
Tm	0.30	0.30	0.28	0.21	0.23	0.17	0.32	0.28	0.29	0.34
Yb	2.16	2.05	1.89	1.49	1.47	1.10	1.82	1.84	1.65	1.94
Lu	0.28	0.33	0.25	0.22	0.23	0.16	0.28	0.27	0.26	0.30
Mg#	35	36	36	57	61	71	55	48	53	53
KO/NaO	1.99	1.97	2.42	10.51	13.37	24.52	0.25	0.77	0.84	1.11

976

977 **Table 8.** Major, trace element and REE data for a selected group of island-arc volcanic rocks from the Ankara Mélange.

Sample no	CE.962	CE.964	CS.07	CS.11	CE.96	CE.98	CS.99	MS.34	MS.35	MS.36	COR.6	COR.7	COR.9	COR.10
Rock-type	**Basanite**	**Basanite**	**Basanite**	**Basanite**	**Basalt**	**Basalt**	**Basalt**	**Basanite**	**Basanite**	**Basaltic-trachyandesite**	**Basanite**	**Trachy basalt**	**Trachy basalt**	**Basanite**
Oxide, wt %														
SiO_2	42.28	42.78	44.35	42.69	51.27	48.78	48.28	44.49	44.56	54.26	44.13	48.08	46.26	42.86
TiO_2	0.88	0.9	0.78	0.82	0.78	1.74	1.71	1.00	0.92	0.50	0.84	0.84	0.85	0.93
Al_2O_3	16.57	16.84	16.10	16.55	15.91	14.85	14.89	17.60	15.63	17.93	17.26	17.21	18.47	17.03
Fe_2O_3	12.07	12.26	11.44	11.98	9.57	12.69	12.69	9.35	10.31	6.34	9.40	10.17	9.49	10.21
MnO	0.27	0.24	0.21	0.20	0.14	0.20	0.20	0.16	0.19	0.14	0.18	0.19	0.16	0.20
MgO	8	7.37	7.67	6.68	6.44	5.78	5.72	6.82	8.84	2.44	7.21	4.22	4.13	4.74
CaO	10.83	10.42	10.47	9.48	7.64	8.26	8.54	9.17	9.84	5.97	8.84	6.9	8.19	13.37
Na_2O	2.7	2.47	3.29	3.88	4.73	3.84	3.48	2.09	2.15	3.75	2.89	4.32	2.35	1.28
K_2O	0.73	1.57	0.51	1.06	0.12	0.59	0.75	2.39	2.33	4.10	2.82	2.51	3.01	2.41
P_2O_5	0.38	0.43	0.33	0.39	0.06	0.18	0.16	0.31	0.31	0.27	0.39	0.46	0.34	0.44
LOI	5	4.3	4.5	6.0	3.1	2.7	3.1	6.2	4.5	4	5.6	4.6	6.4	6.1
Total	99.71	99.58	99.65	99.69	99.81	99.57	99.47	99.64	99.61	99.67	99.56	99.48	99.67	99.62
Mg#	57	54	57	52	57	47	47	59	63	43	60	45	46	48
Trace, ppm														
Cr	21	14	68	14	14	41	41	21	82	14	55	14	27	41
Ni	29	37	31.00	19.70	20.40	18.60	18.00	12.20	23.00	5.10	16.7	1.9	15.1	17.5
Co	44.5	43.7	44.10	43.40	31.80	40.10	40.70	33.20	40.60	14.70	32.4	26.5	24.1	40.2
Sc	32	31	41	34	35	37	37	34	49	11	31	15	26	33
Rb	46.5	65.1	11.00	42.50	3.20	8.30	10.00	58.50	55.70	129.20	67.7	38.3	92.4	59.3
Ba	636	2044	596.00	613.00	36.00	882.00	1437.00	796.00	700.00	1225.00	885	2166	902	877
Sr	497.4	620.5	471.90	321.40	43.40	1129.10	1385.20	497.00	460.50	546.70	966.6	875.8	579.5	660.2
Cs	1.3	1	2.90	1.50	32.70	0.70	0.40	2.90	2.70	3.70	4.4	2.1	2.8	2.5
Th	3.8	4.3	3.70	3.90	0.30	0.90	0.90	12.70	11.00	22.90	14.3	12.1	14.3	15.8
U	1	1.2	1.50	1.10	0.10	0.20	0.30	3.20	2.90	5.70	3.6	3	3.1	4.1
Nb	3.1	3.8	4.90	5.40	4.70	7.40	7.10	7.40	6.30	10.30	5.9	6.3	6.4	5.9
Ta	0.2	0.3	2.40	1.60	3.30	3.50	3.90	0.90	1.00	1.50	0.3	0.3	0.4	0.3
Zr	63.3	65	50.60	55.20	46.10	107.30	104.80	110.90	106.30	175.80	126.4	94.4	108.3	113.3
Hf	2.2	1.9	1.50	1.60	1.50	2.90	2.90	2.90	2.90	4.10	3.1	2.6	2.6	2.3
Y	19.6	20.7	18.20	19.80	20.30	34.00	34.10	25.80	24.80	27.10	25.3	24.3	20.4	23.8
V	357	357	365	339	335	379	385	364.00	401.00	157.00	292	282	280	388
Pb	3.6	4.8	5.40	8.30	0.7	0.4	0.6	8.9	8.9	7	13.4	17.5	13.1	18.8

978

979 **Table 8.** *Continued.*

Sample no	CE.962	CE.964	CS.07	CS.11	CE.96	CE.98	CS.99	MS.34	MS.35	MS.36	COR.6	COR.7	COR.9	COR.10
Rock-type	**Basanite**	**Basanite**	**Basanite**	**Basanite**	**Basalt**	**Basalt**	**Basalt**	**Basanite**	**Basanite**	**Basaltic-trachyandesite**	**Basanite**	**Trachy basalt**	**Trachy basalt**	**Basanite**
REE, ppm														
La	17.3	17.6	14.90	16.80	3.00	8.40	8.30	37.60	33.30	60.20	43.1	36.2	41.1	43.8
Ce	37.6	39.5	31.60	35.20	7.70	20.90	20.40	73.30	67.00	109.70	90.9	74.4	82.0	92.2
Pr	5.16	5.27	4.16	4.63	1.10	2.90	2.84	8.63	8.13	11.97	9.92	8.46	8.73	9.80
Nd	22.7	23	17.60	20.10	5.20	14.50	13.70	34.50	32.80	43.60	35.3	34.6	31.1	34.8
Sm	4.99	5.22	4.14	4.70	1.86	3.92	3.95	6.88	6.66	7.35	7.23	6.81	5.85	6.93
Eu	1.51	1.53	1.27	1.38	0.74	1.26	1.43	1.94	1.80	1.87	1.96	1.86	1.55	1.79
Gd	4.87	4.94	3.97	4.36	2.49	5.00	5.13	6.21	5.88	5.83	6.42	6	5.30	6.23
Tb	0.72	0.73	0.63	0.70	0.52	0.96	0.97	0.95	0.92	0.90	0.94	0.92	0.76	0.89
Dy	3.92	4.06	3.23	3.47	3.17	5.54	5.76	4.85	4.66	4.68	4.80	4.83	3.66	4.48
Ho	0.71	0.75	0.63	0.68	0.70	1.23	1.23	0.96	0.86	0.91	0.89	0.88	0.76	0.84
Er	1.88	1.96	1.75	1.79	2.17	3.59	3.50	2.46	2.35	2.58	2.44	2.62	2.06	2.28
Tm	0.3	0.31	0.25	0.29	0.33	0.55	0.56	0.39	0.36	0.42	0.35	0.36	0.30	0.34
Yb	1.78	1.78	1.56	1.67	2.11	3.35	3.34	2.38	2.23	2.67	2.27	2.33	1.86	2.19
Lu	0.27	0.27	0.24	0.25	0.33	0.52	0.51	0.36	0.33	0.42	0.35	0.36	0.29	0.33
K_2O/Na_2O	0.27	0.64	0.16	0.27	0.03	0.15	0.22	1.14	1.08	1.09	0.98	0.58	1.28	1.88

Table 9. Major, trace element and REE data for a selected group of lamprophyric dike rocks from the Ankara Mélange.

Sample no	DM2	DM3	DM4	DM5	DM5A	DM6	DM7	DM7A	DM8	DM9	DM10	DM17	CE1206	CE1207	CE2	CE1210	25BM11
Rock-type	**Tephrite**	**Tephrite**	**Tephrite**	**Tephrite**	**Tephrite**	**Trachy-basalt**	**Phono tephrite**	**Tephrite**	**Trachy-basalt**	**Phono tephrite**	**Phono tephrite**	**Tephrite**	**Picro-basalt**	**Picro-basalt**	**Picro-basalt**	**Trachy-basalt**	**Trachy andesite**
Oxide, wt %																	
SiO_2	45.25	43.02	47.41	45.84	46.23	48.59	50.29	50.49	49.34	47.48	47.02	46.45	41.94	47.34	44.89	51.33	58.15
TiO_2	0.69	0.76	0.58	0.64	0.66	0.73	0.62	0.62	0.70	0.73	0.74	0.78	1.12	0.83	1.26	1.24	0.43
Al_2O_3	11.20	10.93	15.79	16.98	17.00	10.34	14.94	14.73	12.10	14.37	14.66	11.40	12.91	15.66	13.36	15.62	17.43
Fe_2O_3	11.16	12.10	9.54	10.86	11.03	11.46	10.85	10.72	10.92	11.07	11.13	12.59	10.8	9.79	11.12	7.33	5.81
MnO	0.23	0.22	0.23	0.21	0.21	0.22	0.20	0.18	0.21	0.24	0.23	0.22	0.2	0.21	0.22	0.08	0.14
MgO	5.41	4.98	2.90	4.66	4.87	6.02	4.02	4.13	4.49	3.43	3.50	5.09	7.71	4.02	8.23	5.99	**1.88**
CaO	14.50	15.89	12.25	10.25	9.57	13.68	7.30	7.53	13.50	8.44	8.53	12.26	16.47	9.11	14.37	8.22	4.04
Na_2O	0.67	0.28	0.36	1.63	1.68	0.56	2.84	2.78	1.96	2.64	2.95	1.58	1.62	2.97	1.70	3.95	5.56
K_2O	5.47	5.54	6.96	4.67	4.99	5.73	5.53	5.50	4.11	6.34	5.82	5.40	**0.72**	4.5	1.01	1.85	4.32
P_2O_5	0.89	0.80	0.45	0.44	0.40	1.08	0.96	0.93	0.89	0.78	0.78	0.90	0.49	0.64	0.55	0.75	0.29
LOI	4	4.9	2.9	3.4	3.0	1.1	2.0	1.9	1.3	3.7	3.9	2.8	5.8	4.6	2.9	3.4	1.6
Total	99.5	99.46	99.42	99.61	99.60	99.49	99.53	99.53	99.52	99.27	99.28	99.48	99.78	99.67	99.64	99.76	99.64
Trace, ppm																	
Cr	13.70	13.70	13.70	13.70	13.70	13.70	13.70	13.70	13.70	13.70	13.70	13.70	89	21	82	**158**	68
Ni	20	20	20	20	20	20	20	20	20	20	20	20	48	28	67	86	45
Co	33.0	39.4	26.9	34.8	34.5	37.9	34.1	33.8	32.2	28.5	28.9	41.2	35.5	24.2	39.7	24.9	12.50
Sc	30	34	10	25	27	45	24	25	30	21	22	36	41	22	39	19	7
Rb	51.4	52.6	94.6	76.9	81.5	46.9	65.0	67.7	29.7	47.3	43.1	50.0	20.8	75.5	13.8	29.9	76.5
Ba	1861	1881	2899	1224	1228	1760	1183	1233	1846	3229	3172	2019	180	1109	257	475	1456
Sr	697.0	864.1	762.5	701.6	811.3	823.9	1483.3	1401.6	758.9	1287.1	1335.2	790.0	1073	1116	805.4	1006	679.1
Cs	0.1	0.1	0.2	0.3	0.2	0.1	0.1	0.1	0.1	0.4	0.4	0.1	0.3	0.6	0.1	0.2	0.1
Th	24.4	14.0	19.7	8.9	9.1	21.9	14.2	14.4	23.1	34.6	33.6	13.2	7.3	14.9	6.9	5.4	25.0
U	6.0	5.6	7.4	2.9	3.1	5.4	7.1	6.9	6.0	10.1	10.5	5.1	2.4	4.9	2.5	1.0	6.9
Nb	18.3	22.7	18.4	7.8	7.9	17.0	13.7	13.9	18.6	34.1	33.9	21.7	9.7	13.1	15.1	7.4	10.7
Ta	0.6	0.7	0.7	0.3	0.3	0.7	0.5	0.5	0.6	1.1	1.2	0.7	0.6	0.9	1.0	1	0.6
Zr	111.4	111.2	117.3	65.0	62.3	103.2	95.1	93.8	112.6	188.1	186.3	101.6	92.9	163.5	111.9	121.9	199.7
Hf	2.8	2.9	2.8	1.6	1.4	2.7	2.5	2.3	2.8	4.7	4.4	2.6	2.5	4.1	2.8	3.1	4.3
Y	23.7	24.5	22.1	16.2	15.1	24.4	21.5	20.4	24.8	34.2	34.4	23.7	21.9	34.8	24.7	16.9	28.9
V	305	403	405	307	299	329	262	269	347	329	329	370	300	245	330	162	116
Pb	32.3	17.0	11.1	16.8	15.5	14.8	9.6	8.8	9.4	12.6	11.3	20.2	2.3	6.6	0.9	1.30	33.9
Mg#	49	45	38	46	47	51	42	43	45	38	38	44	59	45	59	62	39
KO/NaO	8.16	19.79	19.33	2.87	2.97	10.23	1.95	1.98	2.10	2.40	1.97	3.42	0.44	1.52	0.59	0.47	0.78

981 **Table 9.** *Continued.*

Sample no	DM2	DM3	DM4	DM5	DM5A	DM6	DM7	DM7A	DM8	DM9	DM10	DM17	CE1206	CE1207	CE2	CE1210	25BM11
Rock-type	**Tephrite**	**Tephrite**	**Tephrite**	**Tephrite**	**Tephrite**	**Trachy-basalt**	**Phono tephrite**	**Tephrite**	**Trachy-basalt**	**Phono tephrite**	**Phono tephrite**	**Tephrite**	**Picro-basalt**	**Picro-basalt**	**Picro-basalt**	**Trachy-basalt**	**Trachy andesite**
REE, ppm																	
La	60.0	41.8	49.5	26.4	25.0	56.6	32.2	30.7	58.4	83.6	81.2	41.4	26.3	43.2	29.3	33.3	69.2
Ce	120.4	87.4	97.8	52.4	49.7	115.9	69.8	67.3	119.6	159.0	156.7	86.5	53.1	88.9	58.1	70.7	124.9
Pr	13.07	9.79	10.41	5.75	5.52	13.12	7.99	7.71	13.19	16.87	16.92	9.76	6.83	10.9	7.52	8.76	13.24
Nd	49.9	39.3	38.7	22.2	22.3	53.9	32.7	32.0	51.5	63.2	63.9	39.6	28.2	42.5	29.8	33.1	46.9
Sm	9.36	8.07	7.17	4.49	4.29	9.83	6.15	5.93	9.48	11.52	11.64	7.84	5.98	8.52	6.96	5.67	7.82
Eu	2.26	2.02	1.86	1.20	1.14	2.35	1.53	1.50	2.27	2.84	2.88	2.00	1.72	2.49	1.98	1.59	1.93
Gd	7.94	7.09	6.23	4.01	3.88	8.37	5.32	5.22	7.97	10.04	10.03	7.19	5.68	8.09	6.36	4.56	6.22
Tb	1.04	0.97	0.88	0.59	0.56	1.07	0.77	0.76	1.07	1.36	1.36	0.95	0.86	1.21	0.93	0.67	0.90
Dy	4.95	4.71	4.31	2.95	2.97	4.94	3.94	3.91	4.88	6.88	6.66	4.72	4.06	6.33	4.68	3.28	4.98
Ho	0.82	0.82	0.73	0.55	0.55	0.79	0.74	0.73	0.84	1.16	1.19	0.80	0.79	1.2	0.81	0.61	0.91
Er	2.05	2.12	2.00	1.50	1.45	2.10	1.96	1.94	2.08	3.08	3.02	2.10	2.09	3.27	2.30	1.64	2.63
Tm	0.29	0.29	0.27	0.22	0.21	0.28	0.29	0.27	0.29	0.43	0.44	0.30	0.32	0.52	0.33	0.25	0.42
Yb	1.65	1.79	1.83	1.41	1.33	1.69	1.74	1.76	1.69	2.67	2.80	1.73	1.76	2.94	1.89	1.47	2.66
Lu	0.25	0.27	0.26	0.21	0.20	0.25	0.27	0.26	0.25	0.41	0.41	0.26	0.27	0.46	0.27	0.22	0.43
$^{87}Sr/^{86}Sr$		0.704786			0.704892			0.704697	0.704720			0.704797			0.704820		
$^{143}Nd/^{144}Nd$		0.512681			0.512686			0.512690	0.512682			0.512680			0.512674		
$^{206}Pb/^{204}Pb$		19.540			19.332			19.939	19.604			19.594			19.418		
$^{207}Pb/^{204}Pb$		15.662			15.655			15.691	15.675			15.659			15.664		
$^{208}Pb/^{204}Pb$		39.376			39.192			39.612	39.536			39.407			39.297		

982